A MULTI-COMPARTMENTAL MATHEMATICAL MODEL OF THE POSTPRANDIAL HUMAN STOMACH

A thesis presented in partial fulfilment of the requirements for the degree of

Doctor of Philosophy

in

Anatomy and Physiology

at

Massey University

Palmerston North

New Zealand

NIKHILA MARY VIJAY

2020

DEDICATION

Achan - aka Vijayan, my father & **Amma** - aka Mary, my mother

Kuttan - aka HemLin, my brother & **Rechu** – aka Harpreet, my SIL

Motta - aka Sameer, my friend

Aaminu - aka Niyati, my daughter & **Dada** - aka Gordon, my partner

Because you extend your shoulders for me to weep in my darkest days, and you celebrate my existence…!

****

Valyachan, Appachan, Echyamma, Indhiramma, Ammachi, and Valyamma

not a single day passes by without missing you and I know you are the 'star of wonder' that guides my wandering soul.

ACKNOWLEDGEMENT

"The teacher who walks in the shadow of the temple, among his followers, gives not of his wisdom but rather of his faith and his lovingness. If he is indeed wise, he does not bid you enter the house of his wisdom but rather leads you to the threshold of your own mind."

Kahlil Gibran (The prophet)

I was privileged enough to have three great teachers in this long journey, Prof. Roger Lentle, Dr Clément de Loubens, and Dr Richard Love. I express my deepest gratitude to my supervisors for their open-door policy, valuable time, expertise and unconditional support throughout this journey.

Roger, you are the one who rephrased the saying, "Brains are not to be found in the beard." However, I shall admit that it wasn't easy for my brain to keep up with yours. But I thoroughly enjoyed your barrel of laughs each time I hit the goal, and that kept my spirit up. Thank you is never enough for allowing me to work with you, encouraging me to do better, and for appreciating me as a person.

Clement, thank you so much for being generous and sparing your valuable family time for me, regardless of our different time zones. Your passion and expertise always surprise me. You never were just a supervisor but a friend who made writing this chapter of my life easier. Thank you!

Richard, you have always shown empathy and helped me with things that were not your assigned duty. I do know that I was a highly demanding student, and you patiently met my needs. I am grateful for the help you extended to support my tuition, other administrative things and for understanding my voyage outside of this university boundary. You will be ever so fondly remembered.

I acknowledge my thankfulness to **Massey University** for providing me with the ***Massey Vice chancellor's doctoral scholarship*** and for the ***Massey Foundation Grant***. I thank the **College of Health** for providing a stipend to support my studies. I use this opportunity to thank **Associate**

Professor Rachel Page, Professor Marlena Kruger, and Dr Wei-Hang Chua for all their help and kindness.

I wouldn't have reached the finishing point in these hurdles if you were not there; **Corrin**-my fellow sailor**, Shampa, Fran, Sarah and all other fellow coffee mates** of the 'secret tea room', thank you for sharing your words and laughs with me.

It is unusual to thank your own family in my culture, but I am here today just because of them, and I want them to know this:

Acha, you have awakened me to a home where everything is in abundance. Every time I feel miserable, I virtually curl up into your arms and 'listen' to all those lullabies you used to sing for me. You mean the universe to me, Acha…!

Amma, you are the one who gave sky to my wings and the nest to my soul. You let me fly freely, but carefully hold the kite reel to get back if I am lost. You have made me flexible yet strong, wild yet rooted. I am so proud and thankful that I am your daughter, Ma.

Kutta, you took away all the attention I received until I was six and made me unhappy and jealous. But you have grown to be an amazing person in whom I seek strength and warmth. You cherish my silly wild dreams and stand by me. I miss all your cuddles and songs, and I want you to know this, even though you are annoying, I love you to infinity and beyond…!

Ammunje, I use this opportunity to thank you for each glass of coffee, lemon drink and plates of lunch you have made for your tired Amma; and for all those head massages and all those worried queries, "Amma, are you all right?!". You stood by me through thick and thin like a best pal. You are an amazing human being, and I am lucky that I got a chance to nurture you. I am forever thankful to this life for you, my child. Love you till the end of my time.

Kanna, this journey would have been appalling if you weren't guarding me against external and internal storms. You nestle me in your roots and navigate the wilderness in me to be the real me. You are the *Genie* who makes my wishes come true and brings smiles to my face. I know I was hard on you and Aaminu during my thesis writing stage, but you both graciously handled me…Umma Kanne !!!

ABSTRACT

Computational fluid dynamics of the human stomach helps to understand the gastric processes such as trituration, mixing, and transit of digesta. Their outcomes give greater insight into the design of food and orally dosed drug delivery system. Current models of gastric contractile activity are primarily limited to the gastric antrum and assume global values for the various physiological characteristics. This thesis developed a unified compartmental gastric model with correctly informed anatomical and physiological data. The gastric geometry incorporated the actions of multiple compartments, such as the gastric fundus, body, antrum, pyloric canal, proximal duodenal cap, and the small intestinal brake. Lattice-Boltzmann Method (LBM) is used to simulate the fluid dynamics within the stomach.

This thesis quantified the effects of transgastric pressure gradient (TGPG) between the fundus and the duodenum, the effect of antral propagating contraction (APC) amplitude, and the viscosity of the gastric contents on gastric flow, mixing, and gastric emptying.

The results of this work suggest that TGPG influences gastric emptying where as APCs do not play major role in gastric emptying. Flow rate without TGPG obtained in this work agrees with previous work (Pal *et al*., 2004); however, it is higher in the presence of a TGPG. Results show that APCs promote recirculation, and the amplitude of APC is vital in this regard. The 'pendulating' flow of gastric content observed in this work is reported previously in duplex sonography experiments (Hausken *et al*., 1992). This work quantified the gastric shear rates (0.6 - 2.0 /s). This work also suggests that the viscosity of the content influences gastric fluid dynamics.

This work is a simplified first step towards a 3D gastric model. Hence, these simulation studies were performed under two simplifications: dimensionality and rheology, i.e., we have assumed a Newtonian fluid flow in 2D gastric geometry. A 3D gastric model with more rheologically realistic fluid to explore the pseudoplastic fluid dynamics within the stomach in the future is recommended.

Table of contents

List of figures

List of tables

List of abbreviations

ACW	Antral contraction wave
ANS	Autonomic nervous system
APC	Antral propagating contraction
ATP	Adenosine triphosphate
CCK	Cholecystokinin
CFD	Computational fluid dynamics
CNS	Central nervous system
CT	Computerized tomography
DEM	Discrete element method
DMC	Dry matter concentration
DPL	Distal pyloric loop
ENS	Enteric nervous system
ER	Endoplasmic reticulum
FEM	Finite element method
FVM	Finite volume method
GC	Greater curvature
GI tract	Gastro intestinal tract
ICC	Interstitial cells of Cajal
ICC - IM	Intramuscular interstitial cells of Cajal
ICC - MY	Myenteric Interstitial cells of Cajal
ICC - SEP	Septal Interstitial cells of Cajal
LBM	Lattice-Boltzmann method
LC	Lesser curvature

MMC	Migrating motor complexes
MLCK	Myosin light chain kinase
MRI	Magnetic resonance imaging
PC	Pyloric canal
PCHIP	Piecewise Cubic Hermite Interpolating Polynomial
PPL	Proximal pyloric loop
Re	Reynold's number
SHIME	The simulator of the human intestinal microbial ecosystem
SM	Smooth muscle
SMC	Smooth muscle cells
SNS	Sympathetic nervous system
TAC	Terminal antral contraction
TGPG	Transgastric pressure gradient
VOF	Volume of fluid

Chapter 1: Introduction

Polyphagous mythical monsters and an 18th-century French showman and soldier named ‘Terrare’, whose unusual diet included corks, snakes, and cats, were my daughter's all-time favourite bedtime stories. She was inquisitive why Terrare's hunger was never satisfied even after a wheelbarrow full of food. I told her that his 'satiety wire' was disconnected, which caused an 'excessive dancing of his belly and bowels’. After having six months of *cat eater's* story, I had told her that he had had a bariatric bypass and lived happily ever after! However, in reality, available medical technologies were insufficient to examine or treat Terrare's condition, and he had a tragic ending (Burns, 2004).

The most proximally situated dilated structure in the gastrointestinal tract (GI tract), the stomach, and the role in pulverizing and partially digesting food has evoked curiosity among physicians, scientists, and physiologists from ancient times. However, real-time visualization of these processes of digestion has only recently been possible. Current technologies such as echo-planar magnetic resonance imaging (Pal *et al*., 2004), ultrasound scanning (Holt *et al*., 1986; Worlicek *et al*., 1989), and two-dimensional spatiotemporal mapping (Berthoud *et al*., 2002; Lentle *et al*., 2010) enables real-time visualization of the contractile behaviours of various components of the stomach. However, such technologies do not provide an integrated overview of their mode of action on gastric contents, notably mixing and triturating solid material. Hence, the incorporation of accurate physiological data regarding the contractile behaviour of various components of the stomach into a real-time computational fluid dynamic model (Ferrua and Singh, 2010; Kozu *et al*., 2010; Du *et al*., 2013; Berry *et al*., 2016) may provide a better understanding of the gastric processes of digestion.

Understanding the biochemical, physiological, and physicochemical parameters that mediate digestion and absorption is essential for the gastroenterologist, food & pharmaceutical industries and nutrition studies (Ferrua and Singh, 2010; Anandharamakrishnan, 2013). The oral route is the most common route for drug administration, and it is the most preferred route by patients due to its advantages, such as ease of use, non-invasiveness, and convenience for self-administration. However, oral drug delivery comes with challenges such as drug solubility, poor drug stability,

low drug permeability across the mucosal barriers and variability in the physiology of the GI tract (Martinez *et al*., 2002). An understanding of the ability of a food matrix to withstand breakdown when subjected to physiochemical processing in the stomach is vital in assessing the bioavailability of nutrients and is essential in maintaining health, particularly in subjects with inherited disorders of uptake of specific nutrients (Garrett *et al*., 1999; Rein *et al*., 2013). Therefore, a versatile gastric model would be helpful to design the drug or food formulation and give the possibility of individually tailored targeted oral drug delivery systems (Ashford, 2002).

The use of a real-time computational fluid dynamic (CFD) model may obviate some of the time and cost involved in human trials of novel foods and drug formulations and circumvent some of the ethical difficulties therein (Barton and Emanuel, 2005; Yoo and Chen, 2006).

While the complexity of form and action of the various components of the stomach and the rheology of the suspension of solid particles in a Newtonian liquid that constitutes a simplified chyme are well known, currently published gastric models have not incorporated these complexities (Pal *et al*., 2004; Dillard *et al*., 2007; Kozu *et al*., 2010; Imai *et al*., 2013; Miyagawa *et al*., 2016;). Instead, published models have concentrated on the contractile activity of particular components, notably the gastric antrum (Pal *et al*., 2004; Ferrua and Singh, 2010) and the pylorus (Dillard *et al*., 2007), and assume global values for the various physiological characteristics.

A wealth of reliable physiological data describing the stomach's various components' actions are available (Pal *et al*., 2004; Lentle *et al*., 2010b; Janssen *et al*., 2011; R.G Lentle *et al*., 2013). This thesis attempts to review and incorporate relevant published physiological parameters to develop a computational fluid dynamic model. This model simulates the consequent flow, mixing, and dispersal of the stomach contents and the influence of fundal tone, antral and pyloric contractions, and the duodenal brake in the postprandial stomach. This work does not consider the outcome of contractile activities of the stomach in the inter-meal interval when pyloric dominance is absent.

1.1 Aim

- This thesis aims to construct a mathematical model of the postprandial human stomach that incorporates published physiological data regarding the action of the gastric fundus, body, antrum, pylorus, proximal duodenum and the concept of the duodenal brake.

1.2 The novelty of the thesis

- All relevant published parameters and geometrical measurements are incorporated to create this anatomically realistic organ model
- Fundic pressure cycles and pyloric pressure cycles are incorporated and are adjustable
- The amplitude of the antral propagating contractions (APCs) is tuneable
- First work to quantify the shear rate within the gastric lumen

To correctly model and simulate the human stomach's mechanical actions, a thorough understanding of the mechanical processes exhibited by the gastric walls and the physical nature and rheological properties of the contained chyme is essential. Since this work required the accurate measurement and demarcations of the stomach, pylorus, and duodenum, and also some relevant physiological data, to accurately create the gastric geometry and its motility patterns, this thesis used a cluster of older references as little has been updated or changed. That is one of the reasons to undertake this study. Chapter 2 of this thesis discusses the broad anatomical and physiological details of the stomach. Chapter 3 details the various published gastric techniques. The details of the development of the CFD model, notably the selection of particular parameters and the lattice-Boltzmann method, the numerical method used in this work to simulate gastric fluid dynamics, is covered in Chapter 4. The fifth chapter details the results and discusses the relevance of those findings. Finally, the general conclusion and future recommendations are given in Chapter 6. More details on the stomach glands, stomach wall motility during inter meal interval are provided in the Appendices.

Chapter 2: Anatomy and physiology of the human stomach

The stomach is a hollow muscular structure located in the epigastric region of the abdominal cavity between the oesophagus and the small intestine (Forte, 1996). The shape of the human stomach is ovid and flattened in the vertical plane with the lesser curvature uppermost and the greater curvature lowermost. Recent advances in medical imaging have allowed a more accurate assessment of the stomach's geometry during various physiological states (Liao *et al*., 2004; Lammers *et al*., 2009). The stomach becomes more acutely ellipsoidal in a vertical cross-section when empty (Leopold, 1975). Its volume reduces to 50 mL from 1-1.5 L after a typical meal (Saladin, 2007). After a meal, an average-sized human stomach is about 10 cm wide at its widest point. The length of the greater curvature is 31.6 cm, and that of the lesser curvature 21.98 cm (Keet, 1982). Likewise, the pyloric ring has a maximum diameter of 1.1 cm (Schulze, 2006).

The stomach has different anatomical regions, and these are the fundus, cardia, body, and pylorus (Figure 1).

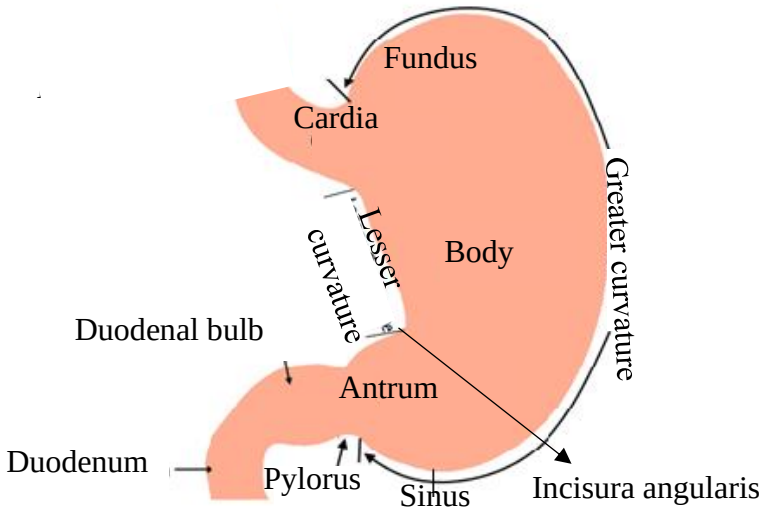

Figure 1. Gross anatomy of the stomach.

The fundus is the dome-shaped distensible pouch that lies to the right of the oesophagus and cardia and forms the apex of the stomach. The fundus convexes upward from the horizontal level of the cardia, and when distended, it is 2 - 4 cm in height (Code, 1968; Groedel, 1909), providing the bean-like shape of the stomach.

The corpus, otherwise known as the body, extends from below the gastric inlet (distal oesophageal opening and cardia) to the incisura angularis and is often collapsed when empty (Terragni *et al*., 2012). The cone-shaped (Code, 1968) thick distal part of the stomach that connects the corpus with the pylorus is called the antrum (Groedel, 1909). The angular notch in the junction of the body and the antrum is called the incisura angularis. The sinus, the lowermost part of the stomach, is wedge-shaped and bulges opposite the incisura (Brown *et al*., 1993). The distance between the tip of the fundus to the lowermost pole of the sinus averages 20 cm in men and 22 cm in women (Schulze, 2006).

The pylorus is a 3-4 cm long segment of thickened muscular extrema that extends to a distal-most point where the circular muscle fibres are sharply demarcated from those of the duodenum by a fibrous septum (Keet, 1982). There are complex changes in the geometry of the pyloric sphincter during contraction and relaxation (Figure 2). The proximal margin of the pylorus is contiguous with the distal end of the greater curvature and is defined by the indentation produced by a thick loop of circular smooth muscle termed the proximal pyloric loop (PPL). Similarly, the distal edge of the pylorus is defined by a loop termed the distal pyloric loop (DPL). The DPL and PPL fuse at their dorsal limit to form the downwardly projecting torus, which is 2 cm long (Keet, 1982) and projects 3.7 mm (Schulze-Delrieu and Wall, 1983) into the lumen.

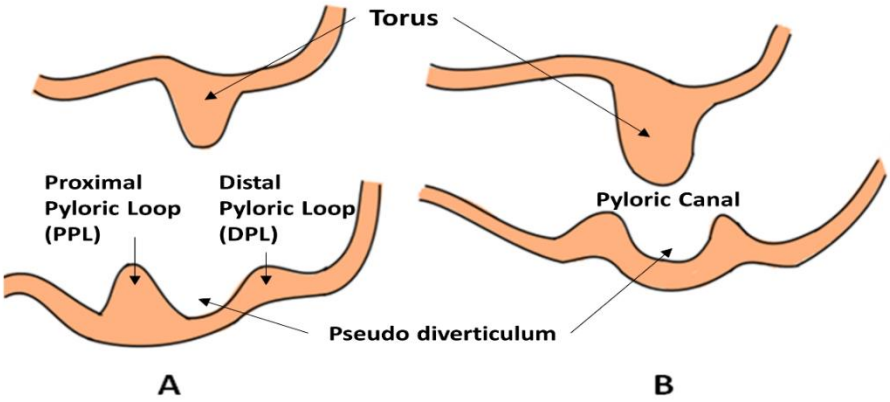

Figure 2. The pylorus in (A) relaxed and (B) contracted state. PPL- proximal pyloric loop; DPL- distal pyloric loop (Adapted from Ramkumar and Schulze, 2005).

The pylorus exhibits a degree of tone (Cristensen *et al*., 2000) that provides baseline resistance to gastric outflow (Keinke *et al*., 1983). During the postprandial period, resistance to outflow is supplemented by short-lived phasic pyloric closures known as the pyloric cycle (Dooley *et al*., 1985). The pylorus connects the stomach to the proximal small intestine. This part of the small intestine, known as the duodenum, has a more dilated proximal part known as the duodenal bulb. The mean diameter of the proximal duodenal bulb is approximately 5 cm (Kararli, 1995). The combined contractile activity of the stomach wall, pylorus and the duodenum helps in physical digestion of the gastric content.

Contractile activity of the gastric wall smooth muscle cells propels the gastric contents between gastric segments during the postprandial period. The contractile activity also generates a significant admixture of ingested food with gastric secretions and breakdown of solid food. The myenteric plexus of the enteric nervous system is primarily responsible for controlling motility, while the submucous plexus regulates mucosal secretion or absorption. These functions involve an integrated response to sensory input from the chemoreceptors or the mechanoreceptors (Adil *et al*., 2005).

The following section presents essential information on the stomach and its wall motility.

2.1 The Gastric Wall

As in the rest of the gastrointestinal system, the gastric wall consists of four distinct layers of tissue (Forte, 1996; Koppen *et al*., 2008; Mitra, 2015) named the:

1. Mucosa: This inner lining of the cavity of the stomach consists of a single layer of columnar epithelial cells that is folded into gastric glands.
2. Submucosa: The sub-mucosal layer contains the nerve trunks, blood vessels and lymph vessels.
3. Muscularis propria: The muscle layer in the stomach. Comprises of three layers of smooth muscle cells and their associated interstitial cells.
4. Serosal layer: This is the outer covering of the stomach wall that consists of a single layer of squamous mesothelial cells adjacent to the peritoneal cavity.

Since this thesis focuses on gastric motility, a detailed discussion on the muscularis propria is given in upcoming sections.

Muscularis propria largely comprises smooth muscle cells organised into three tissue layers, as mentioned earlier. They are the outer longitudinal muscle (LM), middle circular muscle (CM), and inner oblique muscle (Figure 3).

2.1.1 The Longitudinal Layer

The outermost longitudinal layer has two parts. The first part is an extension of the longitudinal muscle fibres of the oesophagus. This begins at the cardia, radiates in a stellate manner and only found in the fundus and body of the stomach. The second part is the intrinsic longitudinal layer that starts at the body and extends to the pylorus, merging with the pyloric sphincter (Mitra, 2015).

2.1.2 The Circular Layer

The most complete and thickest layer of the muscularis propria is oriented circumferentially (Koppen *et al*., 2008). The circular layer is continuous with the oesophagus at the cardiac end and merges with the pyloric sphincter at the pyloric end. It is separated from the circular layer of the duodenum by a connective tissue septum.

2.1.3 The Oblique Layer

The oblique layer is the innermost layer of smooth muscles covering the anterior and posterior surfaces of the stomach (Kelly, 2004). It fuses with the adjacent layer of circular muscle; however, it leaves a free margin at the lesser curvature. The free margin forms the magenstrasse, a temporary canal that runs from the incisura cardia to incisura angularis (Pal *et al*., 2007).

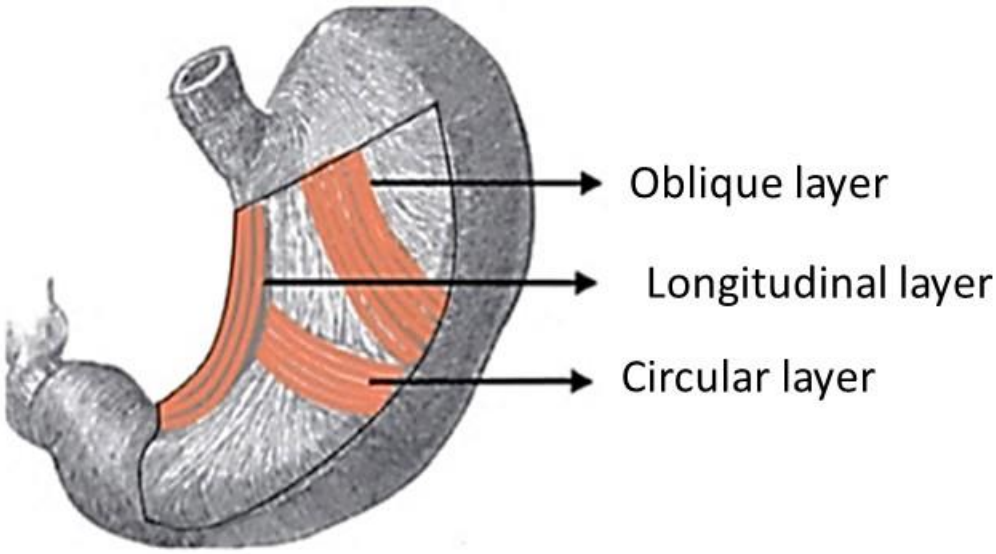

Figure 3. The three different muscle layers of the stomach (Adapted from https://www.theodora.com/anatomy/the-stomach.html).

The motility of the gastric wall results from the contractile activity of the gastric musculature. A detailed discussion on smooth muscle cells (SMCs) and their control mechanism is provided in the following section.

2.2 Smooth muscle cells

A single smooth muscle cell (SMC) is 30-200 µm in length and 5-10 µm in width (Saladin, 2007). Each SMC is covered by a bi-lipid plasma membrane that has longitudinal rows of pits called caveolae which increase the surface area available for signal reception absorption and transport

(Koppen *et al*., 2008). The mitochondria within the smooth muscle cell generates the ATP that is necessary for cellular contraction in association with the endoplasmic reticulum (ER) that act as storage sites for calcium ions (Horowitz *et al*., 1996; Koppen *et al*., 2008). As in other excitable tissues, depolarization depends on the changes in the permeability of several ion channels in the plasma membrane.

2.2.1 Connectivity of smooth muscle cells

SMCs have been broadly classified as unitary (or visceral) smooth muscle and multi-unit smooth muscle (Barrett *et al*., 2010). The SMCs in the GI tract are of the unitary type and form dense sheets or bands with each component cell connected to its neighbours via gap junctions and adherens junctions. Unitary smooth muscle cells are also surrounded by the bead-like varicosities located on the distal ends of the autonomic nerve fibres.

2.2.1.1 **Gap junctions**

Gap junctions are low resistance signal transduction pathways (Koppen *et al*., 2008) that enable a group of myogenic cells to respond to a neural or mechanosensory stimulus in an orchestrated manner (Sanders *et al*., 2014). The minimal distance across a gap junction is about 1.2 nm in vertebrates. This allows the passage of charged or neutral small molecules (Bennett *et al*., 1991) up to a molecular weight of ~1000 Da such as sugars, amino acids, nucleotides and mediates electrical and chemical coupling. These channels are formed of proteins called connexins (Loewenstein, 1981).

2.2.1.2 **Adherens junctions**

These structures are thought to provide a mechanical linkage between cells (Horowitz *et al*., 1996). Elements of actin (a contractile protein present in the cell) extend into the adherens junctions, aiding the transmission of contractile forces generated within a smooth muscle to its neighbours.

2.2.1.3 **Varicosities**

Neural varicosities on elements of the enteric nervous system (ENS) and extrinsic efferent nerves from the autonomous nervous system (ANS) release a range of neurotransmitters that may variously stimulate or antagonize the activities of various ion channels on the SMCs (Westfall, 2006). It is noteworthy that varicosities are located some distance from the plasma membrane of the myocytes and their associated cells (Huizinga, 2001; Sanders *et al*., 2010) and do not fuse with

them to form structures analogous to the motor end plates of smooth muscle. Hence neuro-transmitters must diffuse some distance to influence the ion channels of the plasma membrane (Ward *et al*., 2004).

2.2.2 The contractile apparatus

Within the smooth muscle cells are the thin actin and the thicker myosin filaments that enable SMCs to contract and relax (Bohr, 1964; Horowitz *et al*., 1996; Koppen *et al*., 2008). SMC contraction results from the interaction of actin and myosin proteins initiated by depolarization and an increase in free cytosolic calcium (Webb, 2003). Skeletal or cardiac muscle cells contain multiple repeating parallel bundles of the proteins actin and myosin along the myofibrils and have a striated appearance. In contrast, the contractile apparatus in smooth muscle is arranged in an irregular way.

The actin filaments of the smooth muscle are anchored to the cell membrane at sites known as the dense bodies. These dense bodies are functionally equivalent to the Z-disks in skeletal and cardiac muscle. Contraction of a smooth muscle myocyte initiates longitudinal shortening and a reciprocal increase in its circumference so that the total volume of the cells remains unchanged (Koppen *et al*., 2008 . Figure 4).

The actin filament is a double-stranded helical protein. Myosin filaments are formed from overlapping strands of myosin. Myosin is a large protein that consists of two heavy chains, each with a head region and a long α-helical tail region, and two pairs of light chains (Cooper, 2000). In a smooth muscle cell, the actin and myosin filaments are interdigitated so that two actin filaments are located on each side of a myosin filament. One side of each actin filament is attached to a dense body located in the plasma membrane, whilst the other side overlaps with the thick end of a myosin filament (Craig *et al*., Megerman, 1977; Xu *et al*., 1996; Sobieszek, 2016).

During smooth muscle contraction, each myosin head is moved to pull on the actin filament and thus reduce the length of the myocyte. Some smooth muscle cells can reduce their length to one-quarter of the original length, which constitutes a greater degree of shortening than occurs in skeletal muscles (Xu *et al*., 1996).

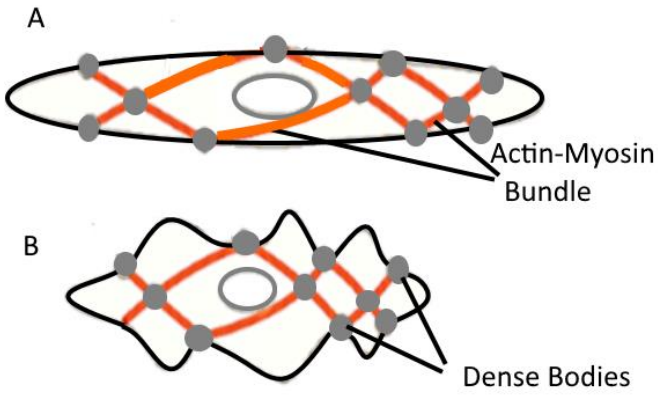

Figure 4. Contraction of a smooth muscle myocyte showing longitudinal shortening and a reciprocal increase in circumference (A) relaxed smooth muscle, (B) contracted smooth muscle.

2.3 Smooth muscle control mechanisms

Smooth muscle contraction in the gut is under three different control systems:

1. Myogenic control: The intrinsic rhythm of the GI musculature imparted by the interstitial cells of Cajal (ICC) generated slow-waves. Myogenic contraction of SMCs can be initiated by ICCs or by intrinsic and/or extrinsic neural control systems.
2. Neural control: This control system includes the intrinsic enteric nervous system and the autonomic nervous system.
3. Hormonal control: This control mechanism operates by various hormones, including cholecystokinin, gastrin, and secretin (Sayegh *et al.*, 2005).

An understanding of the different layers of the control mechanism and the components involved in it will aid in improving understanding of the contractile activity present in each anatomical regions of the stomach.

2.3.1 Myogenic control:The interstitial cells of Cajal and their role in smooth muscle contraction

The slow-waves produced by ICCs achieve myogenic control of the gastric wall. A slow-wave potential is a rhythmic change in transmembrane potential that propagates along the gastrointestinal tract wall and synchronizes smooth muscle contractions (Daniel, 1992). The slow-waves interact with the smooth muscle via gap junctions (Hansen, 2003; Sanderss *et al*., 2006; Hirst and Redwards, 2006; Lees-Green *et al*., 2011), causing them to depolarise by activating Ca^{2+} influx (Sanders *et al*., 2014) triggering muscle contraction (Huizinga *et al*., 2014).

Dickens *et al*., (1999) tried to identify the rhythmically active cells in the guinea pig stomach and identified the smooth muscle cells, and two sets of the interstitial cells of Cajal (ICC). They identified interstitials cells in the myenteric plexus, later termed as myenteric interstitial cells of Cajal (ICC-MY), as the slow-wave generating cells of the stomach and this is confirmed later by various other studies (Mostafa *et al*., 2010; Cheng and Farrugia, 2013; Blair *et al*., 2014; Huizinga *et al*., 2014; Sanders *et al*., 2014). ICCs are distinctive stellate or tubular myogenic cells of mesodermal origin (Mostafa *et al*., 2010, Sanders *et al*., 2014). The structure of ICCs differs from that of smooth muscle cells in that they contain more mitochondria, caveolae and rough endoplasmic reticulum (Hansen, 2003; Mostafa *et al*., 2010; Blair *et al*., 2014; Sanders *et al*., 2014).

Some ICCs, namely the intramuscular interstitial cells of Cajal (ICC-IM), are scattered discretely through muscle layers whilst others, such as. ICC-MY, form communicating layers in various parts of the wall in all segments of the gut (Mostafa *et al*., 2010; Cheng *et al*., 2013; Huizinga *et al*., 2014)

2.3.1.1 **Myenteric interstitial cells of Cajal**

The ICCs located between the circular and longitudinal muscle layers around the myenteric plexus, termed ICC-MY (Mostafa *et al*., 2010; Blair *et al*., 2014; Huizinga *et al*., 2014; Sanders *et al*., 2014) are the principal cells that pace the contraction of smooth muscle cells (Mostafa *et al*., 2010, Blair *et al*., 2014). The ICC-MY are multipolar in shape (Blair *et al*., 2014) and responsible for the generation of slow-waves (Takayama *et al*., 2002). They extend within the myenteric plexus from the orad corpus around greater curvature to the pyloric sphincter (Ördög *et al*., 1999). The slow-

waves generated by thes ICC-MYs are ultimately relayed to smooth muscle cells via ICC-IM and gap junctions (Daniel *et al*., 1999).

2.3.1.2 Intramuscular interstitial cells of Cajal

ICC-IMs are bipolar (Blair *et al*., 2014) in form and are found scattered within the longitudinal and circular muscle layers of the stomach (Hirst *et al*., 2006). They can be further sub-classified according to location as ICC-CM (within the circular muscle layers) and ICC-LM (within the longitudinal muscle layer (Hanani *et al*., 2005; Lees-Green *et al*., 2011; Sanders *et al*., 2014)). ICC-IM relay the slow-wave potential from the ICC-MY to the SMCs, notably in the distal gastric antrum. Further, they bear mechanoreceptors that enable them to respond to th physical phenomena (Mostafa *et al*., 2010). ICC-IMs are closely associated with the varicosities of efferent vagal nerves in the fundus. Likewise, they associate with afferent vagal nerves to relay mechanoreceptive information from the fundus, body, and antrum to the higher centres (Mostafa *et al*., 2010). Whilst ICC-IMs can themselves generate a slow-wave, the change in myogenic cell potential alone is insufficient to depolarize neighbouring SMCs. However, the slow-wave that is generated by the meshwork of ICC-MY and propagates through the tissues reinforces this change in potential to a sufficient level to depolarise the adjacent SMCs.

2.3.1.3 Septal interstitial cells of Cajal

These cells are found within the septa between circular muscle bundles and carry the slow-waves generated by the ICC-MY deep into the circular muscle (Mostafa *et al*., 2010).

The type of ICC present in the stomach wall determines the type of contraction in that wall segment. The types of ICCs present in various anatomical regions of the stomach are summarised in Table 1.

Table 1.Types of ICCs present in the human stomach and their location. ICC-IM - Intramuscular ICC, ICC-MY - Myenteric ICC, ICC-SEP - septal ICC (Adapted from Berridge, 2008).

REGION	TYPE OF ICCs
Fundus	ICC-IM, ICC-SEP
Corpus	ICC-MY, ICC-IM, ICC-SEP
Antrum	ICC-MY, ICC-IM, ICC-SEP
Pylorus	ICC-MY, ICC-IM, ICC-SEP

Isolated regions of the stomach have different slow-wave frequencies (Hashitani *et al*., 2005). For example, the isolated corpus exhibits a slow-wave that has a frequency of 4.5 waves per minute while the antrum generates 3 waves per minute. However, when coupled together, the motor activities are synchronized (Hashitani *et al*., 2005), and the frequency of slow-waves in the antrum and in the corpus are the same (Rhee *et al*., 2011).

The maximum amplitude (Lammers *et al*., 2009) and most significant inherent frequency of the slow-waves (Hashitani *et al*., 2005; Lammers *et al*., 2009) is observed at a point in the mid corpus around 14.5 cm orad to the pylorus along the greater curvature (Pal *et al*., 2004) and hence this location is known as the 'gastric pacemaker' (Pal *et al*., 2004; Imai *et al*., 2013). The first cellular recordings of gastric slow-wave activity from SMCs were made in 1954 (Szurszewski, 1997). Van Helden *et al*. (2010) demonstrated a delay in the propagation of slow-waves (Figure 5), proving that slow-waves are generated at the pacemaker region and propagates to other sites of the stomach.

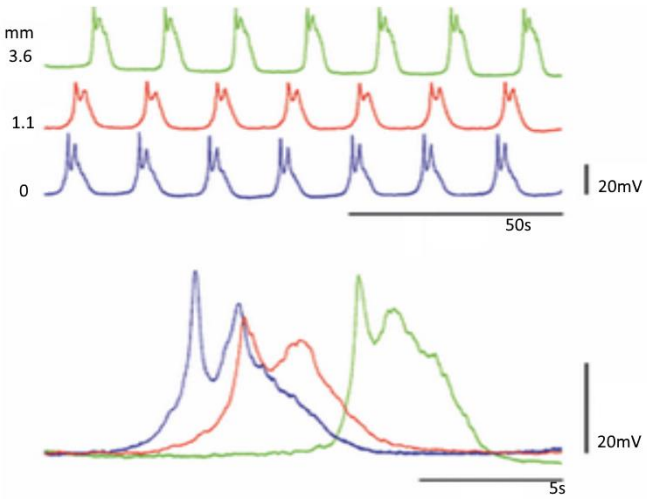

Figure 5. Slow-waves recorded from a sheet of the circular smooth muscle of the guinea pig' distal gastric antrum using intracellular microelectrodes exhibits slow-wave propagation delays. The electrodes were placed at three different sites located transversely (i.e. oro-anally) with a separation of 1.1 and 3.6 mm from the most orally located electrode. The blue peak indicates the slow-wave from the most orad electrode; the green indicates the most caudad electrode; the orange indicates the intermediate electrode (Adapted from Van Helden *et al.*, 2010).

2.3.2 The extrinsic and intrinsic neural control mechanism

Elements of the autonomic nervous system (ANS) and the central nervous system (CNS) can influence gastric contractile activity. In general, elements of the sympathetic nervous system (SNS) inhibit gastric contractile activity (Campbell, 1966), whilst elements of the parasympathetic nervous system promote it. The former acts via the splanchnic nerves (Brookes *et al*., 2013) and the latter via the vagus nerve (Furness, 2009). The afferent elements of the vagus nerve can influence both phasic and tonic contractile activity (Sanger *et al*., 2002), whilst efferent elements can relay mechanoreceptor information to the CNS. Vagal motor control is the principal arbiter of gastric tone. Hence vagotomy generates an increase in fundal tone (Anvari *et al*., 2000) and can influence the amplitude of phasic contraction in the distal stomach (Gleysteen *et al*., 1988). Again, vagotomy may influence pyloric closure. Hence truncal vagotomy suppresses antral contractions and increases pyloric contraction during both the interdigestive and the postprandial state (Mochiki *et al*., 2001).

The enteric nervous system (ENS) is part of the ANS that regulates the digestive functions of the gastrointestinal tract. It receives sensory input from the gastrointestinal tract and efferent input from the brain and other parts of the ANS to regulate digestion. The ENS is "a collection of neurons

in the gastrointestinal tract, that constitutes the brain of the gut and can function independently of the central nervous system" (Raj *et al*., 1996). The ENS consists of 200–600 million neurons, distributed in many thousands of small ganglia (Schemann, 2005). There are three different types of neurons in the ENS: efferent (motor), afferent (sensory), and interneurons. Efferent nerves carry messages from the CNS and are responsible for peristaltic movements of the gastric wall. Afferent nerves react to what a person eats and drinks and carries messages away from the digestive tract and towards the CNS. The ENS can also control exocrine and endocrine secretions and micro-circulation of the gastrointestinal tract (Bornstein *et al*., 2004, Furness *et al*., 2014).

2.3.3 The hormonal control system in the stomach

The gastric cells (G cells), the delta cells (D cells), enterochromaffin-like cells (ECL) and enterochromaffin cells (EC) found in the mucosal layer of the gastric wall are neuroendocrine or enteroendocrine cells of the stomach (Gunawardene *et al*., 2011). They are located around the base of the gastric glands and secrete several different types of hormones and paracrine messengers. These, along with other messenger chemicals produced in other regions of the gut, can regulate gastric motility and other aspects of digestion (Saladin, 2007, Marieb *et al*., 2013). Since this is not the focus of this thesis, a detailed discussion on gastric glands or hormones will not be presented.

2.4 Types of stomach wall contraction

The stomach wall exhibits two types of contraction; phasic and tonic contractions. Examples are phasic antral propagating contractions (APCs), tonic generalized pyloric contractions and global tonic contractions.

2.4.1 Phasic contractions

Phasic contractions are relatively short-lived and can be superimposed on tonic contraction (Kelly, 1980). The phasic contractions on the stomach wall (known as APCs) are initiated at the pacemaker region situated 14.4 cm from the pylorus (Pal *et al*., 2004) and travel distally, progressively narrowing the gastric lumen. They result from the synchronised contraction of the circular and longitudinal muscle layers (Feher, 2012).

The frequencies of phasic contractile patterns of the stomach vary during the fed state (postprandial) and the inter meal interval. APCs in the inter-meal interval occurs in runs (Deloose *et al*., 2012) and are known as migrating motor complexes (MMC) (Takahashi and Toku, 2012). They are inhibited following a meal. The focus of the thesis is the contractile activity of the stomach wall during the postprandial period; MMC are not discussed here, but a discussion on them can be found in Appendix 1.C.

2.4.2 Tonic contractions

Tonic contraction controls the resistance of a muscle to stretch (Indireshkumar *et al*., 2000), i.e. compliance (Lentle *et al*., 2013). The tone has been further classified as tetanic (fused phasic tone) or specific (Cristensen and Gregersen, 2000; Indireshkumar *et al*., 2000). However, recent video-spatiotemporal mapping of the fundal wall indicates that fundic contraction is patchy, rhythmic and alternates locally (Lentle *et al*., 2016).

The type of contractions present in each segment of the stomach are essential to model the gastric geometry, which is the boundary of the flow regime. The following section details the type of contraction present in each segment of the stomach.

2.4.3 Type of contraction present in the gastric fundus

Neurogenic (Cannon, 1898) or myogenic (Sanders *et al.*, 2014) triggering mechanism can activate the fundic muscle tissues. The contractile activity present in the fundus is the myogenic tone (Gregersen and Christensen, 2000), which is modulated by neurogenic and mechanical stimuli.

The postprandial decrease in tone termed 'receptive relaxation' (Lind *et al*., 1961b) causes a generalized reduction of tone, enabling the lumen to accommodate incoming food with little increase in intraluminal pressure (Azpiroz and Malagelada, 1985). A subsequent vagally-induced (Troncon *et al*., 1994) increase in the tone causes the fundal contents to be displaced into the lower stomach (Janssen *et al*., 2011).

As noted above, ICC-MYs are absent in the human fundus; thus, slow-wave mediated peristaltic motion does not occur in the gastric fundus (Hanani *et al*., 2005; Sanders *et al*., 2014). However, the cyclic mechanoreceptive responses of groups of ICC-IMs, present in the fundus may act as local sensors to trigger fundic motor activity (Powley *et al*., 2008). As mentioned, vagal afferent

and efferent innervation are the principal arbitrators of fundic tone. Hence vagotomy causes a generalised increase in the tone of the gastric fundus (Cannon, 1898).

Rhythmic tonic contractions detected in a rat stomach maintained *in vitro* (Lentle *et al*., 2016) were similar to the rhythmic variations in intragastric pressure observed in dogs and human subjects (Azpiroz and Malagelada, 1985). This observation indicates that fundic oscillations play a significant role in maintaining intragastric pressure. This is important in our work as we try to look at the importance of the intragastric pressure gradient in the gastric process.

2.4.4 Type of contraction present in the gastric corpus and the antrum

Displacement of digesta from the gastric reservoir regions to the antrum is mediated by the tonic contractions present in the fundus and the phasic (peristaltic wave) antral propagating contractions (APCs). Peristaltic contractions present in the corpus (Schulze, 2006c), stimulated by cholinergic enteric neurones, can produce a small circular constriction that can push the gastric content. However, this contractile activity is insufficient to mix the entire digesta but mixes and evacuates only the superficial layer of the digesta, which is diluted by gastric juice (Ehrlein and Schemann, 2005).

APCs originate at the pacemaker region and expand radially, then axially, to travel towards and through the antrum (Lammers *et al*., 2009) and terminate 3 cm orad to the pylorus (Pal *et al*., 2004). The tapering profile of the distal antrum causes the degree of lumen constriction to increase as the APC travels distally, becoming maximal just proximal to the pylorus. However, it does not appear to entirely occlude the lumen at any point (Janssen *et al*., 2011).

A real-time ultrasound study in human subjects (Brown *et al*., 1993) showed that the overall shape of the antrum changes according to the gastric content volume. Hence the form of the antrum becomes less tubular and more funnel-shaped as its volume increases. The change to a more tubular form on emptying may aid the transit of solids in the sinus to the gastric outlet.

2.4.5 Type of contraction present in the pylorus

Like other sphincters, the pyloric sphincter exhibits sustained myogenic tone (Cristensen *et al*., 2000), which provides a baseline resistance to the gastric flow (Keinke *et al*., 1983). The connective tissue between the circular muscle of the pylorus and the duodenum prevents the

propagation of electrical slow-wave potentials from the stomach to the duodenum and vice versa (Ramkumar and Schulze, 2005).

The pyloric sphincter exhibits different contractile patterns during the postprandial period and inter meal interval. It opens and closes briefly and squirts a small amount of chyme during the postprandial period; however, it remains open during the inter meal interval. The gradated action of the pylorus may promote the fragmentation of food particles by direct compression and by shear, the selective retention of larger particles by graded retropulsion and the effective advectional mixing of chyme (Dillard *et al*., 2007). It also aids in controlling the rate of gastric emptying (Houghton *et al*., 1988). While pyloric contraction frequency generally matches that of APCs, the two cycles are not under the same local means of control (Indireshkumar *et al*., 2000; Pal *et al*., 2004; Kong *et al*., 2008) and may vary independently (Houghton *et al*., 1988).

Pyloric dominance and the virtual impactor phenomenon

When in synchrony, pyloric contraction commences when an APC is propagated within 2-3 cm of the pylorus. As noted above, such synchrony occurs during the postprandial period and is termed pyloric dominance (Indireshkumar *et al*., 2000; Pal *et al*., 2004; Kong *et al*., 2008). This action causes any distal flow of the gastric contents to be retro-pulsed against a closed pylorus into the gastric lumen. This action is similar to that of a virtual impactor that causes the larger/denser particles of the digesta to be retropulsed farther than finer or less dense particles (Lentle *et al*., 2008; Lentle *et al*., 2010).

The velocity of retropulsion from a closed pylorus that appeared on CFD is around 7.4 mm/s (Pal *et al*., 2004). This may generate a shear force that promotes mixing and the fragmentation of particulate matter. However, these shear forces are likely to be lower than those generated during outflow and backflow through a narrowed pylorus, as the flow is not acting against a closed surface.

2.4.6 Type of contraction present in the duodenum

The duodenum exhibits peristaltic contractions that commence at the duodenal bulb (Ehrlein and Schemann, 2005). The duodenum exhibits both myogenic (segmentation and pendular contractions) and neurogenic (peristaltic) contractions (Loubens *et al*., 2013).

The fed state motor patterns of the duodenum are susceptible to modification due to the nutrient content of the contained chyme (Katschinski *et al*., 1996; Schulze, 2006b). An infusion of isotonic saline traverses the duodenum quickly, compared with hypertonic saline that elicits tonic contraction that can almost occlude the lumen (Schulze 2006). Duodenal tone may increase following the arrival of certain nutrients and causing the mean duodenal diameter to reduce (Rao *et al*., 1996) a phenomena known as the duodenal brake. Similarly, changes may be induced by various hormones (Lee *et al*., 1980), such as. motilin, gastrin, cholecystokinin (CCK), secretin (Konturek *et al*., 1986). The overall effect of these changes is to slow the rate of transit of chyme through the proximal small intestine to increase the residence time and extend the duration of digestion and absorption (Bueno *et al*., 1975).

The stomach wall concerted contractile activity enables storage of ingesta, mixing of ingesta with gastric juices, physical and chemical digestion of ingested food and absorption of a limited number of nutrient (Thomas, 2006). Details of stomach functions can be found in Appendix 1.B.

The functionality of the stomach is very much dependent on the contractile activity of each anatomic region. The motor activities of the distal stomach move the gastric content between and within various anatomical regions, resulting in the mechanical and chemical digestion process. These digestion processes change the digesta into a slurry-like chyme that moves into the proximal part of the small intestine. The next two-sections briefly discuss the functions of the stomach and the properties of digesta. This information would be helpful to determine fluid parameters like viscosity while simulating the gastric flow.

2.5 Functions of the stomach

The stomach is responsible for storing the ingesta, mixing and trituration of ingested food with gastric enzymes and slowly emptying the chyme to the small intestine (Schulze, 2006).

2.5.1 Storage

The proximal stomach consists of the fundus, and the proximal body acts as a reservoir for the masticated food and helps in the orderly progression of this stored food to the distal stomach. When the first bolus enters the stomach, it slides to the lesser curvature region of the stomach and the next bolus stack over the first bolus. As the amount of food increases, the first bolus is pushed

toward the greater curvature region and may even get shifted orad and spread them into thin layers (Schulze, 2006).

The tone of the proximal stomach wall reduces following the consumption of a meal via a change in the vagally mediated motor pattern known as accommodation (Cannon, 1898). The lowering of the tone increases the compliance of the walls so that more significant volumes may be accommodated without undue increase in lumen pressure. A subsequent selective increase in fundal tone promotes outflow (Lind *et al*., 1961b, Azpiroz and Malagelada, 1985).

2.5.2 Mixing and digestion

The motor activities of the distal stomach move the gastric content between and within various anatomic regions of the gastric lumen that triturate the ingested food (mechanical/physical digestion) and mix it with the gastric enzymes (chemical digestion). The resultant slurry-like chyme get emptied into the proximal small intestine called the duodenum. During trituration, solids and fat globules are dispersed in the gastric juices to mediate chemical breakdown, and this process reduces the size of solids and fat, changes the pH or osmolality and viscosity of liquids and is essential for the bioavailability of nutrients.

2.5.3 Sieving

The stomach selectively retains larger particles of digesta, which are greater than 1 mm in size and more or less dense than water (Meyer *et al*., 1981) whilst allowing the liquid phase to exit. Gastric sieving may result from a combination of the action of the pylorus (i.e. larger/heavier particles undergo greater retropulsion by the retropulsive jet generated by pyloric contraction) and subsequent distal carriage resulting from the coordinated actions of the component segments (Janssen *et al*., 2011). The pyloric orifice diameter plays a significant role in gastric sieving (Shahidullah, 1975).

Regarding the general action of the other components, the vorticeal flow of fluid around the axial retropulsive jet may convey particles with a density similar to water (Meyer *et al*., 1981) towards the pylorus whilst particles heavier than water sink below (Schulze, 2006a) and fat and other buoyant materials float (Brown *et al*., 1993) (Figure 6). Subsequently, the decrease in gastric volume and the consequent change in profile may allow the upper and lower positions of the APC to sweep both toward the pylorus directly.

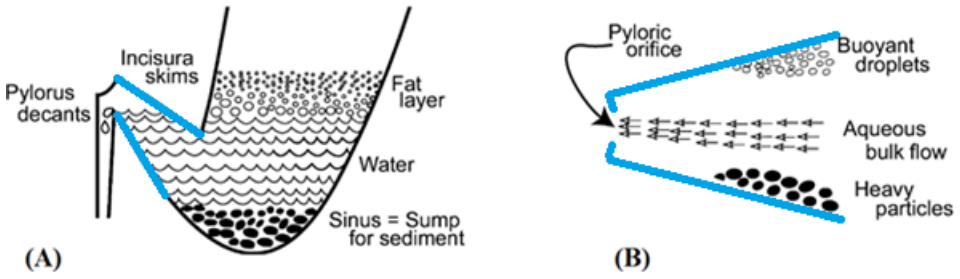

Figure 6. Phase discrimination of the gastric content. (A) Layering of contents according to their density. (B) Deflection of particles through the inverted funnel-shaped distal antrum indicates that buoyant particle and denser particles are away from the pyloric opening (Adapted from Schulze, 2006).

However, the transit of fats is compounded by their poor water solubility and tendency to adhere to the solid food and thus get empty at the end of the gastric cycle (Hasler, 2003).

A further mechanism is the physical sieving of finer particulate material through a bridge of impacted larger particles (Janssen *et al*., 2011). Such bridging may occur postprandially when coarser and more viscous material is driven into the distal stomach.

2.5.4 Gastric emptying

Gastric emptying is the process that determines how fast the chyme is delivered to the small intestine in the postprandial state, and this process is a resultant of coordinated motor activity of the stomach and the duodenum (Hausken *et al*., 1992).

The gastric metabolic load, neural regulatory mechanisms and hormonal influences all play a role in gastric emptying (Hellström PM *et al*., 2006). However, the factor mediating gastric emptying relevant to this thesis is the trans-gastric pressure gradient (TGPG).

The TGPG is established between the tonally contracting fundus (Azpiroz *et al*., 1984), and the resisting small intestinal brake (Shahidullah *et al*., 1975; Schulze-Delrieu, 1992), is vital in gastric emptying of liquids (Okike and Kelly, 1977; Kelly, 1980b). However, its role in emptying solid food has been questioned previously (Wilbur, 1973).

Again there has been an ongoing debate regarding the relative contributions of contractile activity (APC) in the body and antrum. However, relative contributions of forces, from the 'pressure pump'

of fundal tone and the 'peristaltic pump' of APCs (Indireshkumar *et al*., 2000b, Kwiatek *et al*., 2009) in regulating gastric emptying have not been quantified.

The rate of gastric emptying is directly proportional to gastric volume (Hunt and Spurrell, 1951). However, this relationship is not linear. In a real-time ultrasound study of human subjects, it was found that the gastric emptying of liquid was log-linear with a mean half-life of 22.0 ± 2.5 min (Bateman and Whittingham, 1982). Hormonal reflexes can also modulate this rate.

Pappas *et al*. (1986) conducted a study to determine the physiological role of cholecystokinin in the inhibition of gastric emptying. Four dogs were administrated CCK intravenously to simulate the physiological condition. By monitoring the gastric emptying of the volume, they proved that CCK is a potent inhibitor of gastric emptying. They observed that penta gastrin and heptadeca peptide gastrin also inhibited gastric emptying, but the dosage required was much higher. No difference was observed between men and women in postprandial antral motility parameters or gastric emptying (Hutson *et al*., 1989; Tougas *et al*., 2000).

2.6 Properties of digesta

As mentioned earlier, mechanical and chemical digestive processes change the structure and composition of food (Kozu *et al*., 2010), and the physical properties of digesta may influence mixing, the efficiency of digestion, and absorption (Lentle *et al*., 2008).

The digesta in the proximal stomach is a suspension of particulate matter in a fluid phase (Takahashi *et al*., 2004; Dikeman *et al*., 2007). The solid particle concentration in the digesta is generally measured as the dry matter concentration (DMC) by weight, and a high DMC increases the viscosity of digesta (Lentle *et al*., 2008), making it viscous and non-Newtonian (Takahashi *et al*., 2004; Dikeman *et al*., 2007).

Lentle *et al*. (2010) proposed that the presence of macromolecules increase the apparent viscosity and exhibit shear thinning behaviour. The apparent viscosity of the digesta largely depends on the ratio of the volume fraction (denoted by ϕ) of the particulate matter of digesta to the maximum packing fraction (denoted by ϕ_m) as shown in Figure 7 (Krieger *et al*., 1959). The volume fraction(ϕ) is the volume of a particular constituent divided by the volume of all constituent of

that mixture. The maximum packing fraction is the maximum number of constituent particle in a given volume.

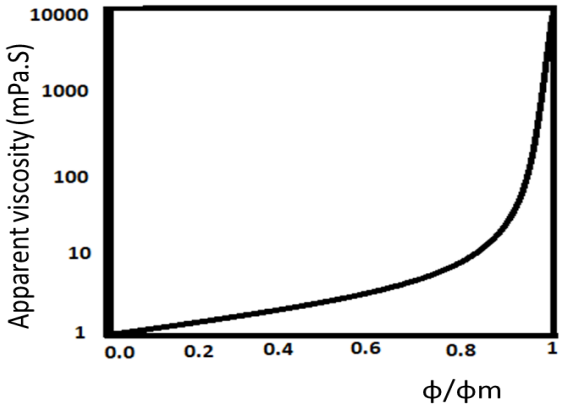

Figure 7. Relationship between apparent viscosity and solid volume fraction relative to the maximum packaging fraction (Adapted from Krieger *et al*., 1959).

If the digesta is modelled as a suspension of particles in a liquid phase, the liquid phase viscosity stays constant; however, the viscosity of the suspension as a whole depends on the volume fraction that changes in time due to the sieving action of the stomach. When the gastric process happens, the sieving of gastric content happens in many ways. The larger and denser particle may be sieved out by pylorus, and another critical sieving process called bridging of particles also happen during the gastric process. Here, the larger particles get closer and smaller particles to get trapped in it, which acts as a sieve.

The whole digesta exhibits a shear-thinning behaviour (apparent viscosity decreases with increased shear rate), and this characteristic is known as pseudoelasticity (Barnes, 1989). Even though a high viscosity meal may increase the apparent viscosity of the gastric contents, rapid intragastric dilution minimalizes this effect (Kong and Singh, 2008). A study conducted by Marciani *et al*. (2000) reported that the zero-shear viscosity of a meal (containing 1.5 g locust bean gum per 100 g) fell from 11 - 2 Pa·s immediately after ingestion, and decreased to 0.3 Pa·s after 30 min.

Also in another study the liquid phase of the caecal digesta of pigs (1.3 ± 0.2 mPa.s) (Takahashi and Sakata, 2004) and ileal digesta of dogs (6.5 – 9.5 mPa.s) (Dikeman *et al*., 2007) showed low viscosities and were Newtonian. This finding justifies the usage of a Newtonian fluid to simulate the gastric flow in this thesis.

Chapter 3: Gastric Modeling

3.1 An overview

Early gastric studies were conducted *in vivo* (within the living body) of a rodent, canine or porcine (Yoo *et al*., 2006) to understand digestion as conducting a human trial is typically resource intense and the ethical aspect is often challenging. Computer-controlled mechanical models were developed to mimic a human gastric system (Aoki *et al*., 1992; Molly *et al*., 1994; Blanquet *et al*., 2004; Yoo *et al*., 2006). These *in vitro* mechanical models simulate the gastric environment and fluid dynamics but can barely mimic the real gastric geometry and motility.

The simulator of the human intestinal microbial ecosystem (SHIME) developed by Molly *et al*. (1994), was a five-step reactor to simulate the gastro-intestinal microbial ecosystem. They used two reactors to mimic the small intestine and three reactors to mimic the large intestine and added another six reactors to simulate the stomach (Molly *et al*., 1996). An *in vitro* GI tract model to investigate the dissolution of drugs in the GI tract (Aoki *et al*., 1992) and for simulating Bucco-gastric digestion to assess the physical and chemical changes of food (Hoebler *et al*., 2002) have been developed. A multi-compartmental (stomach, duodenum, jejunum, and ileum), the computer-controlled *in vitro* gastric system was developed, known as the TNO model (Minekus, 1995).

Mattila *et al*. (1999) used the TNO model and SHIME reactor and found some probiotics with known clinical survival could not survive TNO and found conflicting results in SHIME for feeding treatments with trivial changes. A potential weakness of these models is that they simulate the gastric environment but not the gastric muscle motility patterns, which is vital in the physical digestion of ingested food.

To overcome the limitations of *in vivo* and *in vitro* systems, researchers adopted computational fluid dynamic technology to create virtual human GI systems (Pal *et al*., 2004; Cheng *et al*., 2007; Liao *et al*., 2008; Yassi *et al*., 2009; Kozu *et al*., 2010; Maria J Ferrua *et al*., 2011; Xue *et al*., 2012; Imai *et al*., 2013; Miyagawa *et al*., 2016). These are capable of mimicking the contractile activities of the GI tract and help to understand the gastric process of physical digestion and fluid dynamics within the GI tract. The advantage of such a system is that it reduces the cost and time

involved in *in vivo* trials and capable of introducing non-existing conditions such as gastroparesis. Usually, parameters in use are adaptable.

3.2 Published computational fluid dynamic gastric models

A complete gastric compartmental model that incorporates all different motility patterns is yet to develop; however, a detailed list of available published *in silico* gastric models is given in Table 2 and most relent works are discussed in the following section.

Table 2. Published works on gastric models.

Title of the paper	Numerical method used	Aim	Reference
Antral recirculation in the stomach during gastric mixing	Free-surface	To determine the effect of different postures on gastric flow velocity and antral recirculation	(Imai *et al*., 2013)
Granular flow in the stomach	CFD–FVM	To explore the multiphase mixture (solid and liquid) model	(Xue *et al*., 2012)
Computational modelling of gastric digestion and the role of food material properties	CFD–FVM	To determine the gastric fluid flow velocity, pressure and effect of viscosity on particle shear	(Ferrua *et al*., 2011)
Modelling intragastric fluid motions induced by human peristalsis	CFD–FVM	Explore the shear force induced by peristaltic flow	(Kozu *et al*., 2010)
Modelling the mechanical function of the human gastroesophageal junction	Finite element method (FEM)	To determine the intraluminal pressure values (pressure inside the junction) due to the muscle contraction	(Yassi *et al*., 2009)
Gastric flow and mixing	Lattice-Boltzmann Method (LBM)	To understand the gastric motility pattern	(Pal *et al*., 2004)
Simulation of anatomically realistic gastric slow-wave activity	FEM	To predict the slow-wave activity within the stomach	(Cheng *et al*., 2007)
Relationship between gastric motility and liquid mixing in the stomach	LBM	To establish the relation between gastric motility and the mixing of liquid food in the stomach.	(Miyagawa *et al*., 2016)
Peristaltic transport of a particulate suspension in the small intestine	Smoothed Particle Hydrodynamics (SPH) and Discrete Element Method (DEM)	Transient behaviour of chyme in the duodenum using a suspension of rigid particles in a viscous Newtonian fluid.	(Sinnott *et al*., 2017)

In general, all *in silico* gastric models developed so far can be grouped as either an antral model or a pyloro-duodenal junction model. The antral models simulate the motility of the gastric chamber orad to the pyloric sphincter, whereas the pyloro-duodenal model deals with simplified anatomy and motility patterns of the pyloric sphincter and duodenum. A detailed discussion on crucial *in silico* gastric models are given in the following section

Although several works have published models regarding the action of the stomach, the work by Pal *et al*. in 2004 is considered the substantial first mathematical model of the gastric antrum. Subsequent works have published modified versions of this work (Pal *et al*., 2004; Ferrua *et al*., 2010; Samer *et al*., 2019; Ishida *et al*., 2019; Li *et al*., 2021).

The first and detailed 2D model of the stomach was developed using the lattice-Boltzmann method (LBM) to study the flow and mixing in the human stomach (Pal *et al*., 2004). The stomach geometry was modelled from magnetic resonance imaging (MRI) images and used open and closed pyloric states (Figure 8). However, this work did not incorporate the complex pyloric anatomy or the TGPG but focused on the stomach's APC-induced flow patterns.

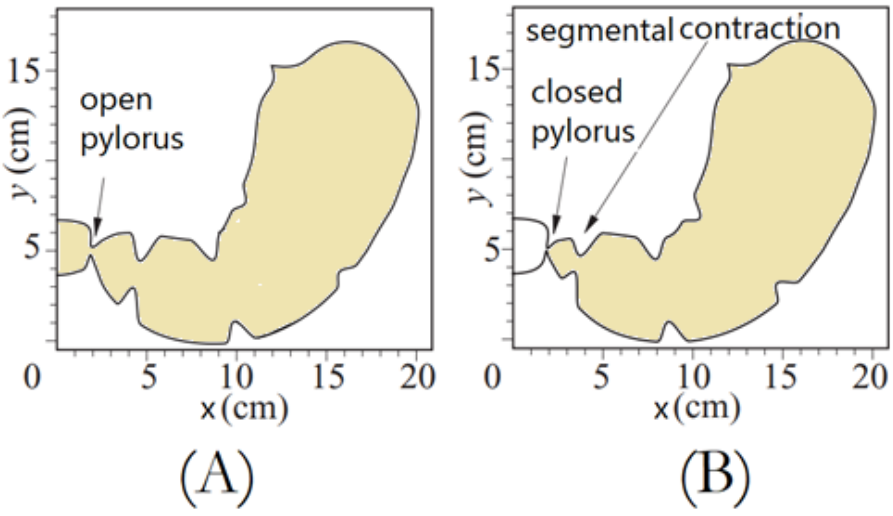

Figure 8. Gastric geometry created from MRI images by Pal *et al*. (A) open pyloric state and (B) closed pyloric state (Adapted from Pal *et al*., 2004).

This study found that mixing occurs through a combination of circulatory motions and jets. The jets propagate in the opposite direction to the antral propagating contraction (APC) waves. A well-

defined 'zone of mixing' was observed in the antrum. It was noticed that multiple and narrower APCs enhanced the circulatory motions and the pressure waves in the distal antrum had a much lower pressure amplitude than manometric data. However, the high manometric pressure value could result from direct contact of the catheter with the gastric wall. This work concludes that the APCs are central to gastric mixing and gastric emptying.

Ferrua *et al*. (2010) developed a 3D model of an average-sized human stomach and incorporated the motility pattern of the stomach wall during digestion (Figure 9). They used it to characterize the fluid dynamics of gastric contents of different viscosities using the software Fluent™. This can be considered as a 3D extension of the work done by Pal *et al*. (2004).

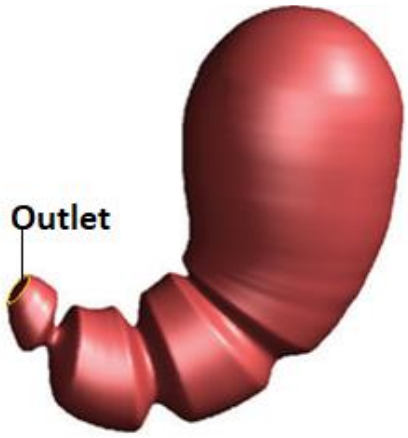

Figure 9. 3D gastric geometry developed by Ferrua *et al*. (Adapted from Ferrua *et al*., 2010).

The APC waves in this work introduced up to 80% relative occlusion to the geometry. The flow field within the model was strongly dependent on gastric contents' viscosity, and they noticed that the retropulsive Jet-like motion and eddy structures were significantly diminished by increasing the viscosity. Even though this work agrees with Pal *et al*. (2004) on the flow patterns, and open pyloric ring with a diameter of 1.1 cm used in the simulation is physiologically incorrect. Neither the fundic motility nor the trans gastric pressure gradient is considered in this work.

Samer *et al*. (2019) modelled a stomach that consists of an axisymmetric tube of varying diameter to represent the antrum and the other end to represent the pylorus (Figure 10).

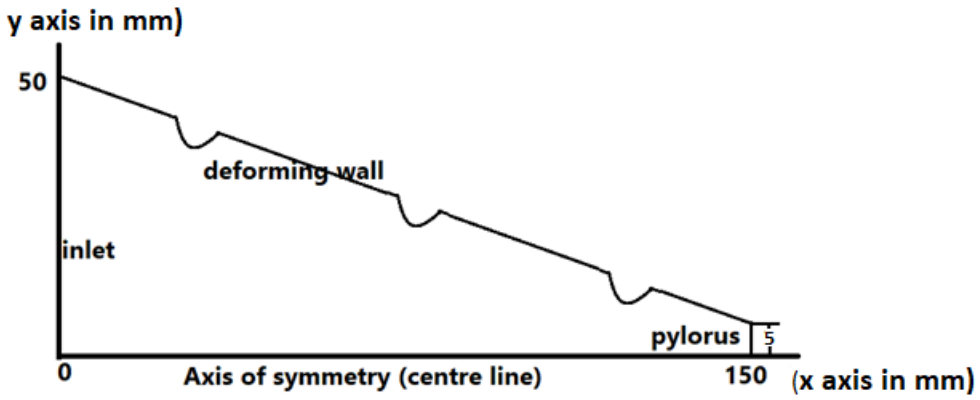

Figure 10. Computational domain for the axisymmetric conical model of the antrum created by Samer *et al*. (Adapted from Samer *et al*., 2019).

In this work, APCs are modelled as travelling waves that deform the computational mesh using an open-source code called OpenFOAM. A set of parameters such as the fluid viscosity, wave speed, wave width, and maximum relative occlusion were varied. The effect of these parameters on the retropulsive jet and the recirculation was investigated. According to this study, both of these flow features contribute to the mixing and digestion process, which is in line with the findings of Pal *et al*.(2004) and Ferrua *et al*. (2010). This work found that the flow velocity decreased, and the jet length increased as the viscosity increased. Also, the mixing efficiency increased as the relative occlusion due to APC increased, and the viscosity or wave width decreased. However, it is noteworthy that they did not incorporate the *J*-shaped stomach anatomy, fundic cycle or pyloric structure and cycle. Moreover, they had a permanently open pylorus and simulation was limited to the antrum.

Ishida *et al*. (2019) showed how coordination between the pyloric closure and antral contraction affects the emptying of liquid contents. They numerically simulated fluid dynamics using an anatomically realistic 3D gastrointestinal geometry.

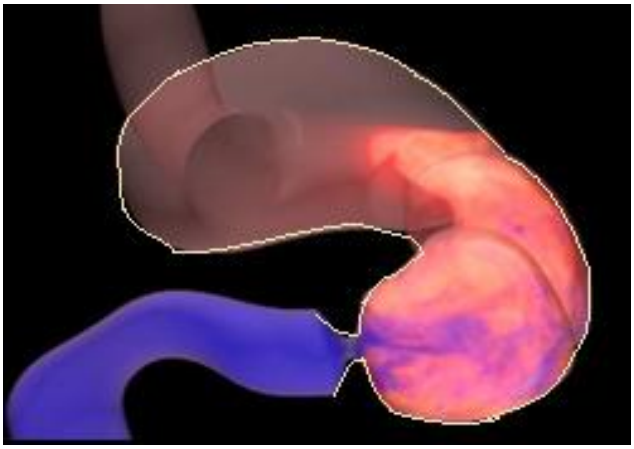

Figure 11. 3D gastric geometry used by Ishida *et al*. Gastric chamber is outlined with yellow lines (Adapted from Ishida *et al*., 2019).

The emptying rate increased from 8-10 mL to 10–30 mL per minute when the pylorus was in a constant open state. Instantaneous inflow from the duodenum to the antrum occurred during antral relaxation. Rapid emptying occurred when the pylorus began to open during the terminal antral contraction, and the emptying rate was negative if the pylorus only opened during the antral relaxation phase. Their results also showed that impaired coordination between antral contraction and pyloric closure could result in delayed or rapid gastric emptying. Another interesting observation from this three-dimensional model was that a road-like region appears from the pylorus to the proximal antrum with highly viscous contents but on the greater curvature side. In low-viscosity contents, the road-like region disappears, as the gastric contents are mixed homogeneously in few minutes. This observation disagrees with Pal *et al*.(2006) on the formation of magenstrasse. This work is vital as this shows the importance of incorporating the pyloric cycle in the simulation, even though the pyloric anatomy and intragastric pressure gradient were not included in this work.

A recent work by Li *et al*.(2021) developed a computational fluid dynamics (CFD) model of the stomach to study liquid food and gastric juice mixing. The gastric juice secretion is modelled as sources of mass and hydrogen ions continually added into the stomach lumen. Gastric emptying rates of different foods are determined according to their calorie content. This work looked at the role of antral contraction, known as the terminal antral contraction (TAC), in mixing gastric juice

with liquid food. The numerical results showed that the TAC significantly increased the averaged kinetic energy in the stomach, and the maximum velocity nearly doubled. When a TAC contracts the terminal antrum, the gastric contents were forced away from the pylorus sphincter by a retropulsive jet. The numerical results of this work confirmed the phenomenon observed in previous studies (Pat *et al*.,2004; Ferrua *et al*., 2010).

A single published model of the pyloro-duodenal junction (Dillard *et al*., 2007); examines the effect of the pyloric sphincter anatomy (Figure 12) on gastric flow. However, this model did not incorporate the distinctive pyloric sphincter anatomy or the duodenal bulb. This work also failed to look at the integrated picture of gastric emptying from the stomach to the duodenum. It also failed to incorporate the pyloric motility cycle and the fluctuating duodenal pressure at the duodenum injected by duodenal motility.

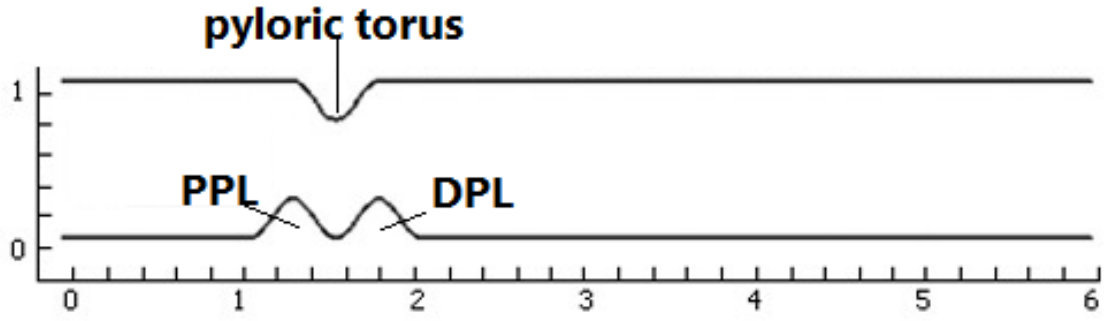

Figure 12. The anatomy of the pyloric sphincter used in Dillard's work shows that it is oversimplified compared to the actual anatomy of a human pyloric sphincter (refer to Figure 2 of this thesis). PPL - proximal pyloric loop, DPL - distal pyloric loop (Adapted from Dillard *et al*., 2007).

It is evident from the published works (Pat *et al*.,2004; Dillard *et al*., 2007; Ferrua *et al*., 2010; Ishida *et al*., 2019) that each of them focused on the stomach and APCs or just the pylorus and failed to look at the integrated effect of the fundic, antral, pyloric and the duodenal motility on digestion. The alternative opening and progressive closing of the pylorus occur 3 times in every gastric cycle, which is not included in any of these models. Gastro-duodenal pressure gradient mediated trans-pyloric flow (Kelly, 1980; Lentle *et al*., 2016) is not studied in any of these models.

The current published pyloro-duodenal junction model assumes a sufficiently open pylorus (Dillard *et al*., 2007).

There is no unified model that incorporates both antral and pyloro-duodenal junction models. So there is a need to unify both models and verify the results. The effect of the fundic pressure cycle, pyloric cycle, and pyloric dominance and the concepts like duodenal brake need to be incorporated into a model, which is the focus of this work.

Chapter 4: Methodology

This model incorporated the entire functional ensemble of the stomach, proximal duodenum, and the contractile characteristics of the gastric body, antrum, pylorus and the duodenal bulb, along with an overall constriction of the duodenal outlet that simulated the operation of the intestinal brake. This work is accomplished in different steps, and the four significant steps involved in modelling the fluid dynamics of the human stomach are (1) collection of correct anatomical gastric data to create the 2Dgastric geometry; (2) implementation of region-specific gastric wall motility patterns; (3) execution of fluid flow in the gastric chamber, pylorus, and the duodenum; (4) analysis and validation of results. It is noteworthy that all physiological information in the physical unit were converted to a lattice unit using a dimensionless system and converted back to the physical unit before analysing the results. This work modelled and simulated the flow within a fed stomach of an adult human male from the published physiological literature. Scaling the gastric geometry to suit the child stomach or female stomach is possible but not attempted in this work.

The baseline gut anatomy was drawn using Microsoft Visio-2017 by incorporating correct anatomical information collected from published papers. Detail discussion of data and geometry creation is discussed in the following section.

4.1 Collection of anatomical and physiological gastric data

The transverse diameters of the body and proximal antrum were based on a geometric gastric model reconstructed from computed tomographic (CT) images of the fundus, body, and antrum of a healthy human male subject (Cheng *et al*., 2007) obtained after the consumption of 473 mL of radio-opaque fluid (Figure 13A). The linear distance from the distal limit of the gastric antrum to the lowest limit of the greater curvature was shorter than that given by Schulze (2006). This difference is because Cheng *et al*., 2007 only recreated the stomach proximal to the pyloric aperture over which slow-wave did not propagate. Even though this work did not provide the complete geometry information required for this work, critical anatomical curvatures given in this

work were used to draw the proximal stomach's line drawing, including the proximal antrum (Figure 13B).

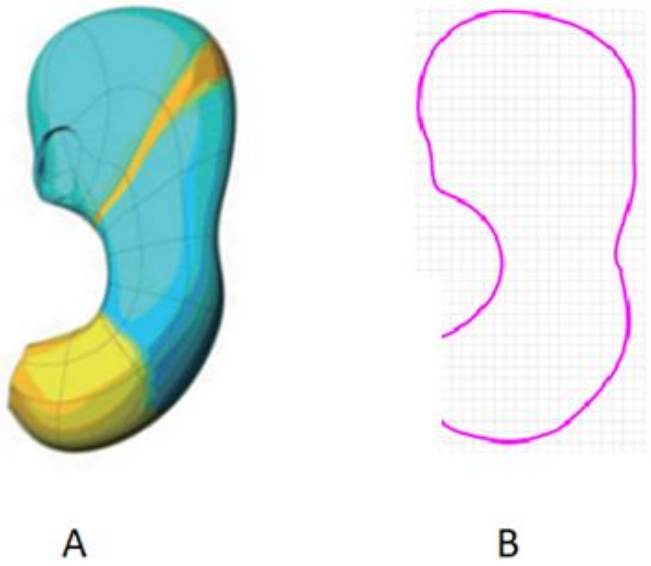

Figure 13. (A) The human stomach geometric model reconstructed from a series of CT images by Cheng *et al*., 2007). (B) Line drawing of the gastric geometry drawn work based on (A).

Information collected from various published papers that were used to create the missing parts of the gastric geometry is as follows:

- A vertical linear distance from the apex of the fundus to the lowest point on the greater curvature of 20 cm (Schulze, 2006).
- A horizontal linear distance from the lowest point oo the greater curvature of the stomach to the distal margin of the pylorus of 8 cm (Schulze, 2006).
- A radius of the hemispherical uppermost border of the fundus of 4 cm (Schulze, 2006).
- A horizontal linear distance from the gastro-oesophageal junction to the greater curvature of 10cm (Schulze, 2006) is the widest part of the stomach.
- The fundic distal limit was marked by a transverse line extending from the gastroesophageal junction to a point 18.2 cm along the greater curvature. This was obtained by adding to the reported distance of the gastric pacemaker from the pyloro-

duodenal junction measured along the greater curvature (14.4 cm) (Pal *et al*., 2004) to 3.8 cm, a published distance along the greater curvature at which the proximal propagation of slow-wave ceases (O'Grady *et al*., 2010).

- The diameter of the pyloric aperture at rest 1.8 cm (Keet Jr, 1962) was taken as the distance from the innermost limit of the torus, which is a 2 cm long dorsal mass of muscle formed by the fusion of the distal pyloric loop and proximal pyloric loop (Keet, 1982). The torus projects vertically 3.7 mm (Schulze-Delrieu and Wall, 1983) into the lumen, to the innermost limit of the ventral indentation formed by the DPL, which projects 3.7mm into the lumen (Schulze-Delrieu *et al*., 1983).
- The sphincteric musculature proximal pyloric loop is reported to be 2-3 cm proximal to the distal pyloric loop (Ramkumar *et al*.,2005). Since this distance is not specified as linear or curvilinear along the pylorus, it was assumed that PPL is at a curvilinear distance of 3 cm from the distal limit of DPL to accommodate the pseudo-diverticulum.
- The maximum diameter of the relaxed pyloric lumen is 5.6 cm, taken at right angles to the longitudinal axis (Keet Jr, 1962). This value is incorporated immediately proximal to the proximal limit of the torus and distal to the distal edge of the PPL.
- The mean diameter of the proximal duodenal bulb is reported to be 5 cm (Kararli, 1995). It was decided to incorporate 5cm of the duodenal bulb and a 3 cm long extension of the duodenal lumen to offer a duodenal brake while pylorus closing.

Based on the details of the pyloric and duodenal geometry given above and the diagram (Figure 14, upper) provided by Ramkumar *et al*. (2005), a series of line drawings were created (Figure 14, lower) to represent an open pylorus and closed pylorus.

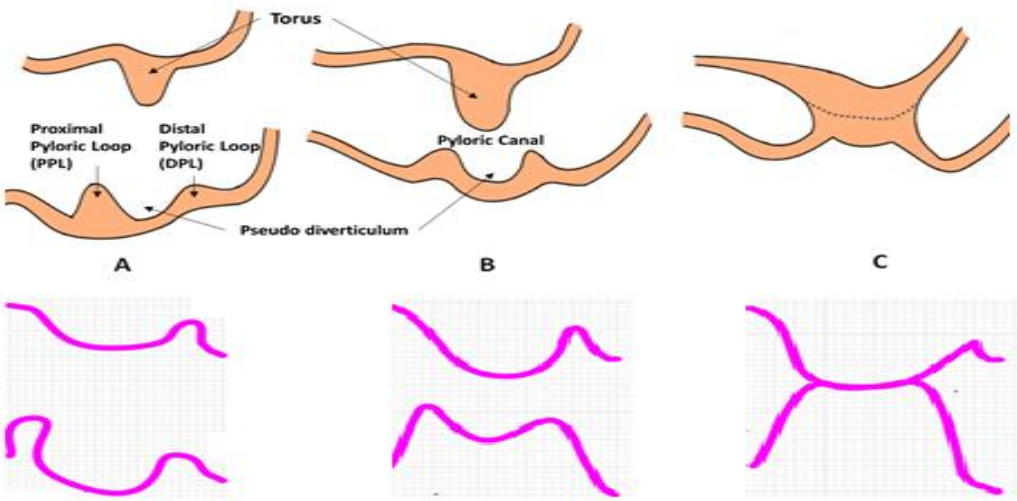

Figure 14. Anatomy of the pylorus at three different stages of a pyloric cycle. Upper: Anatomy of the pylorus (A) Open position (B) contracted pylorus (C) closed pylorus (Adapted from Ramkumar *et al*., 2005). Lower: Line drawing of the anatomy of the pylorus created using Microsoft Visio based on the upper figure. (A) Open Pylorus (B) contracted pylorus. (C) closed pylorus. DPL- distal pyloric loop, PPL - proximal pyloric loop.

A line drawing of the duodenal bulb and 5cm of the proximal duodenum was created (Figure 15) and joined to the relaxed pyloric geometry (Figure 14, lower diagram A). This is then connected to Figure 13 B to complete the gastric geometry used in this work.

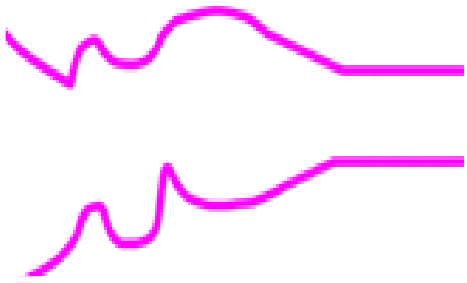

Figure 15. Line drawing of the anatomy of the relaxed pylorus, duodenal bulb and part of proximal duodenum created from the collected data.

A detailed figure with all dimensions and values discussed in this section to create the gastric geometry in its relaxed position (pink colour) and after the first appearance of an APC (grey colour) is given (Figure 16). It is noteworthy that 2.4 cm of the fundic segment is removed to introduce the fundic pressure cycle.

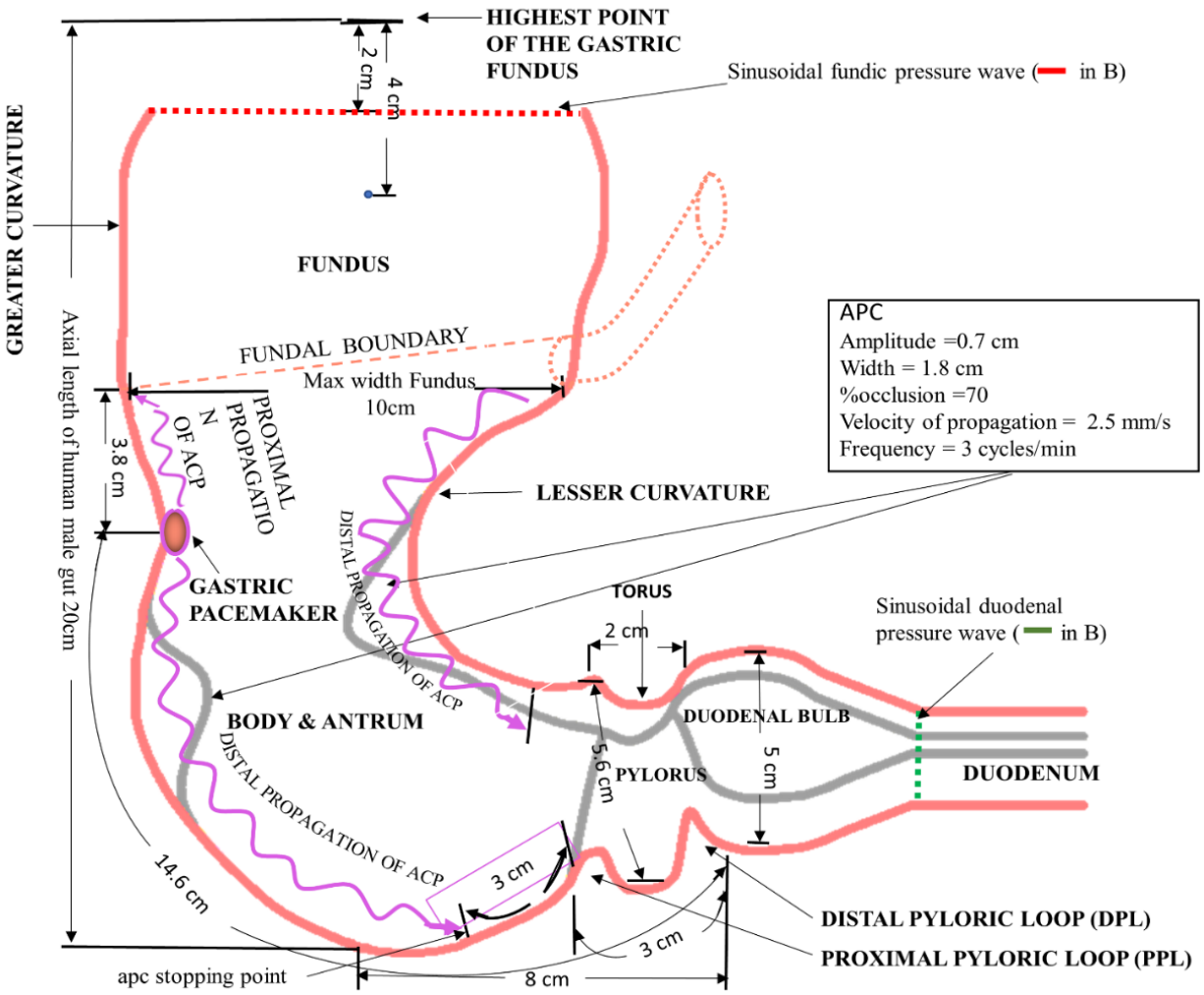

Figure 16. The final stomach geometry developed for this work. The pink contour shows the relaxed gut wall, while the grey line shows the contracted gut wall after 20 s (Note the presence of a single APC in the grey line).

4.2 Conversion of line drawing into a fluid simulation flow boundary

The line drawing created using Microsoft Visio-2016 was then exported to Matlab (Version R2015b) as an image using its image processing toolbox of Matlab. This image then underwent a segmentation process to ease the curve fitting task and avoid recursive data points (i.e., a unique Y coordinate value for each X coordinate value in each segment). We then used the Piecewise Cubic Hermite Interpolating Polynomial (PCHIP) curve fitting method to yield the best curve fitting for the gastric geometry data points.

This segmentation process also helped introduce each segment's motility pattern separately, and these were tested before combining to provide the entire geometric gastric model. For example, the geometry proximal to the pylorus was segmented and recombined first, as shown in Figure 17. The distal antrum, pylorus and duodenum are joined to this in the next stage of geometry development.

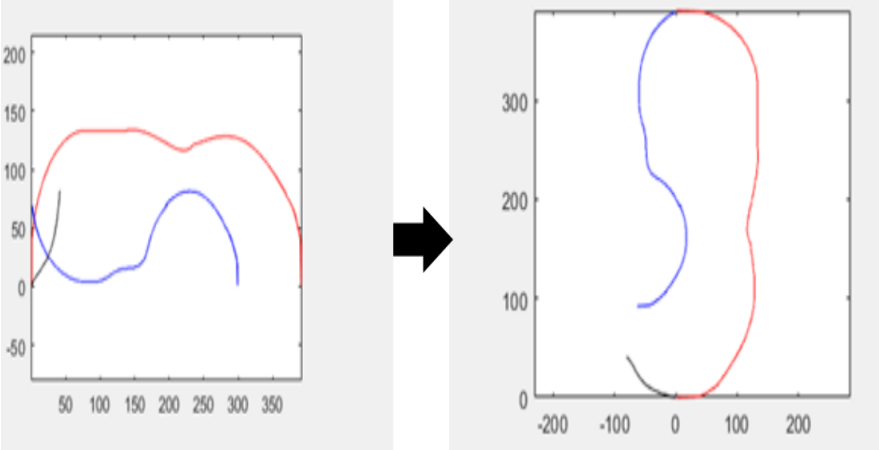

Figure 17. Pictorial representation of segmentation of the gastric geometry and reconstruction sequence without the pylorus and the duodenum. The first figure shows that the gastric geometry is segmented into three pieces (represented in three different colours) and underwent curve fitting. The second figure is the recombined final geometry without distal antrum, pylorus and duodenum.

4.3 Implementation of gastric motility

Two distinct motility patterns were implemented in this work:

- Phasic contractions with a frequency of 3 cycles/minute (Pal et al., 2004) start from the mid-corpus and terminates 3 cm proximal to the pylorus (Janssen *et al*., 2011), known as the antral contraction wave (ACW) or antral propagating contractions.
- The pyloric contraction has a frequency of 3cycles/minute (Edwards, 1961; Rovelstad, 1976; Schulze-Delrieu and Shirazi, 1983) but are independent of each other (Pallotta *et al*., 1998).

Even though the frequency and the pyloric cycle frequency are the same, two separate timers are used to trigger the pyloric contraction and the APCs. By doing so, we made both motility patterns independent of each other. This independence gives the flexibility to introduce asynchrony between motility patterns and study their effect on each other, but this is not attempted in this work.

4.3.1 Creation of antral propagating contractions

An antral propagating contraction wave looks like a bell curve with a width of 1-2 cm, and amplitude of 0.5 - 0.8 cm (Marcini, L. 2001; Monica A, 2006; Schulz,2006) travels along the entire gastric lumen from the origin to the distal antrum with a velocity of 0.0025 m/s (Pal *et al*.2004). Three APCs originates and travels to the distal stomach in a gastric cycle (Marciani, L. 2011).

An ACP's shape as a function of time and characteristic size parameters was simulated using Equation (1). The advantage of using such an equation is that parameters like amplitude and width are tunable.

$$APC = A\sum_{k=1}^{n} exp\left[\ln(\epsilon)\frac{2}{\sigma}(P(k)-ut)^2 + \left(\frac{2}{D}P(k)\right)^2\right] \quad (1)$$

Where:

A - Amplitude (m)

ϵ - a constant (0.99 in this case)

σ - a constant (0.02 in this case)

P - current position (m)

D- Distance to be travelled (m)

u - propagation velocity (m/s)

t – time (s)

A typical APC wave created using (1) for this work is given in Figure 18; however, the orientation may differ when mounted over the greater curvature (GC) and lesser curvature (LC) of the gastric geometry.

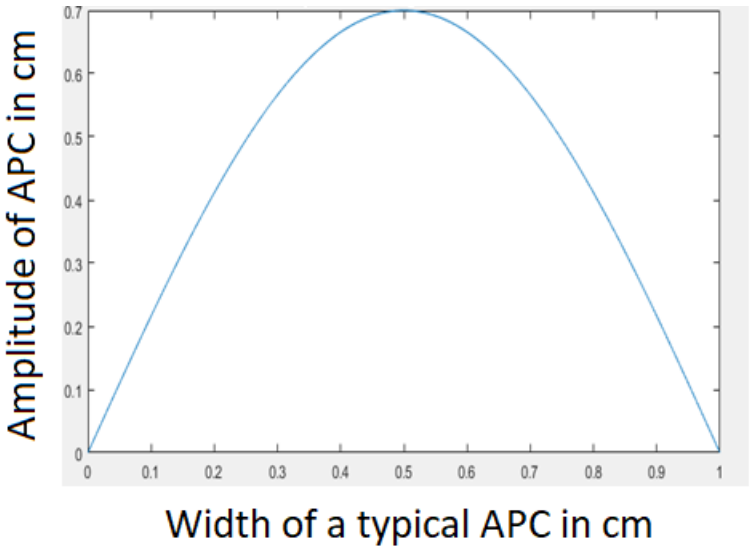

Figure 18. A typical single antral propagating contraction wave (APC) generated using Equation (1) with 0.7 cm amplitude and 1 cm width.

After creating the APC, the next step is to mount them on either side of the stomach wall and fix their initial position. The APCs commence at the site of a 'pacemaker' area situated at the mid corpus along the greater curvature. Despite recent precise electrophysiological localization of this site (O'Grady *et al*., 2010), the exact distance along the greater curvature at which an APC becomes fully apparent has not been reported. Therefore, the location described by Pal *et al*. (2004), which was based on the first appearance of indentations on the greater curv ature in an MRI film of the

profile and was approximately 15 cm distal to the pylorus along a horizontal line from the pylorus, was used in this work. The distal point to which an APCs propagate is reported to vary, with 43% stopping within 1cm of the pylorus and 50% stopping within 2 cm of the pylorus (Pallotta *et al*., 1998). We assumed in our model that all APCs propagated within 2 cm of the pyloric proximal end.

To study the effect of APC amplitude on the gastric processes, two sets of APCs were modelled, one with 0.7 cm amplitude/height and another one with 1.4 cm amplitude/height. A 20 s time lag between two APCs (Kwiatek *et al*., 2006; Singh *et al*., 2010; Xue *et al*., 2012) were introduced to ensure that three APCs are generated from the pacemaker region in a gastric cycle (60 s). Figure 21 shows the stomach wall after one complete gastric cycle with a standard APC (0.7 cm height, Figure 19A) and a double APC (1.4 cm height, Figure 19B).

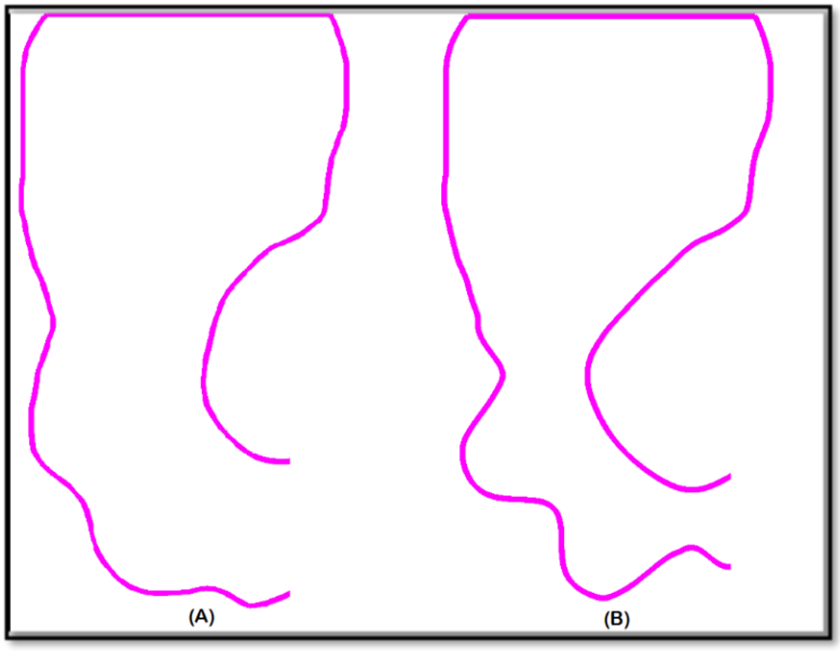

Figure 19. Placement of APCs on the gut wall after one gastric cycle (1 gastric cycle = 60 s). (A) APC with 0.7cm amplitude. (B) APC with 1.4 cm amplitude.

4.3.2 Pyloric contractile cycle

Three pyloric cycles (one cycle consists of closing and opening of the pylorus) occur in a 60 s period. So pylorus takes 20 s to move from the open state to the closed state and back. In this work, in a 20 s long pyloric cycle, the pylorus remained closed for 30% of the time (6 s) and opened for 70% (14 s). The open position included every position except the completely closed position of the pylorus.

While simulating the pyloric contractile activity to achieve a smoother transition to support LBM, we implemented a 7-6-7 pattern. The pylorus took 7 s to reach a completely occluded state from a fully open state and remained closed for the next 6 s and another 7 s to come to the original form from the completely closed state.

Whilst it is broadly accepted that the mechanism of pyloric contraction is distinct from that of phasic antral contraction (Pallotta *et al*., 1998), there is an ongoing debate as to whether the approaching APCs trigger its closure. The contraction of the pyloric canal (PC) may be triggered by the approach of APC (Keet Jr, 1962), which generally stop 2-3 cm short of the proximal limit of the pylorus (Pallotta *et al*., 1998), and hence acts in phase with them, but it may on occasion contract independently of APCs (Indireshkumar *et al*., 2000). In this work, APC and pyloric contraction are in phase.

4.3.3 Introduction of fundic and duodenal pressure cycles

It is known that fundal tone and consequent intraluminal pressure influence the gastroduodenal pressure gradient contributing to gastric emptying (Lentle *et al*., 2016). However, in this model, fundal tone and duodenal motility were not implemented but were introduced as an overall pressure difference between the distal fundal and the proximal duodenum is set. Hence, the work emulated the reported pulsatile variation in fundal pressure (Lentle *et al*., 2016) in the model by a uniform sinusoidal fluctuation in lumen pressure from a maximum of 10 Pa to a minimum of 0 Pa on the line of division between the fundus and the body of the stomach (Figure 20).

The duodenal brake was simulated as a periodic sinusoidal reduction in the mean diameter of the distal-most (tubular) portion of the duodenum and a sinusoidal variation of the pressure wave with an amplitude of 10 Pa at the reported postprandial frequency of 12 cpm (Figure 20). Even though this maximum was much lower than that of reported 400 Pa duodenal pressure (Faas *et al*., 2001),

it was sufficient to promote periodic influx and efflux from the stomach. Also, the pressure reported by Faas *et al*. (2001) was not specific whether the reported pressure was lumen pressure or the pressure between the transducer and the mucosa.

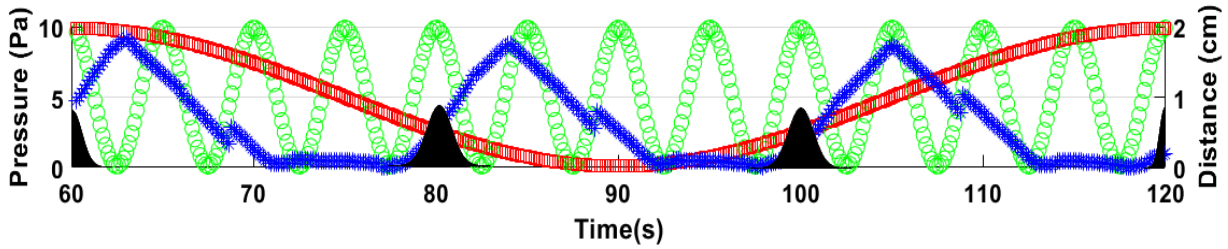

Figure 20. Oscillating inlet/fundic pressure (red) and outlet/duodenal (green) pressure waves and open/close state of the pyloric sphincter (blue) in a gastric cycle. The black bell curve indicates the time when a new APC originates at the pacemaker region.

4.4 Development of the CFD Model

Fluid flow inside the gastric geometry created using line drawings as explained in the previous section, was modelled using the mesoscopic lattice-Boltzmann method (LBM). In fluid dynamics, the transport equation (a differential equation) that transports mass, momentum, and energy by a moving fluid can be simulated in two different approaches (Mohamad, 2011). One is the continuum method in which mass, momentum, and energy conservation are applied to an infinitesimal control volume (Mohamad, 2011). Nevertheless, this approach is incapable of handling nonlinearity, complex geometry, and complex boundaries most of the time.

The second approach is to discretize the entire domain into a small volume (finite volume method, FVM), grid (finite-difference method, FDM) or elements (finite element method, FEM) (Mohamad, 2011). This is a macroscopic approach, and the 'parameters' like velocity or pressure are rather 'assumed' or 'averaged' over a large number of particles, which demands a high computational cost (Mohamad, 2011). The primary three discretization schemes, the finite difference, the finite element, and the finite volume methods, are very similar and are collectively referred to as computational fluid dynamics (CFD). All these methods have difficulties dealing

with multiphase systems and complex shape geometries (Mohamad, 2011). Moreover, they struggle to handle complex moving interfaces that need computationally expensive geometry remeshing at each time step.

CFD techniques often struggle with complex moving boundaries and multiphase-non-Newtonian particulate suspension. So an intermediate mesoscopic level approach is getting popular in recent years, called the lattice-Boltzmann method (LBM), to model the fluid flow simulations (de Loubens *et al*., 2013).

Parallel processing capacity (Succi, 2001) and the ability to handle complex geometries (Ladd *et al*., 2001) makes LBM ideal for simulating biological systems with multicomponent flows and complex moving boundaries (Feng *et al.,* 2010; Browning *et al*., 2011; Bao *et al*., 2011; Guo *et al*. 2013). This capability is significant in our work as the gastric geometry is complex and constantly moving. LBM can simulate particulate suspension flows (Ladd *et al*., 2001; Aidun *et al*., 2010). This would be useful in the next stages of our work, where the pseudoplastic gastric content flow will be studied. Since gastric geometry is time-variant, complex and moving, and the gastric content is non- Newtonian, we will be using LBM as our simulation tool.

4.5 Lattice-Boltzmann Method

LBM was developed to model the gas system, and it is a direct descendant of the Lattice gas automata (LGA). LGA simulates the behaviour and interaction of many single particles in a gas (Succi, 2001; Sukop, 2006; Mohamad, 2011). However, LBM replaced this discrete particle concept with a particle distribution function (PDF), where several particles with predefined velocities in a small volume are considered rather than individual particles (Succi, 2001). The PDF gets updated at each time step by lattice Boltzmann's governing equation (equation 2), also known as the evolution equation. The evolution equation gets updated in two distinct steps, (a) collision step (b) streaming step. The collision step updates the distribution function with a relaxation time factor and an equilibrium density distribution factor, and this updated distribution function then transported using the streaming step (Succi, 2001). The streaming step is the transfer of the direction-specific densities. It can be understood as if a group of the molecules located on the node moved to the nearest neighbour modifying its density and its velocity. The classic LBM model is

the lattic-Boltzmann model with the BGK (Bhatnagar-Gross-Krook) collision operator and is often used to solve the incompressible Navier-Stokes equations (Succi, 2001; Sukop, 2006; Mohamad, 2011) as they are accurate enough and efficient for simulation of fluid flows with low Reynolds numbers (Eslam Ezzatneshan, 2019).

In LBM, the solution domain is divided into lattices (discretization), with the particle distribution function evaluated at each node. The lattice arrangement is denoted as DnQm, where n represents the problem's dimension (1 for 1-D, 2 for 2D, and 3 for 3D), and m denotes the number of directions that each particle that resides in a specific node can have (Bao and Meskas, 2011). For example, a D2Q5 model has four velocity vectors issued from the central nodes (Figure 21).

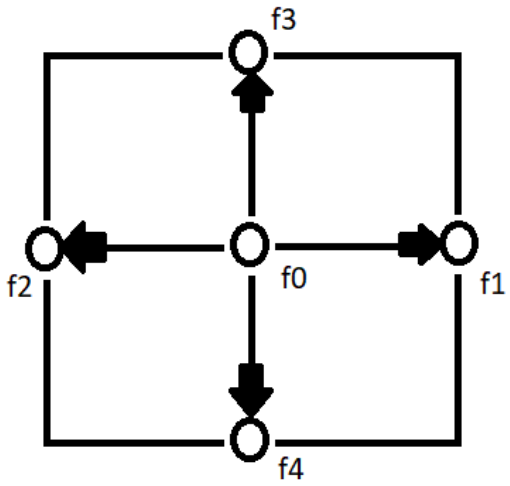

Figure 21. D2Q5 lattice arrangement. The particles, denoted by f that resides at the central node, has a speed of zero, noted as c(0,0): The distribution function f1and f2 move with c(1,0) and c(-1,0) (to the east and west), respectively, while f3and f4 move with speed c(0,1)and c(0,-1) (to the north and south), respectively.

Since this work modelled a two-dimensional stomach model, the lattice arrangement for this work was D2Q9 (Figure 22).

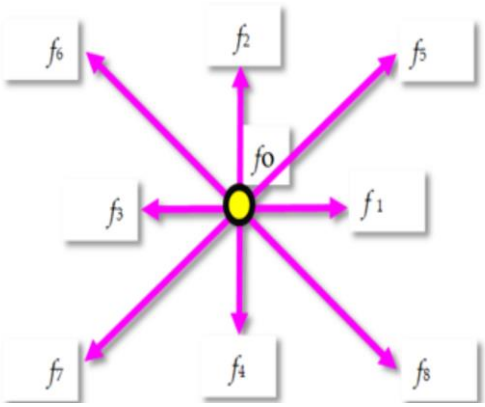

Figure 22. D2Q9 lattice arrangement, where f indicates the particle and the number shows the nodes at which each particle resides. For instance., f1 indicates a particle resides in the (0,1) node or particle position while f7 suggests a node or particle position of (-1,-1).

The lattice arrangement also determines the lattice weight factor (W_i) that a particle gains by moving in one specific path. In other words, this is the possibility of a particle following the possible lattice path. The sum of the weighing factors in all directions must be unity (Succi, 2001). The weight factor for the D2Q9 model is; W_i = [16/36 4/36 4/36 4/36 4/36 1/36 1/36 1/36 1/36]. The two lattice parameters δx (the spacing between two adjacent nodes) and δt (the time defined for a single time step) are generally user defined and commonly specified as unity. This simplifies the governing equation of LBM.

Lattice Boltzmann's governing equation (BGK Model)

Consider LBM as a discrete-time, discrete space, and discrete momentum version of lattice gas automata (Zhang, 2011), where the transportation process happens in two different steps, known as streaming and collision. This can be expressed as equation (2).

$$\underbrace{n_i(x + \mathrm{e_i}, t + 1) = n_i(x, t)}_{\text{Streaming step}} + \underbrace{\Omega_\mathrm{i}\big(n(x, t)\big)}_{\text{Collision step}} \qquad (2)$$

Where , e_i is the microscopic particle velocities, Ω is the collision operator, and n_i is the boolean particle occupation variables.

In LBM, particle occupation variables (n_i) is replaced by a particle distribution function (PDF) f_i ; where $f_i = \langle n_i \rangle$ ($\langle \quad \rangle$ denotes the ensemble average). Hence the evolution equation of Boltzmann becomes

$$\underbrace{f_i(x + e_i, t + 1) - f_i(x, t)}_{\text{Streaming step}} = \underbrace{\Omega_i\big(n(x, t)\big)}_{\text{Collision step}} \qquad (3)$$

Where $f(x, t)$ is the Particle distribution function (PDF), and Ω is the collision operator. Even though there are various lattice arrangements in LBM, and that may change the PDF, our discussion will be restricted to D2Q9 as we used this lattice arrangement in our work.

As mentioned earlier, in the D2Q9 arrangement, particles are restricted to move to nine directions, including the resting position. Macroscopic fluid density is the sum of these microscopic particle distributions (PDF).

$$\rho(x, t) = \sum_{i=0}^{8} f\,(x, t) \qquad (4)$$

Where, ρ – Macroscopic fluid density,f(x,t) – Particle distribution function.

Here we are no longer tracking single particles but averages over many particles; hence, we are not operating at the microscopic but mesoscopic levels. From equation (4), macroscopic velocity can be derived.

$$u(x, t) = 1/\rho \sum_{i=0}^{8} C.\, f_i \qquad (5)$$

Where, C - Lattice speed ($c = \frac{\Delta x}{\Delta t}$) which is related to the fluid speed of sound Cs; $Cs = C/\sqrt{3}$.

LBE (equation 1) can be modified with a simplified collision operator proposed by Bhatnagar-Gross-Krook (BGK) single relaxation time approximation as

$$f_i(x + ce_i\Delta t, t + \Delta t) - f_i(x,t) \;=\; -\frac{1}{\tau}[\, f_i(x,t) - f_i{}^{\mathrm{eq}}(\mathrm{x,t})] \tag{6}$$

Where $f_i{}^{\mathrm{eq}}$ - the equilibrium distribution function

$$f_i{}^{\mathrm{eq}}(x,t) = W_i\rho + \rho S_i(u(x,t)) \tag{7}$$

Here,

$$S_i(u) = W_i[3\frac{e_i.u}{c} + \frac{9}{2}\frac{(ei.u)^2}{c^2} - \frac{3}{2}\frac{u.u}{c^2}] \tag{8}$$

Where, W_i – Weight factor, τ is the dimensionless relaxation time towards an equilibrium that relates to kinematic viscosity in the D2Q9 model using

$$\nu \;= \frac{2\tau - 1}{6}\,\frac{\Delta x^2}{\Delta \mathrm{t}} \tag{9}$$

The pressure of flow is calculated as given by (Guo *et al*., 2013)

$$\mathrm{P} = \mathrm{c}^2/4\sigma \sum_{i=0}^{8} f_i + \mathrm{S0(u)} \tag{10}$$

Where, C - lattice speed of light, σ is calculated from two other parameter $\lambda + \mathrm{r} = \sigma$ and $2\mathrm{r} + \lambda = 1/2$, f_i – Particle distribution function, $\mathrm{S0(u)}$ can be calculated from equation (8) where i=0.

4.5.1.1 **Boundary Conditions**

Boundary conditions define the particle streaming direction and change in distribution function when particles collide with a boundary. The boundary condition in hydrodynamic problems is usually a macroscopic variable, such as velocity and pressure. But in the lattice Boltzmann method, the basic evolution variable, the distribution function f_i, at the boundaries must be obtained from the given macroscopic variables using appropriate methods (Zhao-Li *et al*., 2002). Boundary conditions are critical for the stability and accuracy of numerical solutions. Options include bounce back boundary conditions (Succi, 2001; Goodarzi *et al*., 2014), half bounce back boundary conditions, Zou-He velocity, and pressure boundary conditions (Zou and He, 1997).

We have moving stomach wall boundaries and pressure boundaries at fundic inlet and duodenal outlets in this problem. Bounce back boundary conditions (modified to accommodate the momentum injection to the fluid from the moving boundary) are the most appropriate to represent the moving stomach wall (the gastric wall). Pressure boundary conditions are appropriate to represent the inlet and outlet (Zou and He, 1997).

Moving Boundary condition

The moving boundary conditions imposed by the APCs on the stomach wall was modelled by the methods of Zou and He (Zou and He, 1997). Bounce back is used when the boundaries are solid stationery, moving boundary, non-slip boundary, or flow-over obstacles. This boundary condition states that when the streaming particle touches the boundary from the medium (say from a node Xm), it will bounce back to the node Xm with a reversed lattice velocity (Figure 23. Illustration of bounce-back from a stationary boundary).

$$f_i\,(Xm, t + \Delta t) = f_i^{\#}\,(Xm, t) \qquad (11)$$

Where, $f_i^{\#}$ is the distribution function leaving Xm after the collision and, $f_i^{\#}$ is opposite in direction, f_i

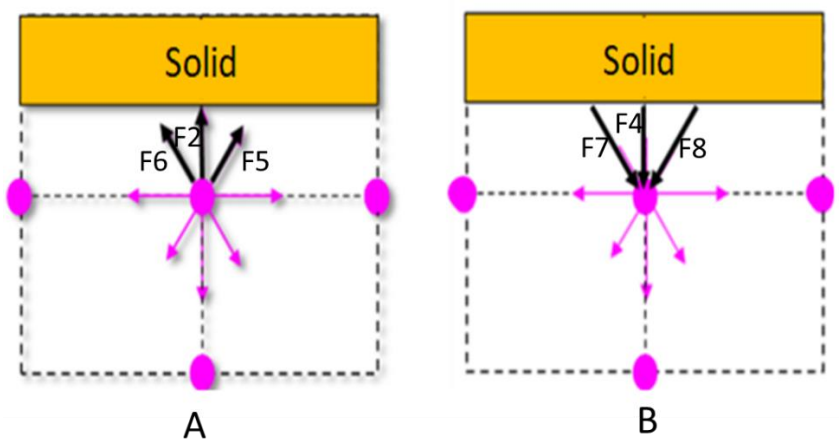

Figure 23. Illustration of bounce-back from a stationary boundary. The central node is considered as Xm, and solid lines represent the propagation direction.
(A)Three particle distributions (f2,f5, and f6) from Xm propagated towards the boundary (represented in black arrow), and after colliding with the solid boundary (B), Propagating back to Xm as f4, f7, and f8.

When the boundary is moving, this scheme can be modified to incorporate an extra impulse to the particle to represent momentum transfer to the particle from the boundary (Ladd 1994). This gives:

$$f_i\,(Xm, t + \Delta t) = f_i^{\#}(Xm, t) - \frac{2\rho\, W_i}{Cs^2}\,\mathrm{Ub.e_i} \qquad (12)$$

Where Ub is the boundary velocity at the bounce-back point, *ei* is the microscopic velocities, Cs speed of sound in the fluid. If there is no bounce back, the term Ub becomes zero, and the last part of the equation gets removed and becomes (9).

Pressure Boundary condition

It is common to encounter problems where there is an inlet and/or outlet flow. In this case, either the velocity profile or pressure at the boundary is set. In both cases, similar approaches are used. In our case, the inlet is set to be the pressure exerted by the fundus, and the outlet is set as the pressure introduced by duodenal movements.

Consider a situation where the fluid enters the channel from the Northside (physical boundary) and leaves the channel via the south boundary (fluid boundary) where the entrance pressure is higher than the exit pressure (Figure 24).

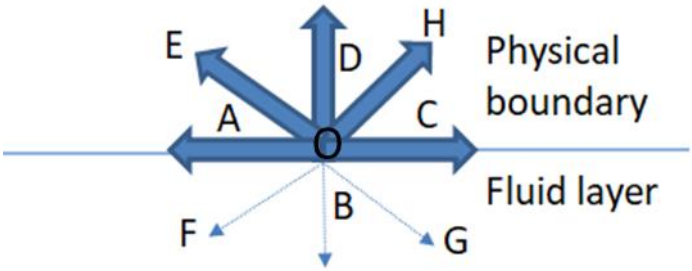

Figure 24. Illustration of an inlet pressure boundary. Here each particle is assigned a letter. Central particle f(0,0) is called 'o' , f(0,1) is C, and so on.

Here the fluid velocity has only x and y components as this is a 2Dproblem. In this situation, we need to determine the distribution function of nodes F, B, and G after the streaming process. This is achieved by the equation given by (Zhao-Li *et al*., 2002).

$$f_i(o,t) = f_i^{\,0}(o,t) + (1-\omega)[f_i(B,t) - f_i^{\,0}(B,t)] \qquad (13)$$

A similar procedure can be used to derive the pressure boundary condition of all other nodes.

4.5.2 Physical to LBM unit conversion

The LBM methodology requires every physical quantity (such as lengths, pressures, velocities, fluid properties.) in lattice units. The procedure converts physical quantities into dimensionless values and then converts the dimensionless intermediate numbers into the final lattice units. The reverse must be done with the results; results in lattice units need to be converted back into physical units.

The dimensionless Reynolds number (Re) and the Strouhal number (S) were the basis for setting up fluid flow velocity and the pressure oscillation frequency of the fundus and duodenum.

Reynold number (Re) is a dimensionless quantity and is the ratio of inertial to viscous forces in the fluid (equation 14), and it indicates a flow regime. Generally, if Re is less than 2,000, the flow is laminar, and if Re is above 4,000, the flow is turbulent; in-between is transitional.

$$Re = \frac{\rho u L}{\mu} \quad (14)$$

Where,

ρ is the density of the fluid (kg/m^3)

u is the velocity of the fluid (m/s)

L is a characteristic linear dimension of the flow channel (i.e., pipe diameter) (m)

μ is the viscosity (Pa·s or N·s/m^2 or kg/m·s)

The dimensionless Strouhal number (St) describes an oscillating flow mechanism (equation 15), which is the movement ratio due to oscillation to movement due to flow.

$$St = \frac{f L}{U} \quad (15)$$

Where,

f is the frequency of oscillation (Hz)

L is the characteristic length (m)

U is the fluid flow velocity (m/s)

Table 3 below gives a clear and comprehensive idea of unit conversion used in our problem. The technique is:

- The Reynolds number and Stouhal number for the physical problem are calculated.
- All physical quantities are scaled to dimensionless forms so that the Reynolds and Strouhal numbers are preserved.
- The characteristic dimensions of the lattice are selected. These are quantities such as the number of lattice nodes.
- The dimensionless forms of the physical quantities are then scaled into lattice units.

Table 3. Different systems used in converting physical unit to lattice units

Physical System (SI unit)	**Dimensionless System**	**Lattice System**
Simulation Time = 181 (s)	Absolute Simulation time $A_{time}=\frac{SimulationTime}{\frac{L}{U}}$	Number of iterations Nt= $A_{time}(\frac{L_{lb}}{U_{lb}})$
Length (L) =0.2 (m)	The Reynold's number (Re) = $LU(\frac{\rho}{\mu})$	Viscosity $\mu_{lb} = (\tau - 0.5)Cs^2\Delta t$
Velocity U = 0.003 (m/s)	Strouhal Number $Sr_{APC} = APC_{freq}(\frac{L}{U})$	Macroscopic velocity $U_{lb} = Re(\frac{\mu_{lb}}{L_{lb}\rho_{lb}})$
Frequency _freq = 0.05 Hz (3 cycles per minute)	Strouhal Number $Sr_{FP} = FP_{freq}\frac{L}{U}$	Frequency $Flb_{APC} = \frac{Sr_{APC}U_{lb}}{L_{lb}}$
Fundic pressure wave frequency FP_freq=0.02Hz (1cycles per minute)	Strouhal Number $Sr_{DP} = DP_{freq}(\frac{L}{U})$	Fundic frequency $Flb_{fun} = \frac{Sr_{fun}U_{lb}}{L_{lb}}$
Duodenal Pressure wave Frequency DP_Freq=0.2Hz (12 cycles per minute)	Fundic pressure $Pfun_d = \frac{p_{fun}}{\mu}(\frac{U}{L})$	Pyloric cycle frequency $Flb_{pyl} = \frac{Sr_{pyl}U_{lb}}{L_{lb}}$
Pyloric cycle frequency = Freq (3cycles per minute)	Duodenal pressure $P_{duo_d} = \frac{p_{duo\ U}}{\mu L}$	Duodenal frequency $Flb_{duo} = \frac{Sr_{duo}U_{lb}}{L_{lb}}$
Density =1000 (kg/m^3)		Fundic pressure $Pfun_{lb} = Pfun_d\mu_{lb}\left(\frac{U_{lb}}{L_{lb}}\right)$
Viscosity ($\mu = \tau/\dot{\gamma}$) = 0.1 Pa.s; $Where,\ \tau$ = stress (Pa), $\dot{\gamma} = strain\ rate\ (S^{-1})$, μ= *modulus of viscosity (Pa.S)*		Duodenal pressure $Pduo_{lb} = t_d\ (\frac{L_{lb}}{U_{lb}})$
Fundic pressure, Pfun= 4.9001 Pa		User-Defined: L_{lb} (lattice length), ρ_{lb} (density), τ (relaxation time), Δx /Δt -lattice position/time steps

An example problem to convert physical flow velocity to lattice velocity based on our work is given below.

Characteristic length of stomach, L = 0.21 (m)

Flow velocity, U = 0.003 (m/s)

Density of the fluid, ρ = 1000 (kg/m^3)

Viscosity, μ = 0.2 (Pa. s)

Thus $Re = \frac{\rho u L}{\mu}$ = 3.15 (refer eqn (14))

In our problem, user defined LBM parameters were:

Characteristic length, *L_lb =100* (number of lattice nodes).

Density, ρ_{lb} =1.

Viscosity (μ_lb) is a function of relaxation time (τ) and microscopic particle velocity (Cs); $\mu_{lb} = (\tau - 0.5) * Cs^2 * \Delta t$, where $Cs^2 = 1/3(dt/dx^2)$; and dt = dx = 1 in our case (one step increment in time and position for the particle).

Thus, μ_lb =0.03 (LB unit).

Reynolds number in LBM units, $Re = \frac{\rho_{lb} U_{lb} L_{lb}}{\mu_{lb}}$

Thus, tteso maintain the Reynolds number of the physical units, the LBM flow velocity

$U_{lb} = Re.\mu_{lb}/(\rho_{lb} L_{lb})$

A similar procedure was employed to derive all other parameters in LBM from physical parameters and a reverse conversion to display and interpret results in later stage.

4.5.3 Testing of LBM code

The LBM code was tested against the problem of Poiseuille flow in a pipe before introducing it to the final geometry. The velocity profile in Poiseuille flow has a well known analytical solution derived from Navier stoke's equation, so it can be used to test a numerical scheme such as LBM by checking whether the analytical and numerical solutions agree.

The Poiseuille flow is a flow pattern of an incompressible, viscous flow with non-slip boundary conditions. The problem of Poiseuille is a positive pressure-induced channel flow inside a pipe of length L and radius R, where R<< L.

$$U = \frac{\Delta_P R^2}{4\mu L} \tag{16}$$

Where, U – max. Newtonian flow velocity, Δ_P - Pressure gradient, L - length of the pipe, R - radius of the pipe, and μ - viscosity.

For simulating the flow, a homogeneous velocity profile was assumed at the inlet, and the outlet of the pipe and the pipe walls were considered non-moving and non-slip. This translated to microscopic boundary conditions as bounce-back boundaries to simulate the pipe and velocity boundaries at the inlet and outlet.

It usually takes several iterations to develop its final shape. The velocity profile resulted from the LBM should agree with the parabolic profile of the Poiseuille flow.

The analytical solution is the blue line in Figure 25 (A and B); the simulation result obtained using the LBM method is given in red. The simulation result converged with an analytical solution after 4,000 iterations (Figure 25B). This shows that the numerical implementation of LBM is correct for the Poiseuille problem.

.

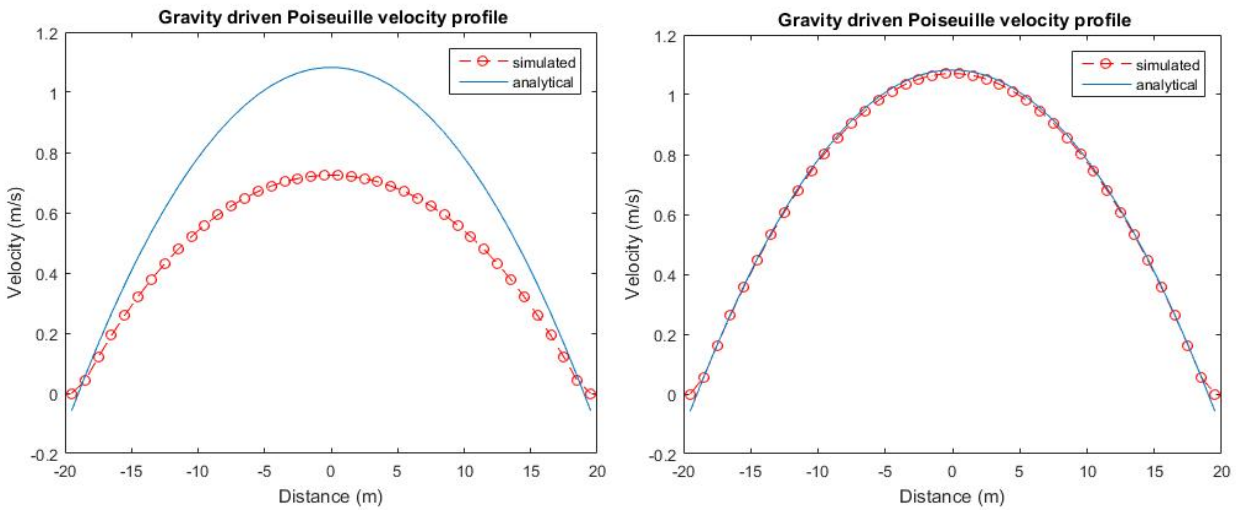

Figure 25. LBM analytical vs simulation plots. (A) after 1,000 iterations (B) after 4,000 iterations.

4.6 Gastric flow simulation and saving the simulation data

After satisfactory testing of the gastric motility and the LBM code, we extended the LBM code into the gastric geometry to simulate the gastric flow. The general flow diagram (Figure 26) and the fluid flow domain within the gastric geometry are explained in the following sections.

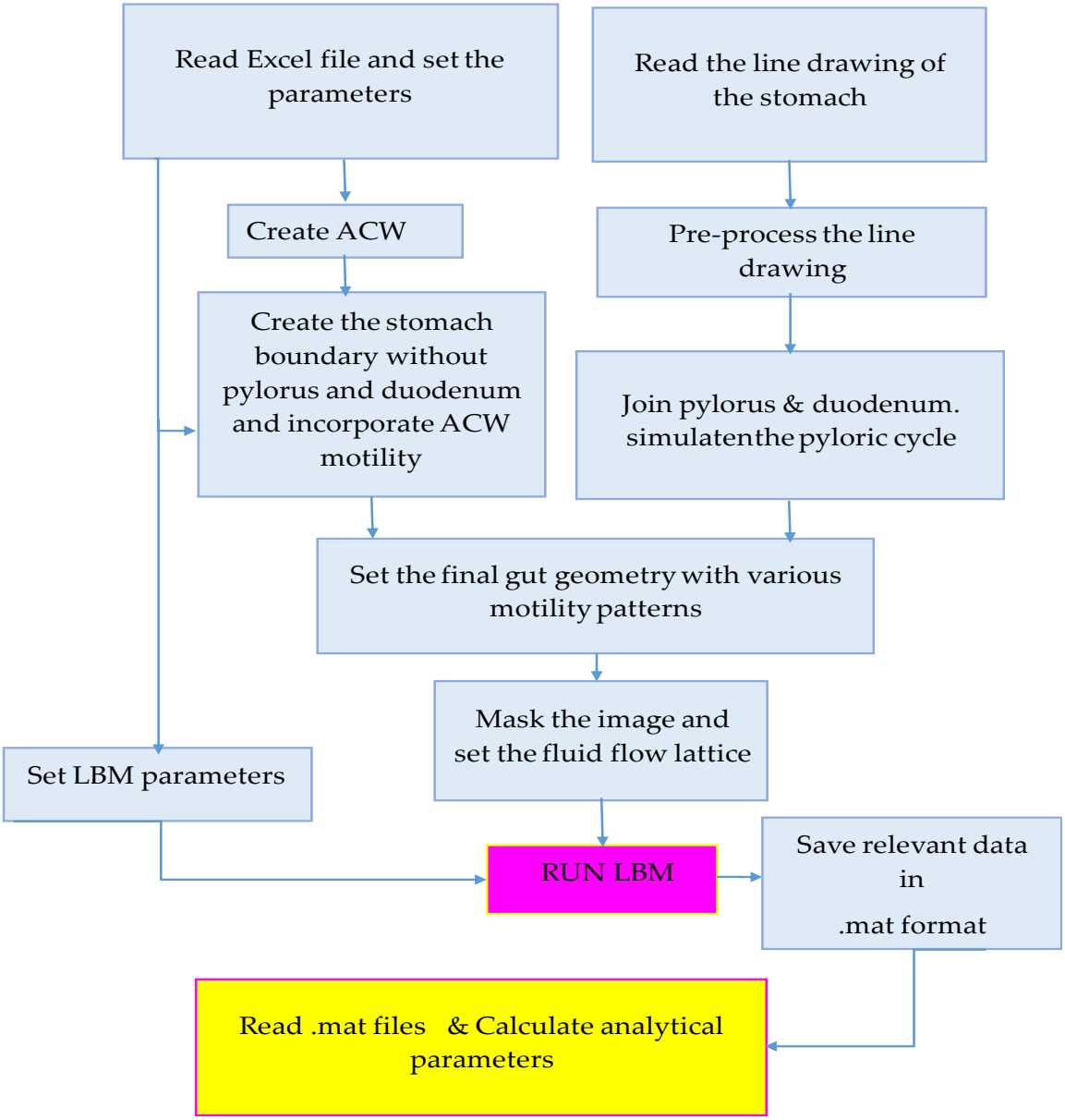

Figure 26. Block diagram representation of the workflow.

Before starting the simulation, the fluid flow field must be created, which is nothing but the discretized gastric geometry.

4.6.1 Creation of the fluid flow domain

We have created a 100 x100 lattice on the gastric geometry after removing 2 cm of the fundus (Figure 27 A). A mask was then created to differentiate the flow domain from the rest of the lattice (Figure 27 B).

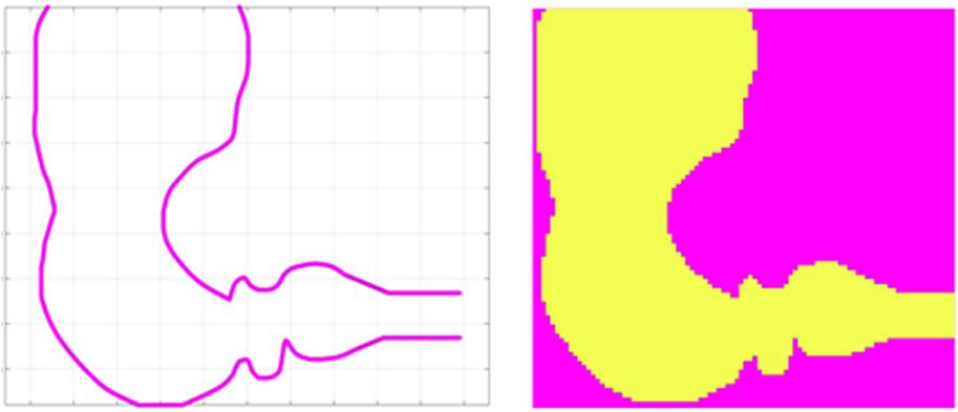

A B

Figure 27. (A) Original image of the gastric geometry (B) Masked gastric geometry to create the fluid flow domain. The yellow region is the fluid flow domain.

All physical data relevant to the simulation entered in an excel sheet and calculated corresponding quantities in LB units in the same excel sheet. This information was then exported to the main Matlab program.

Time evolution of gastric geometry, a subfunction, was called before calling the LBM function in the main time loop. The number of iterations was strictly dependent on the number of the gastric cycles simulated. The simulation was run for three gastric cycles (180 s) from a resting state. The first 60 s of the data was discarded from the most analysis since it was not physiologically realistic; because it proceeds from a non-natural rest-state. The time-series data for the x and y position of the geometry, the x and y components of the fluid velocity were saved as a *.mat* file. The saved data was later post-processed to calculate parameters such as the exit velocity and a mixing index at different anatomical regions within the stomach to verify the model.

4.7 Testing the consistency and stability of the model

Consistency (change in mesh size) and stability (sensitivity of the solution to changes in its input values) are primary for *in silico* -models and need to be tested. One way to test the consistency of a model is to change the mesh of the fluid flow domain and verify that the results are comparable.

Consistency was tested using three different mesh sizes. A 100 x 100 mesh was laid on the flow domain and simulated the flow. Then we changed the mesh size to 150 x 150 and then to 250 x 250 mesh size (Figure 28). The simulations were done without applying a TGPG and used an APC of 0.7 cm high to avoid a long simulation time. We have measured the flow velocity and shear to verify the result. We measured the shear rate at the distal end of the pylorus, and in all three cases, we got the same result of 4.8 s^{-1} and a maximum flow velocity of .02 m/s. However, the simulation time almost doubled when we moved from 100 x 100 to 150 x 150 mesh size, so as the data storage space. This is because as the number of nodes increases, the number of iterations and data produced by each iteration increases. Hence to avoid time and storage constraints, it is decided to use a mesh of 100 x 100 for the simulation.

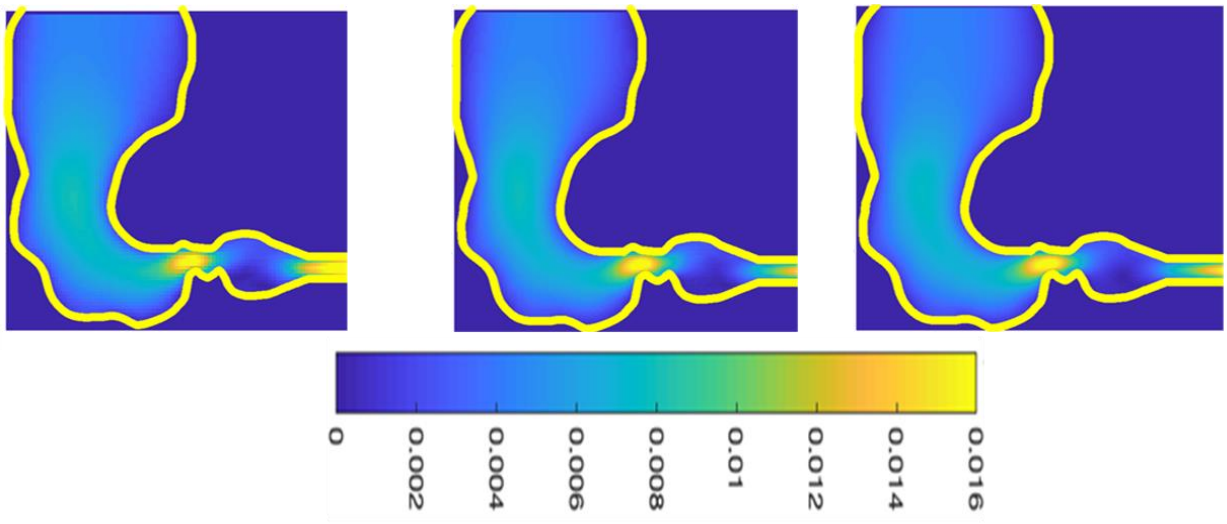

Figure 28. Simulation result with various mesh sizes. (A)100 x 100 mesh at 60 s. (B) 150 x 150 mesh at 60 s. (C) 250 x 250 at 60 s. Unit of flow velocity in m/sLower velocity regions are in blue, and higher velocity regions are shown in yellow.

4.8 Comparing the current model with a published model

There are no published gastric models with the exact physiological information that are incorporated in this model. So a comparison of this model with a published model parameter by parameter is not possible. However, the work by Pal *et al*. (2004) is the closest to this model, even though they have not incorporated the pyloric or duodenal geometry. So we have decided to look only at the flow patterns inside the stomach and compare them with Pal's work (Figure 29). It is noteworthy that the published work has closed pylorus, so we have chosen when the pylorus is closed. There was no mention of the trans-pyloric pressure gradient in Pal's work, so we had kept the TGPG to zero. The published work shows a recirculatory mixing profile within the stomach around the APC. Similar recirculatory patterns are observed in this work, with an APC amplitude of 0.7 cm and another APC of 1.4 cm amplitude. More details of these findings can be found in the discussion chapter.

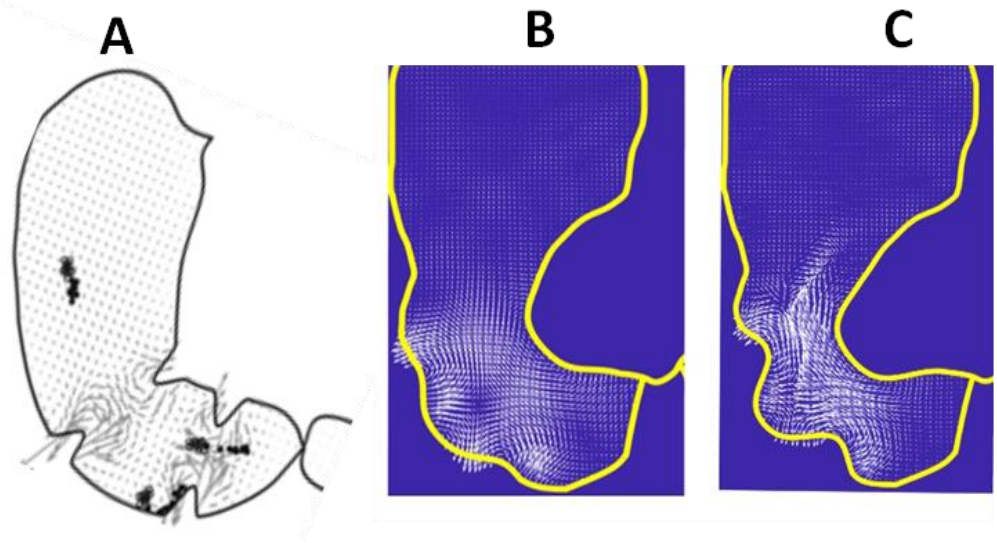

Figure 29. Recirculatory patterns in the stomach. (A) Published model by Pal *et al*.(2004). (B) Current work with an APC amplitude of 0.7 cm. (C) Current work with an APC amplitude of =1.4 cm.

4.9 Quantification of simulation outputs

Different parameters are derived and plotted from the saved simulation data to quantify the output. A brief discussion on those parameters are as follows; however, the plots and analysis of the results are given in the results chapter (Chapter 5).

4.9.1 Flow lines

Flow lines help to get a general overview of the flow directions at various points within the lumen. Flow lines were calculated by dispersing randomLy massless markers in the stomach at time t = 60 s and following their advection for the next 60 s. These trajectories provided the flow directions and a means of distinguishing local recirculation (vortices) that favour mass transfers from the stomach's central axis to its periphery. Each marker's position was plotted in green when it travelled proximally (i.e., from the duodenum to the fundus) and red when it travelled distally (i.e., from the fundus to the duodenum along the central axis of the stomach and duodenum). Apart from showing the general overview of flow directions at various points within the lumen, the trajectories provided a means of distinguishing local recirculation (vortices) that favour mass transfers from the stomach's central axis to its periphery.

4.9.2 Flow rate and velocity

Variation in mean flow velocity and the flow rate in the duodenum were plotted and compared with published physiological data. The flow rate Q was calculated in mL/s by assuming that the velocity profile in the duodenum (calculated in 2D) was axisymmetric, i.e., $Q = S\overline{U}$, with S the section of the duodenum and $\overline{U}$ the mean velocity. Outflow was determined as a positive integer and backflow as a negative integer.

4.9.3 Dispersion of the group of markers

Streaming of 4 groups of massless markers located at the antrum and the pylorus was tracked for a complete gastric cycle and computed the extent of longitudinal and axial dispersion. The axial and radial dispersion would provide better insight into gastric content mixing, outflow, and backflow.

Each step involved in developing this human gastric model described in this chapter is summarised in Figure 30. The next chapter will discuss the outcome of this model in detail.

4.9.4 Shear Rate

Plots of shear rate can give a general view of the extent and the sites where particles were more likely to be fractured due to hydrodynamic stress. The values are useful in understanding the forces which influence the disintegration of particular foods and pharmaceutical delivery systems. The spatiotemporal evolution of the shear rate (i.e., the second invariant of the rate-of-strain tensor) was calculated within the stomach by differentiating the velocity field according to space and averaged in respect to the time for two different time sequences. Plots of shear rate indicated the sites where particles were more likely to be fractured due to hydrodynamic stress.

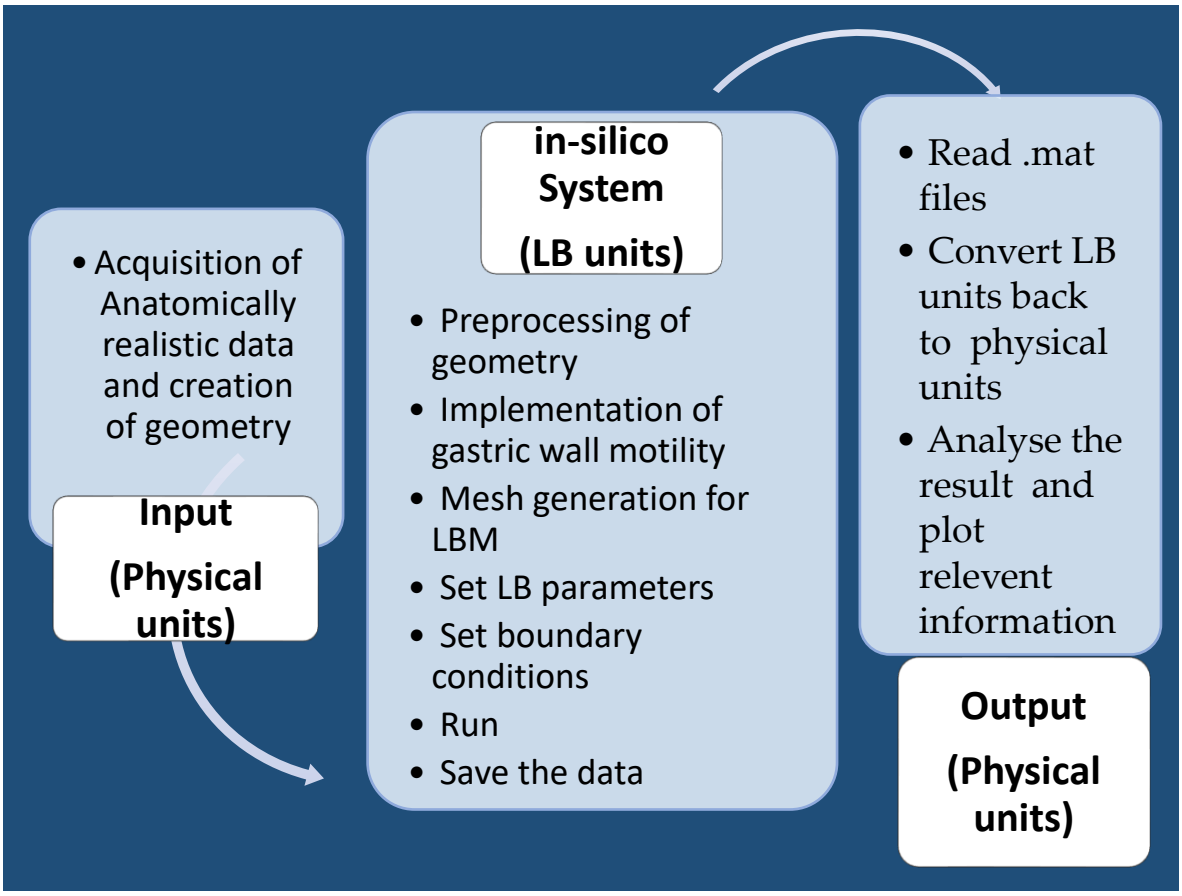

Figure 30. Various steps involved in modelling and simulating the human gastric system.

Chapter 5: Results

There is a significant admixture of ingested food with gastric secretions and the physical breakdown of solid food within the stomach before it is propelled into the small intestine (Camilleri, 2006). Three principal actions may contribute to gastric retention, mixing, and trituration: (1) the forcible cyclic contraction of the pylorus, (2) the phasic contractions of the distal stomach wall, i.e., antral propagating contractions (Melville *et al*., 1975; Pal *et al*., 2004) and (3) the establishment of a trans-gastric pressure gradient (TGPG) between the fundus (Azpiroz *et al*., 1984) and the duodenum (Shahidullah *et al*., 1975; Schulze-Delrieu, 1992). However, the relative contributions of these mechanisms remain unclear and are investigated in this work.

CFD simulations were started by considering no flow conditions at time zero. To suppress these initial condition effect on the results, we omitted the first 60 s of data, and the results were derived from the second gastric cycle (60 s - 120 s). There for in this work, several parameters were plotted and analysed to get insight into the action of the stomach concerning mixing and trituration. These were then used to assess the effects of; the amplitudes of APCs, the apparent viscosity of the gastric content, and the presence or absence of TGPG (

Table 4).

Simulations were done on a desktop computer (Windows 10 Home 64, Intel Core i3 processor, 8 GB memory, and 256 GB storage), and after each simulation, data was stored in a 1 TB external hard disk. To simulate two gastric cycles with 0.1 Pa.s viscosity, it took around 48 hours and generated 4 GB of data. Time and data doubled when the viscosity changed to 0.2 Pa.s.

Table 4. Combination of parameters used for simulations.

	TGPG - Present		TGPG - Absent	
	Viscosity = 0.1 Pa.s	Viscosity = 0.2 Pa.s	Viscosity = 0.1 Pa.s	Viscosity = 0.2 Pa.s
Amplitude = 0.7 cm	X	X	X	X
Amplitude = 1.4 cm	X	NA	X	NA

5.1 Role of trans-gastric pressure gradient

By comparing two sets of simulations, one with applied TGPG and the other one without TGPG, we studied the role of TGPG in the gastric process. The introduction of oscillating fundic pressure waves of 1 cycle per minute at the fundic boundary and oscillating duodenal pressure waves of 12 cycles per minute at the duodenal end, created a transgastric pressure gradient (TGPG). We set both fundic and duodenal oscillating pressure waves to zero magnitudes to simulate the flow without a TGPG.

5.1.1 Flow lines

Flow lines calculated during the 60 s of activity without introducing a TGPG (Figure 31, TGPG absent) showed that the proximally orientated axial flow (red lines) generally exceeded distally orientated flow (green lines) within the antrum and body. Distally located flow lines indicated constant recirculation in the duodenum and within the patent pylorus lumen. When the TGPG was present, the flow lines indicated that backflow was relatively restricted and outflow moderately enhanced in the body and antrum, notably when the fundic pressure was high and the pylorus was open. In other words, in the absence of TGPG the gastric flow tended to directed away from the duodenum and recirculate within the gastric lumen. The imposition of TGPG directed the gastric flow towards the duodenum (Figure 31, TGPG present). This observation was consistent regardless of the amplitude of the APC or the viscosity of the gastric content. Note that the flow lines were broken in the pylorus, i.e., no outflow from the stomach to the duodenum in the absence of TGPG (Figure 31, TGPG absent), but flow lines were continuous when TGPG is present (Figure 31, TGPG present). This result clearly shows that TGPG is the driving force behind gastric emptying.

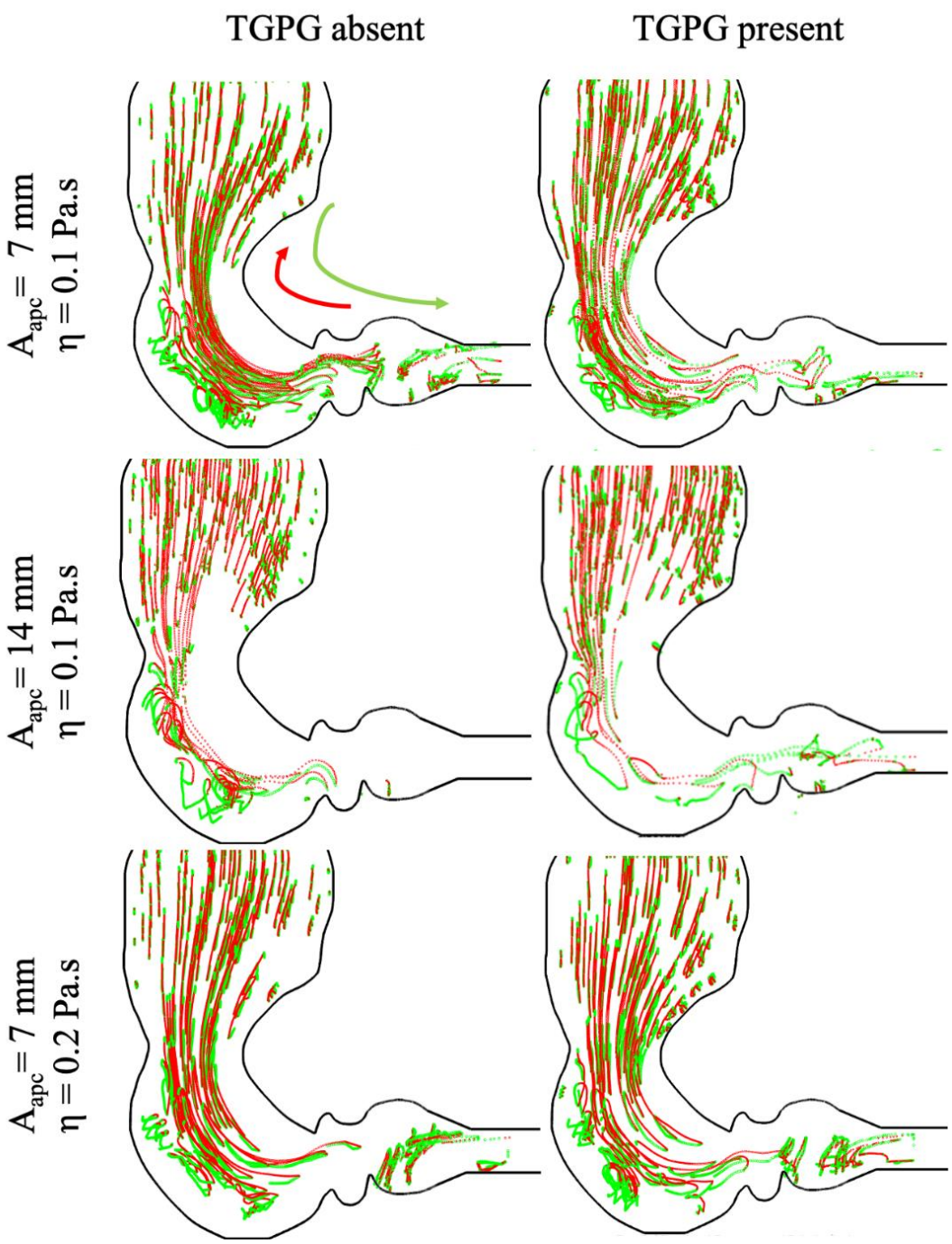

Figure 31. Flow lines within the gastric lumen in the presence and absence of TGPG. Flow lines were calculated after 60 s running time up to 120 s. The stomach outlines are solely for anatomical guidance and were moving throughout time. The distally transiting tracks are shown in green and proximally traversing paths in red. A_{apc}, the amplitude of antral contraction waves; η, the viscosity of the lumen contents; TGPG, trans-pyloric pressure gradient.

5.1.2 Flow rate and velocity

The flow rate and velocity of the gastric content calculated across the proximal duodenum also demonstrated the relative increases in axial flow in the presence of TGPGs (Figure 32). This is consistent with the flow line result. The mean velocities and flow rates in the duodenum were pulsatile. Each sequence was comprised of an inflow and an outflow. The initial brief period of inflow from the duodenum into the pylorus occurred around the pyloric opening. However, a subsequent, more prolonged outflow period occurred from the pylorus into the duodenum during pyloric closure. During the latter event, two peaks occurred, one during pyloric closure and the second coincided with an APC approach to the distal antrum (Figure 32, bottom diagram).

The profiles of both volumetric inflow and outflow obtained with a TGPG were more complex in form than those obtained without a TGPG. When the TGPG was present, dual peaks appeared in both inflow and outflow, which resulted from cyclic variation in the pressure difference between the duodenum and the fundus during a complete cycle of gastric activity. Hence the first and most prominent peak in mean velocity occurred at the time of completion of pyloric opening (t = 63 s) and the second and smaller at the commencement of pyloric closure (t = 65 s). Again, the first peak in pyloric outflow occurred after pyloric opening. The second and larger peak was coincident with an APC's arrival at the distal limit of the antrum and commencement of closure (t = 80 s).

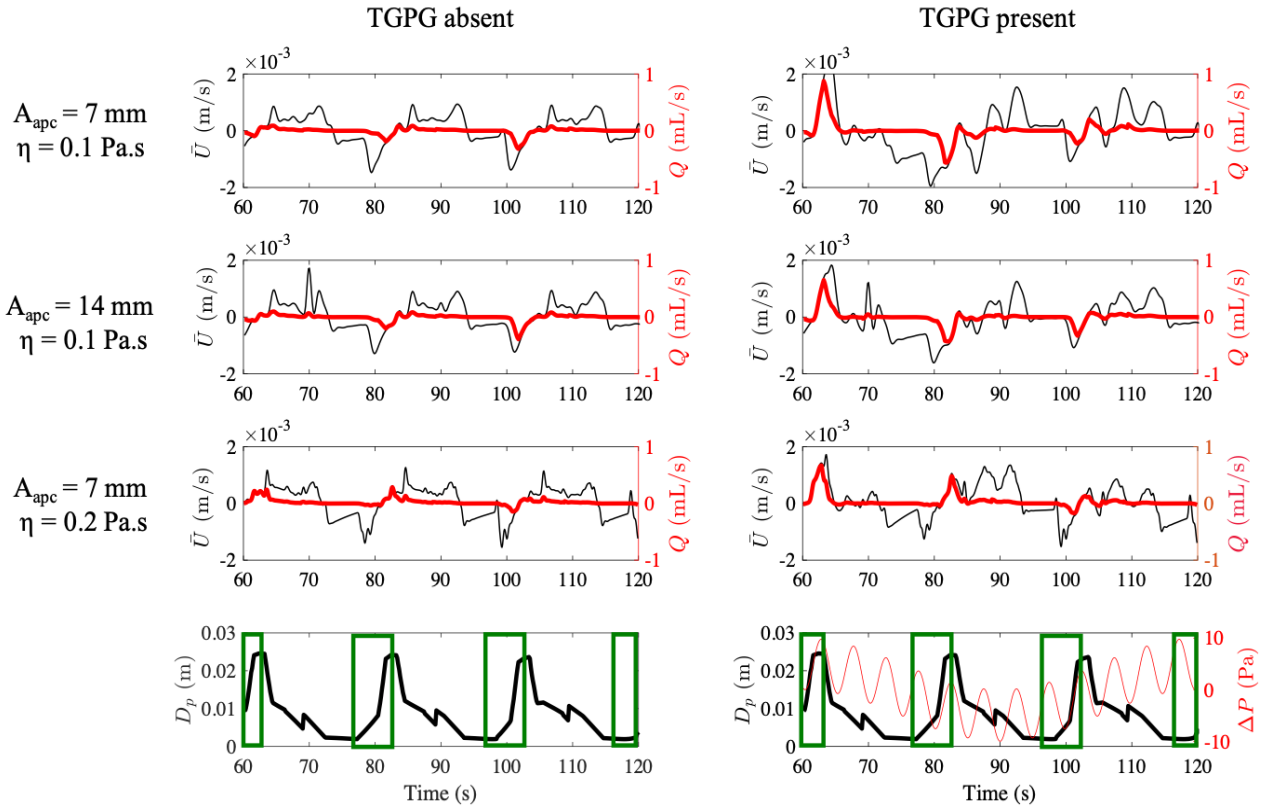

Figure 32. Temporal variation of mean flow velocity $\bar{U}$ (black) and flow rate Q (red) in the duodenum in the absence (left column) and presence (right column) of a TGPG. Top diagram: Temporal variations in $\bar{U}$ and in Q over three successive sequences of pyloric activity that results from phase differences in the components of the TGPG (i.e. P_{fundus} and $P_{duodenum}$).Bottom diagram: Concurrent variation in pyloric diameter (black lines) and the presence of APCs (green rectangle). In the presence of TGPG, the overall pressure difference between the fundus and the duodenum is shown in red, $\Delta P = P_{fundus} - P_{duodenum}$.

5.1.3 Dispersion of groups of markers

The advection of clusters of markers was cyclic but mainly orientated in the proximal direction (backflow) when the TGPG was absent (Figure 33). Radial dispersion of markers located at the central axis of the antrum (red) and near the greater curvature (green) of the gastric body antrum was minimal. Still, they were streamed predominantly longitudinally (advection). Radial dispersion was more evident in the group of markers that were located nearest to the greater curvature (blue) due to the presence of APC. In contrast, axial dispersion in this group was minimal, thus creating recirculatory patterns of displacement. Radial dispersion was also evident in markers near the pylorus, accompanied by more axial dispersion into the antrum and body.

The presence of TGPG increased axial advection in groups of markers near the greater (blue) and the lesser (green) curvatures of the stomach (Figure 33), as well as those that were located closest to the pylorus (black). The total axial dispersion of the markers located near the lesser curvature and closer to the pylorus (green) was most significant and was distributed over the entire region.

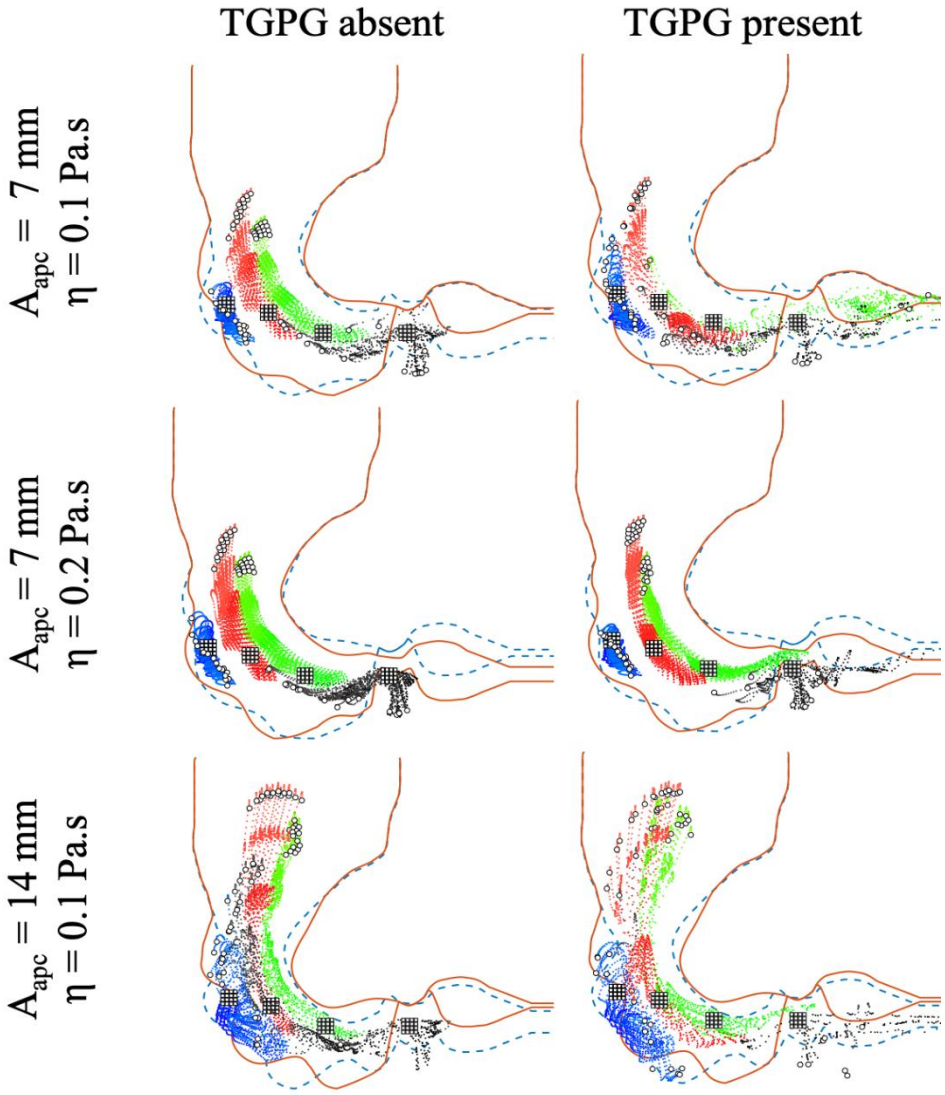

Figure 33.Cumulative dispersion of clusters of markers located at various sites in the stomach during 60 s of activity in the presence and absence of TGPG. The initial location of the four groups of markers (black, blue, red, green) are shown as squares located at 60 s at various sites in the stomach and pylorus (squares). Their cumulative advection over 60 s is shown by an increase in the intensity of the relevant colour (60 s - dark colour / 120 s - light colour). Circles indicate Their final locations. A_{apc}, the amplitude of antral contraction waves. μ, the viscosity of the lumen contents. TGPG oscillating trans-gastric pressure gradient. The two variations in the position of the walls of the stomach are shown solely for anatomical guidance.

5.1.4 Shear rate

The shear rate ($\dot{\gamma}$) was maximal at points adjacent to the distal walls of the greater and lesser curvatures (0.3 s^{-1}), pylorus (2 s^{-1}), and duodenum (3 s^{-1}) before pyloric closure and after its reopening (Figure 34). However, relatively low shear rates were observed at other sites both before (57 - 63 s) and during pyloric closure (63 - 76 s).

At times when the pylorus was open, and the TGPG was present (i.e., between 57 and 63 s, Figure 34, A_{apc} = 0.7 cm, η = 0.1 Pa.s, TGPG present), the mean amplitudes of maximal shear rates ($\dot{\gamma}$), and the area of shear rate present was significantly increased, especially near the distal part of the greater and the lesser curvature (0.6 s^{-1}), in the pylorus (3 s^{-1}), and the duodenum (5 s^{-1}) as shown in Table 5. At other times the presence of a TGPG did not influence the shear rates, notably when the pylorus was closed when TGPG was minimal.

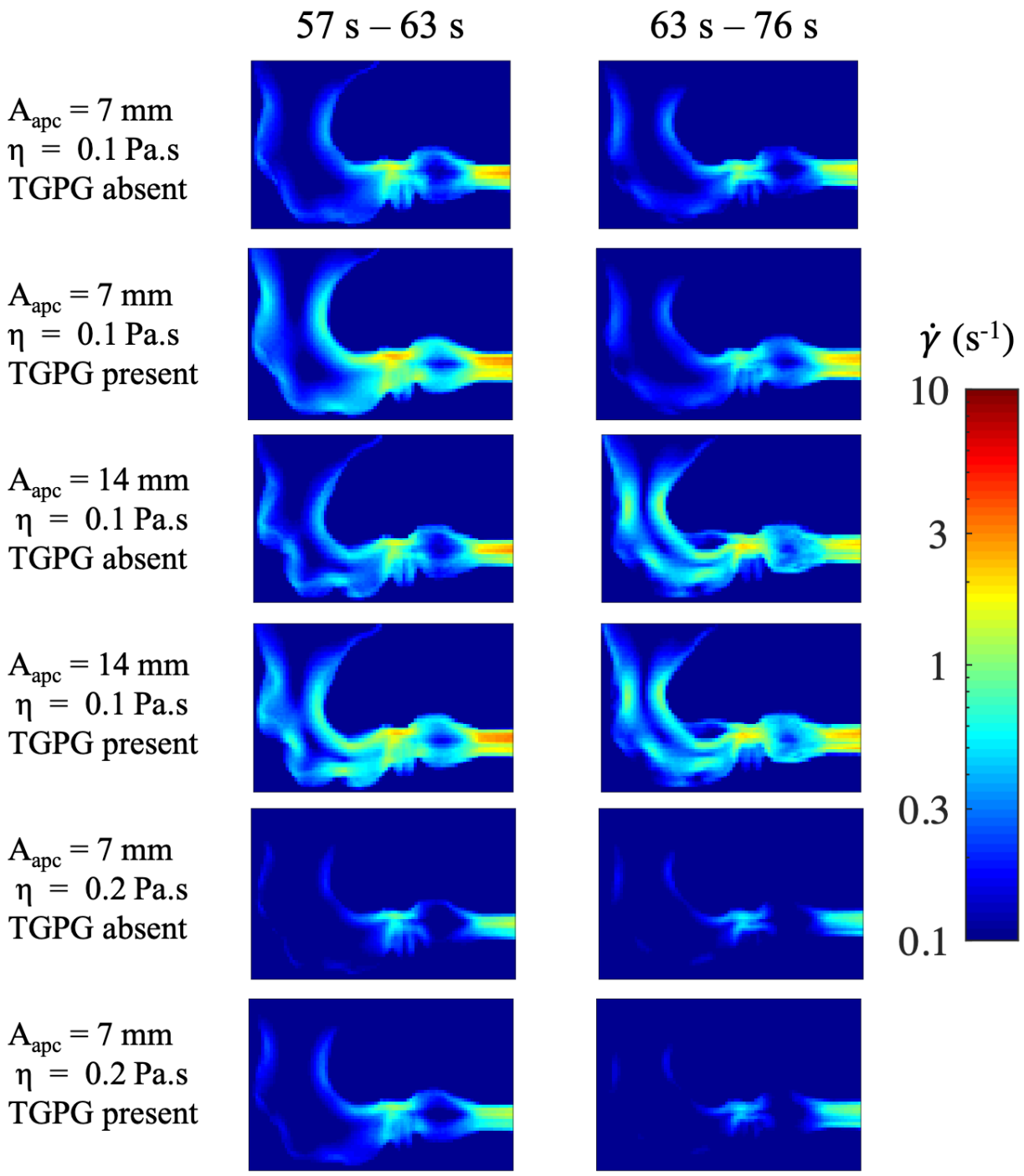

Figure 34. Spatial patterns of shear rate $\dot{\gamma}$ with and without TGPG within the lumen of the stomach during propagation of APCs around the time of pyloric opening (57-63 s, left column) and pyloric closing (63 - 76 s, right column). A_{apc}, the amplitude of antral contraction waves. μ, the viscosity of the lumen contents. TGPG, trans-pyloric pressure gradient. $\dot{\gamma}$ is calculated as the temporal mean of the shear rate for two times periods.

Table 5. Maximum, minimum and mean shear rate values of the entire flow domain obtained from the simulation with and without a trans-gastric pressure gradient (TGPG). APC - Antral propagating contractions

	Maximum shear rate (s^{-1})	Mean Shear rate (s^{-1})
TGPG - present APC Amplitude - 0.7 cm APC Viscosity - 0.1 Pa.s	4.7	0.2
TGPG - present APC Amplitude - 0.7 cm APC Viscosity - 0.2 Pa.s	4.5	0.14
TGPG - present APC Amplitude -1.4 cm APC Viscosity - 0.1 Pa.s	5.6	0.23
TGPG - Absent APC Amplitude - 0.7 cm APC Viscosity - 0.1 Pa.s	4.8	0.17
TGPG - Absent APC Amplitude - 0.7 cm APC Viscosity - 0.2 Pa.s	5.2	0.15

5.1.5 Summary of TGPG results

The TGPG results generally suggest that the presence of a trans-gastric pressure gradient influences the conveyance (as evidenced by the flow lines) and has a role in mixing (as evidenced by the dispersion of markers). However, TGPG does not have a great influence on the trituration of particles (as evidenced by the shear rate plots and shear rate values).

5.2 Effect of antral propagating contraction amplitude on gastric processes

The amount of gastric lumen constriction can be varied by changing the APC amplitude. The following parameters were plotted and studied using two different APC amplitudes (0.7 cm and 1.4 cm) to investigate the effect of APC amplitude on gastric processes.

5.2.1 Flow lines

The flow lines showed a general tendency of greater advection of gastric content with an increased APC amplitude (Figure 35). The same observation was made in the absence of TGPG. However, the advection was limited to the stomach (not beyond the pylorus). The above statement suggests that APC accentuates gastric content's advection; however, no gastric outflow happens without TGPG.

The flow domain narrowed as the APC amplitude increased in the presence and absence of TGPG. Also, larger vortices were formed along the greater curvature as the APC amplitude increased (Figure 35).

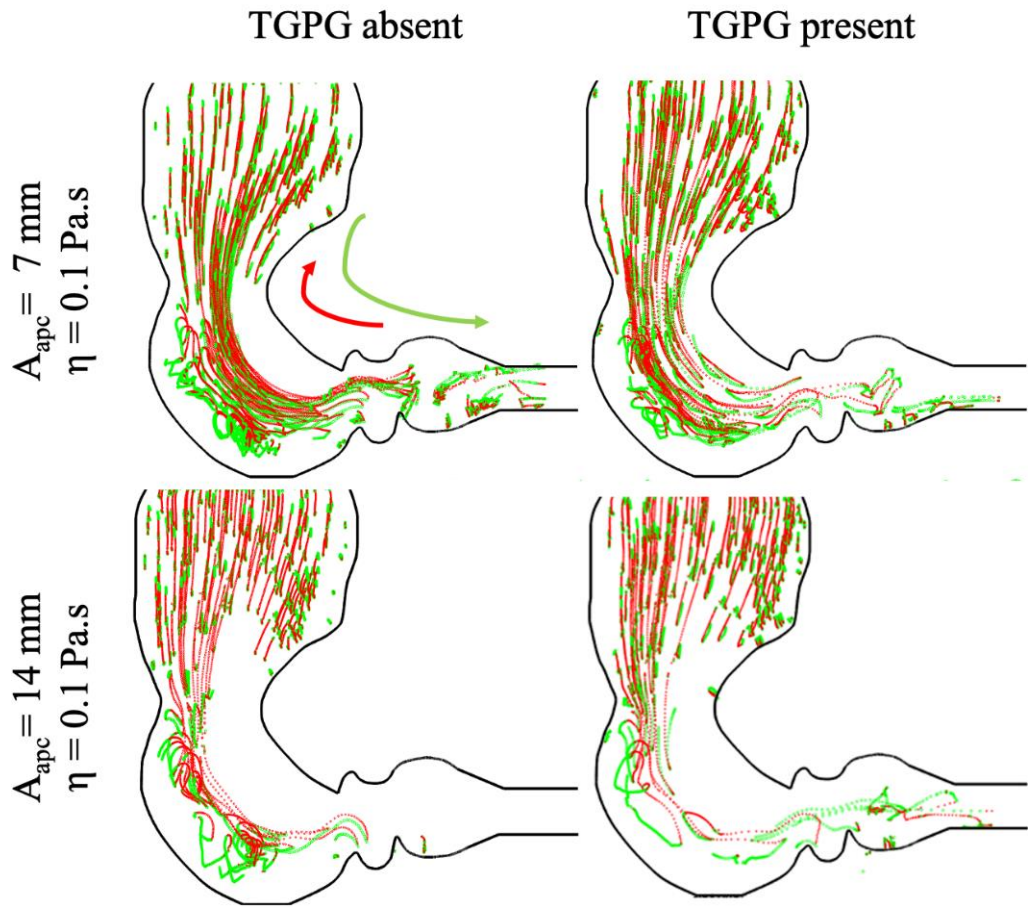

Figure 35. Flow lines within the gastric lumen with two different APC amplitudes. The stomach outlines are solely for anatomical guidance and APCs were present and moving throughout time. A_{apc}, amplitude of APCs. η, the viscosity of the lumen contents.

5.2.2 Flow rate and velocity

The amplitudes and forms of the temporal variations in inflow and outflow (A_{apc} = 1.4 cm) were like those obtained with a lower amplitude of 0.7 cm (Figure 36). The amplitudes of the single pulses in inflow obtained with or without TGPG were similar to those obtained with the lower APC amplitude and viscosity. This suggests that deeper stomach wall contractions may not play a major role in gastric outflow or gastric emptying.

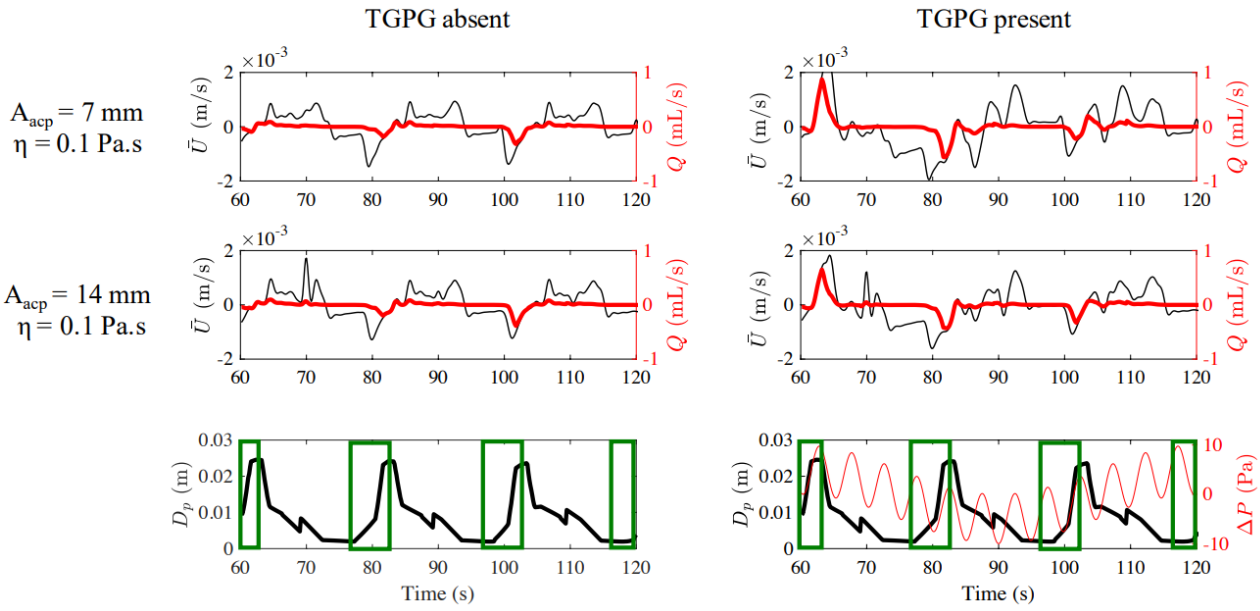

Figure 36. Temporal variation of mean flow velocity $\overline{U}$ (black) and flow rate Q (red) in the duodenum with two different APC amplitudes. Top row: APC amplitude = 0.7 cm. Centre row: APC amplitude = 1.4 cm.

Bottom diagram: Concurrent variation in pyloric diameter (black lines), and the presence of APCs (green rectangle). In the presence of TGPG, the overall pressure difference between the fundus and the duodenum is shown in red, $\Delta P = P_{fundus} - P_{duodenum}$.

5.2.3 Dispersion of groups of markers

Doubling the amplitude of APCs augmented the axial dispersion of markers (Figure 37) in the absence and presence of TGPG. Hence, the markers initially located near the greater curvature were dispersed throughout this curvature after the 60 s of activity. Furthermore, increasing the amplitude of APCs also improved the radial dispersion of groups of markers near the central axis. In sum, an increase in APCs' amplitude appeared to promote advection and radial dispersion of gastric content.

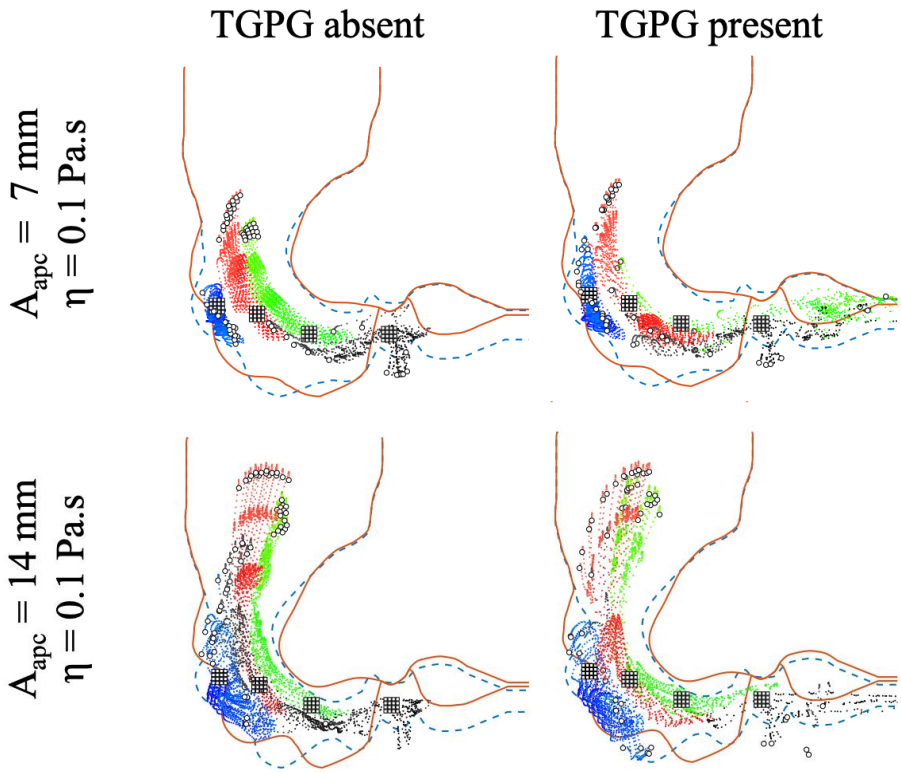

Figure 37. Changes in the cumulative dispersion of clusters of markers located at various sites in the stomach during 60 s of activity with two different APC amplitudes. Top row: APC amplitude = 0.7 cm. Bottom row: APC amplitude = 1.4 cm.

The initial location of the four groups of markers (black, blue, red, green) is shown as squares located at 60 s at various sites in the stomach and pylorus (squares). Their cumulative advection over 60 s is shown by an increase in the intensity of the relevant colour (60 s: dark colour / 120 s: light colour). Circles indicate their final locations. A_{apc}, the amplitude of antral contraction waves. η, the viscosity of the lumen contents. TGPG, an oscillating trans-gastric pressure gradient. The two variations in the position of the walls of the stomach are shown solely for anatomical guidance.

5.2.4 Shear rate

The magnitude and area of the shear rate increased with an increase in APC amplitude, both in the absence and presence of a TGPG (Figure 38). The maximum shear rates developed at various anatomical regions of the stomach when the pylorus was open (57-63 s) were of similar magnitude in both cases. Conversely, when the pylorus was closed (63 -76 s), the magnitude of shear rate was 2-3 times higher with higher APC amplitude than a lower APC amplitude. Trituration of gastric

content due to shear is most likely to happen at the anatomical regions where the shear rate is higher, and from this work, it is most likely at the pylorus.

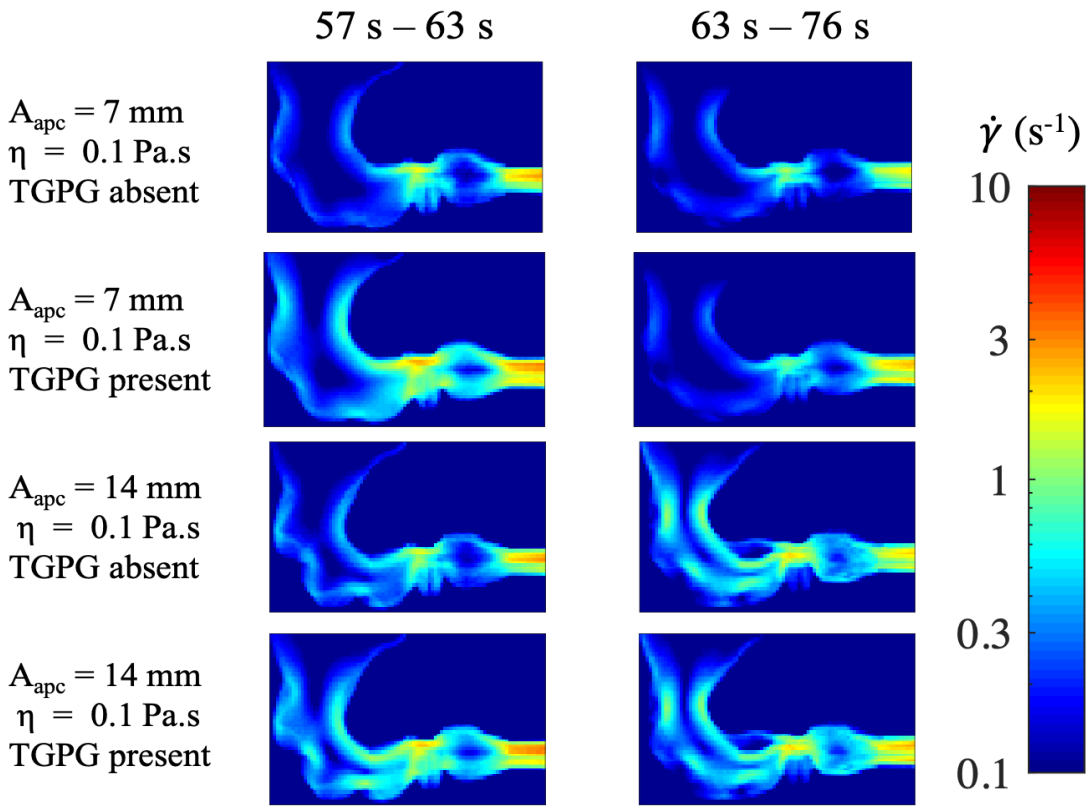

Figure 38. Effect of APC amplitude in spatial patterns of shear rate ($\dot{\gamma}$) within the lumen of the stomach during propagation of APCs with around the time of pyloric opening (57 - 63 s, left column) and pyloric closing (63 -76 s, right column). Top two rows: APC amplitude = 0.7 cm. Bottom two rows: APC amplitude = 1.4 cm. TGPG, trans - gastric pressure gradient.

5.2.5 Summary on the effect of APC amplitude

APC amplitude plays a major role in gastric mixing (as evidenced by the flow lines and the dispersion of particles). Increasing the APC amplitude also increased the shear rate that the particles within the gastric lumen are exposed to, and this might increase the trituration of gastric content (as evidenced by the shear rate plots and shear rate values). However, APC amplitude plays a negligible role in gastric emptying (as evidenced by the flow line and flow velocity plots).

Further, the changes in the dispositions of flow lines suggest that an increase in the amplitudes of APCs, such as could occur with a progressive post-prandial reduction in gastric volume, does not serve to augment shear by promoting vorticeal action at the periphery but by narrowing the width of the stream of axial backflow.

5.3 Effect of doubling viscosity of contents with regular APC

A rheogram study of gastric digesta done on volunteers after ingesting locust bean gum showed a viscosity of 0.1 Pa.s (Marciani *et al*.,2000). Hence a set of simulations were done with the reported viscosity of 0.1 Pa.s and another simulation by doubling the viscosity (0.2 Pa.s) to study the effect of gastric content viscosity in the gastric process.

5.3.1 Flow line

Plots of flow lines with more viscous gastric contents show a reduction in outflow even when a TGPG is present (more red lines than green lines) than those obtained with lower viscosity (Figure 39). However, change in viscosity has no significant effect on the size and extent of vortices formed near the greater curvature.

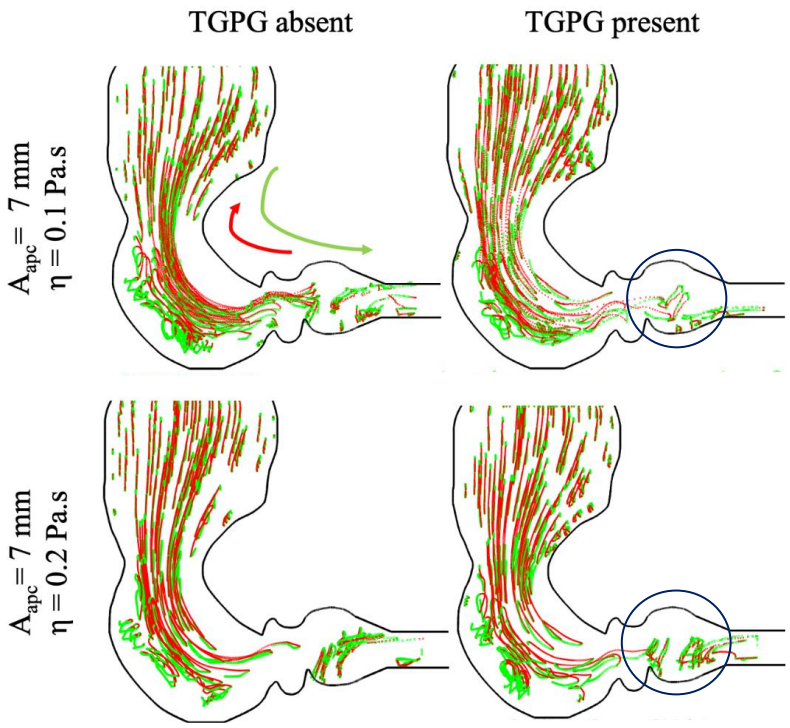

Figure 39. Flow line within the gastric lumen with two different fluid viscosities. The circled area shows the enhanced advection of marker when the viscosity is lower (TGPG present, viscosity 0.1 Pa.s) compared to higher viscous gastric content (TGPG present, viscosity 0.2 Pa.s). An increase in the gastric content viscosity restricts the on flow (green) and the backflow (red)

5.3.2 Flow rate and velocity

The temporal sequences of pulsatile inflow and outflow of the gastric content with a higher viscosity were broadly similar to those with lower viscosity of contents, both in the presence and the absence of a TGPG. In the absence of a TGPG, there was a slight reduction with an increase in viscosity in the magnitude of the single pulse of inflow that was synchronous with the pyloric opening. Similarly, in the presence of a TGPG, there was a slight reduction in the magnitudes of the two peaks in backflow around the time of pyloric opening. Again, both with and without a TGPG, there was a noticeable reduction in the magnitude of the first pulse of outflow coincident with the closing of the pylorus and a slight reduction in the second pulse of outflow on the arrival of an APC.

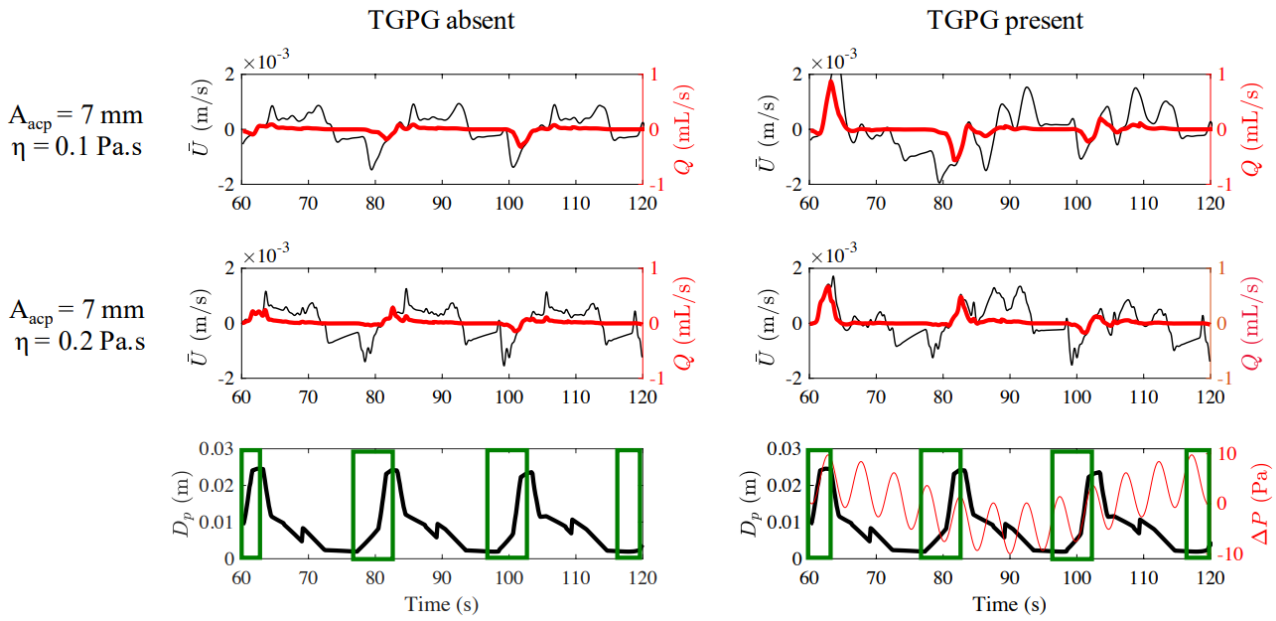

Figure 40. Temporal variation of mean flow velocity U (black) and flow rate Q (red) with two different viscosities. Top row: viscosity = 0.1 Pa.s. Middle row: viscosity = 0.2 Pa.s.

Bottom row: Concurrent variation in pyloric diameter (black lines), and the presence of APCs (green rectangle). In the presence of TGPG, the overall pressure difference between the fundus and the duodenum is shown in red, $\Delta P = P_{fundus} - P_{duodenum}$. TGPG, trans-gastric pressure gradient.

5.3.3 Dispersion of groups of markers

Radial dispersion and advection of markers present in the gastric lumen were reduced in the presence and absence of a TGPG when viscosity was doubled (Figure 41). No outflow of gastric content from the stomach to the duodenum was observed (no green markers are present in the duodenal bulb; Figure 41. Cumulative dispersion of clusters of markers located at various sites in the stomach during 60 s of activity, with two different fluid viscosities. Top row: viscosity = 0.1 Pa.s. Bottom row: viscosity = 0.2 Pa.s. However, a small number of markers (black) present in the pylorus advected to the duodenum.

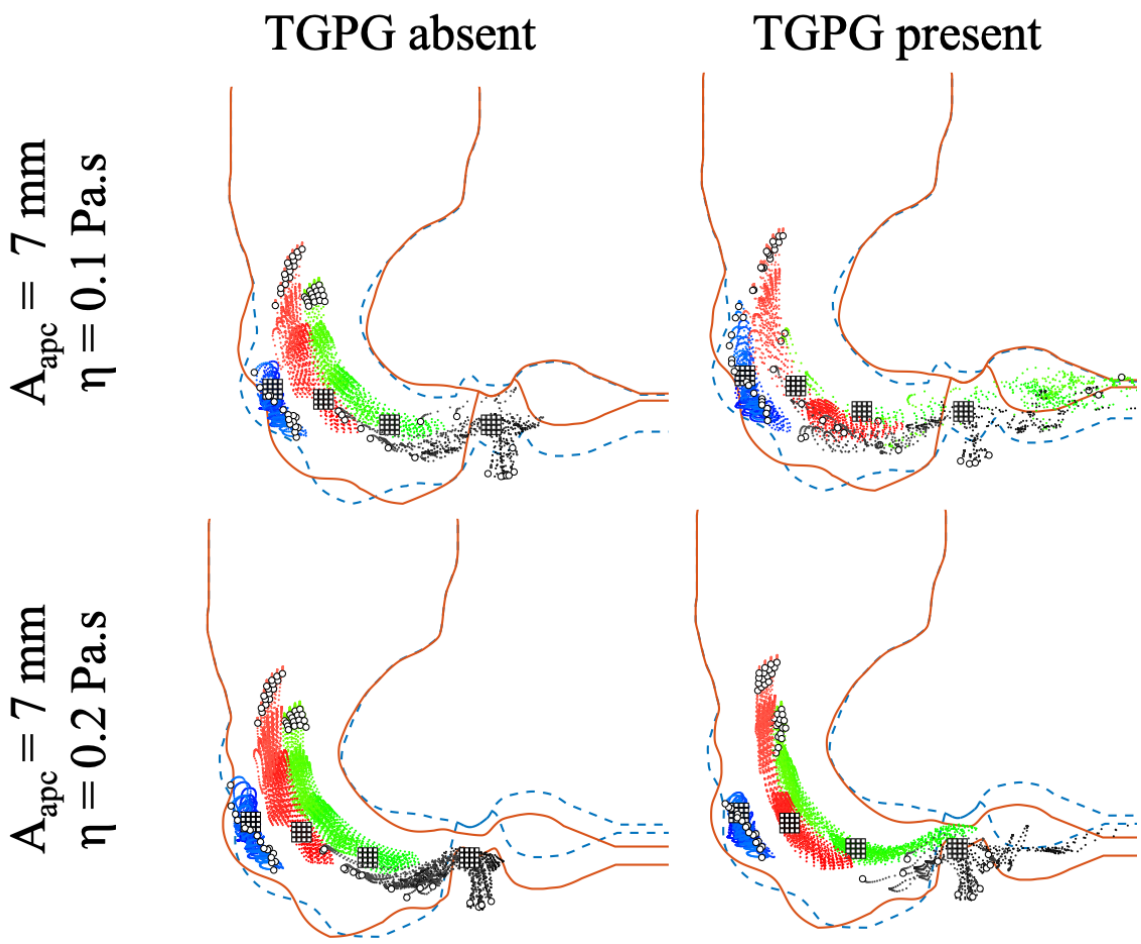

Figure 41. Cumulative dispersion of clusters of markers located at various sites in the stomach during 60 s of activity, with two different fluid viscosities. Top row: viscosity = 0.1 Pa.s. Bottom row: viscosity = 0.2 Pa.s.

The initial location of the four groups of markers (black, blue, red, green) is shown as squares located at 60 s at various sites in the stomach and pylorus (squares). Their cumulative advection over 60 s is shown by an increase in the intensity of the relevant colour (60 s: dark colour / 120 s: light colour), and circles indicate their final locations. A_{apc}, the amplitude of antral contraction waves. μ, the viscosity of the lumen contents. TGPG oscillating trans-gastric pressure gradient. The two variations in the position of the walls of the stomach are shown solely for anatomical guidance.

5.3.4 Shear rate

An increase in the gastric content viscosity reduced the maximal amplitudes of shear rate almost by a factor of 2, both with and without a TGPG (Figure 42).

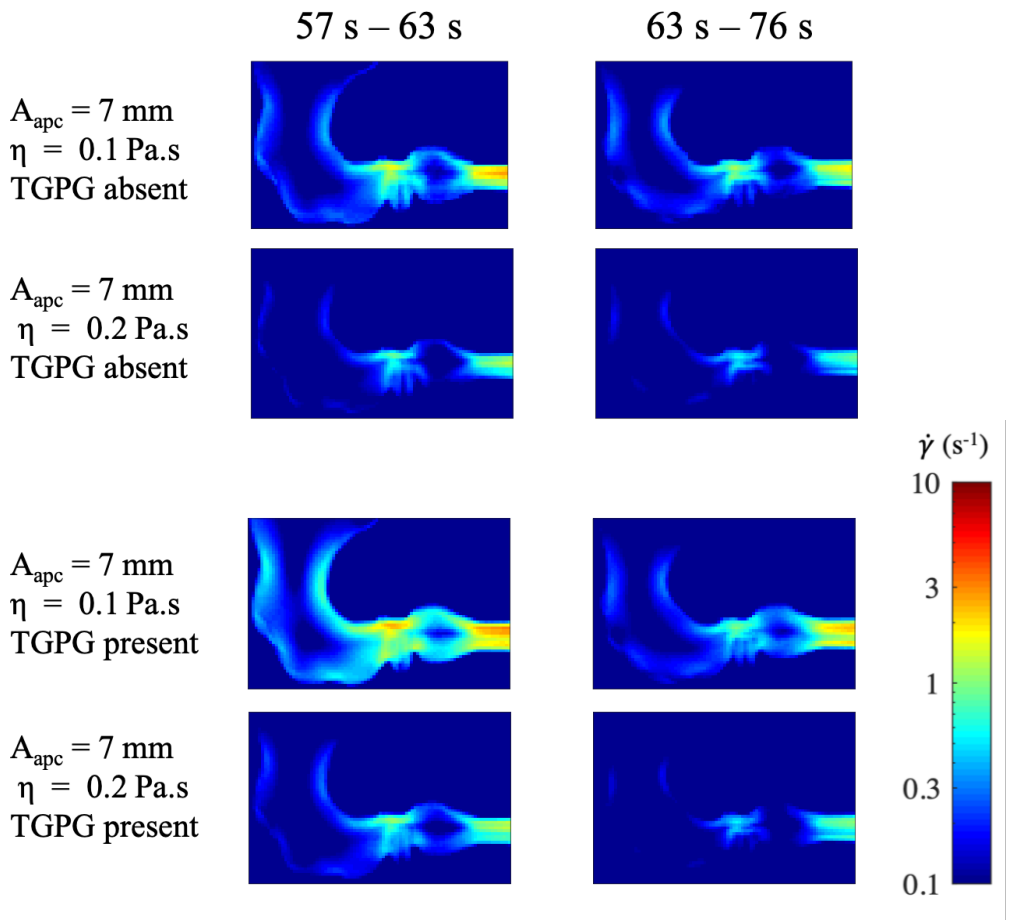

Figure 42. Effect of viscosity on spatial patterns of shear rate ($\dot{\gamma}$)within the lumen of the stomach during propagation of APCs around the time of opening s (57-63 s, left column) and of closing (63-76 s, right column) of the pylorus with two different viscosities. Top set: shows the shear rate in the stomach with two different viscosities (0.1 Pa.s and 0.2Pa.s) when TGPG absent. Bottom set: shows the shear rate in the stomach with two different viscosities (0.1 Pa.s and 0.2Pa.s) when TGPG is present.

5.3.5 Summary of viscosity effects

Even though the gastric wall deformations were modelled, independent of the gastric content properties, the gastric flow (as evidenced by the flow lines and flow rate results), mixing of gastric contents (as evidenced by the dispersion of markers) and the shear rate within the gastric lumen (evidenced by the shear rate plots) were reduced.

5.4 Overall summary of results

According to the results obtained, the trans-gastric pressure gradient (TGPG) plays a major role in gastric emptying. Without imposing a TGPG, the gastric content flow directs away from the duodenum (increased inflow), and hence the content gets mixed inside the gastric lumen but not emptied into the duodenum. Increasing the APCs amplitude narrows the gastric lumen and increases the dispersion and advection of gastric content within the stomach. However, no gastric emptying occurs without a TGPG even if the APC amplitude is doubled. The flow lines suggest that an increase in APC amplitudes increases the shear, not by vorticeal action at the periphery but by narrowing the stream width of axial backflow. The group of markers located around the central axis of the antrum and body have relatively little recirculatory displacement, and mass transport.

Higher shear rates are generated adjacent to the walls of the pylorus and on the tip of the APCs during the period immediately before pyloric closure and during its subsequent reopening. These results also suggest that more excellent shear rates and greater dispersion happen in the antrum during the gastric cycle when the pylorus is open than during the periods when the pylorus is closed. These effects predominate when antral and fundal pressure cycles are in phase, and the overall pressure difference is high. This suggests that trituration and mixing are maximized during these periods. However, these effects are generally reduced when the lumen content is of higher viscosity that likely to occur immediately following the consumption of a meal. Gastric content viscosity plays a significant role in gastric fluid dynamics, and an increase in the gastric content viscosity decreases the outflow and inflow velocity and also the shear rate even in the presence of a high trans-gastric pressure gradient.

Chapter 6: Discussion and conclusions

As far as we know, this is the first work to quantify the gastric shear rates (0.6 s^{-1} - 2.0 s^{-1}) and locate the sites and times at which shear is maximum. Another novelty of this work is that this is the first work to incorporate all unique contractile activities from the fundus to the duodenum in a gastric model. Also, previous gastric models did not investigate the role of TGPG in gastric processes.

Flow line plots show that the flow lines break near the pylorus, and gastric contents were carried back to the gastric chamber and never emptied to the duodenum in the absence of TGPG (refer to Figure 31). This result suggests that the presence of a TGPG, principally generated by rhythmic fundal tonic contractile activity, plays a primary role in gastric emptying (distal gastric outflow). This observation supports the hypothesis suggested by experimental data that the 'pressure pump' is the principal arbiter of gastric outflow (Kelly, 1980) and runs contrary to the view that APCs induce gastric emptying (Indireshkumar *et al*., 2000, Paterson *et al*., 2000). However, Kwiatek *et al*. (2006) reported that APC has no role in the outflow from the stomach, and our results support this finding.

Cumulative dispersion of clusters of markers located at various sites in the stomach shows that APC promotes recirculation and plays a significant role in advection and radial dispersion of gastric content within the gastric lumen but is less involved in gastric emptying. This finding supports Pal *et al*. (2004) regarding the recirculatory flow patterns but disagrees with their argument that APCs promote gastric emptying. Changing the APC amplitude in this work showed that the amplitude of the APC is vital in mixing the gastric content, which is observed by Pat *et al*. (2004) by stating 'occlusion ratio affects mixing. According to the results, an increase in APC's amplitude augments gastric flow and mixing, but APC alone cannot empty the gastric content without a TGPG.

Results show that TGPG and APCs with higher amplitude generate higher shear rates and better dispersion of gastric content during a gastric cycle with an open pylorus. These effects predominate when antral and fundal pressure cycles are in phase, and the overall pressure difference is high.

Higher shear rates are generated adjacent to the pylorus wall and proximal to APCs during the period immediately before pyloric closure and subsequent reopenings. This result suggests that trituration and mixing are maximized during these periods. However, these effects are generally reduced when the lumen content is a higher viscosity, likely after a meal. The proximal and distal extension of the maximum shear rate area when both TGPG and the APCs with higher amplitude indicates the combined effect of tonic contraction of the fundus and the phasic contraction of the antrum maximizes shear rates. Further, the flow lines suggest that an increase in APCs' amplitudes (such as could occur with a progressive postprandial reduction in gastric volume) does not augment the shear by vorticeal action but by narrowing the width of the flow stream.

The markers located in the centre of the flow domain, near the antrum and the body, predominantly undergo axial flow. They are less affected by recirculatory displacement and advection. This observation fits in with the results of a study that tracked the progressive displacement of ferrite particles in the living human stomach (Weitschies *et al*., 2010). These findings fit with the pattern of distribution of ingested food (Groedel, 1924), indicating the axial central 'maganstrasse' (Pal *et al*., 2007) may function principally as a channel for the propulsion of intact ingesta while the shear is accentuated in the periphery promoting mixing and fragmentation.

The quantitative and qualitative results regarding the sequence and volume of trans-pyloric flow are in line with several existing physiological studies. A ‘pendulating’ (pendulating flow is defined as a to-and-fro movement of luminal contents across the pylorus by Hausken *et al*. (1992) distal-ward and proximal flow of digesta through the pylorus are observed in this study. This pendulating motion has been reported in real-time ultrasound studies of the human stomach (King *et al*., 1984), in duplex ultrasonography studies (Hausken *et al*., 1992), and three-dimensional guided digital colour doppler imaging studies (Hausken *et al*., 2001).

The total volumes of pulsatile outflow recorded in this model are broadly within the bounds of those obtained from electromagnetic flowmeter measurements in dogs (Malbert *et al*., 1991; Malbert *et al*., 1992) and those obtained from cats using force transducers (Schulze-Delrieu *et al*., 1998) at between 0.1 and 75 mL/pulse. Flow rate without a TGPG (0.08 mL/s) obtained in this work agrees with Pal *et al*. (2004); however, it is higher in the presence of a TGPG. Also, the viscosity of the content influences the flow rate and gastric fluid dynamics.

The temporal sequence in the flow direction demonstrated in this model, with inflow preceding outflow, was similar to that obtained on real-time ultrasound of human subjects (King *et al*., 1984) (refer to Figure 35). However, it appeared to be the reverse of that received by duplex ultrasonography in human subjects where events were timed in relation to the arrival of an APC at the pylorus (Hausken *et al*., 1992), and duodeno-gastric reflux was reported to follow rather than precede gastroduodenal efflux in the fed state.

It is noteworthy that this model assumed that pyloric contraction was largely synchronous with the arrival of the APCs, as has been shown in several ultrasound studies. However, recent work suggested a degree of asynchrony between APC and the pyloric cycle, which may augment trituration and dispersion (Ishida *et al*., 2019). Nevertheless, the factors that govern such action remain unquantified and hence was not focused in this work.

It has been postulated in other models (Pal *et al*., 2004; Ferrua *et al*., 2010; Imai *et al*., 2013) and by experimental work (Marciani *et al*., 2001, Kong *et al*., 2009) that the shear rates generated within the distal stomach, and proximal duodenum during the gastric cycle, may be sufficient to fragment fragile food particles. However, as Schulze hypothesized (Schulze, 2006), the trituration of more mechanically robust food particles may happen by direct compression. The latter hypothesis is indirectly supported by the work of Marciani, showing that gel beads are fractured with force between 0.53 N and 0.78 N (Marciani *et al*., 2001). The high shear rate in the pylorus obtained in this work supports the likelihood of particulate matter becoming entrapped within the pylorus and undergoing direct compression. Further, the oscillating trans-pyloric flow shown in this study increases particles' probability of being subject to such an action.

This model indicated that the bulk of ongoing macromolecular mixing, represented by axial and radial dispersion of fluid markers, occurred principally in the distal stomach. In the absence of a TGPG, this resulted mainly from the action of APCs. However, a combination of TGPG with APCs maximized gastric dispersion, indicating that mixing is an outcome of both activities. When the pylorus was closed, there was ongoing vorticeal action within the duodenal cap and high shear at the wall, which is likely to contribute to mixing and trituration. This finding was in line with the results from a recently published duodenal mixing model (Dillard *et al*., 2007).

6.1 General Conclusion

Major points concluded from the results:

- Transgastric pressure gradient (TGPG) is the arbiter of gastric emptying.
- APCs narrow the gastric lumen and increase the radial dispersion and advection; however, no gastric emptying occurs without a TGPG. This observation agrees with the findings of Wilbur *et al*. (1973).
- APCs do not contribute to the outflow from the stomach. This finding contrasts with what was previously thought (Houghton et al., 1988, Pal et al., 2004).
- Increased shear rate is observed on the tip of the APC and in the pyloric canal.
- Viscosity does have a role in gastric fluid dynamics. Increasing viscosity decreases the outflow and inflow velocity.
- This work is the first to qualify the shear rates, which is helpful for the novel food and targeted drug delivery system manufacturers.
- This gastric model is the first unified gastric model to incorporate and study the relevance of TGPG.

6.2 Applications

This model can adjust the shear rate by adjusting the fundic-duodenal pressure gradient (TGPG) or increasing the APC amplitude. Thus this model can be adapted to monitor the maximum shear that food or drugs can withstand. This model may be useful in advanced control drug delivery systems like microcapsules, microemulsions (Scheuble *et al*., 2016; Scheuble *et al*., 2018), where researchers try to tune the interfacial properties of such carriers to adapt to the mechanical and physicochemical conditions in the stomach. Since such a system is micro or nano-sized and highly dispersed, it may not change the flow in the stomach, and hence hydrodynamic stress maps obtained from this study can be directly used for assessing such a system. Although this is a unified gastric model, the contractile activities of each anatomic region are independent. This independence makes the model versatile to test various situations, such as gastric paralysis, the effect of funductomy or vagotomy in gastric mixing and flow.

6.3 Recommendations

It is important to note that this current model is two-dimensional and reports only movements within a single stomach plane. Hence, three-dimensional models are required to expand and further validate these findings. A very simplified 3D gastric model is attempted (Ferrua *et al*., 2011), which lacked physiologically relevant events and parameters. The techniques used in creating this model, such as lattice Boltzmann method, can handle 3D complex geometries. The lattice-Boltzmann method is used to solve 3D biological and non-biological (Peng *et al*., 2004; Iglberger *et al*., 2008; Mösges *et al*.,2010; Rinaldi *et al*., 2012; Zu *et al*., 2014b) scenarios. However, the time efficiency of LBM in a 3D complex geometry like a stomach needs to be studied.

This work has not incorporated the complex fundic physical motility patterns because the fundic motility is patchy, rhythmic, and alternates locally (Lind *et al*., 1961; Lentle *et al*., 2016). Since modelling of fundic activity would take longer than the stipulated time, it was decided to introduce the fundic pressure wave rather than modelling the fundic wall motility pattern. Moreover, it was assumed that the pyloric canal undergoes active dilatation and is not sensitive to pressure forces acting on it.

This current work did not explore the effect of the reported pseudo-plasticity of gastric chyme (Lentle *et al*., 2002, Patarin *et al*., 2015) nor the direct effects of the various contractile processes on suspended particulate matter (Hardacre *et al*., 2018). A change in fluid viscosity from 0.1 Pa.s to 0.2 Pa.s doubled the simulation time and generated around 4 GB of data. Considering the time required to simulate and for post-processing data, we decided to abstain from non-Newtonian fluids. The development of a basic unified gastric model that works and provides some qualitative information was the focus of this work, and we are successful in that regard. This model can be used as a base model can be modified to simulate the gastric fluid dynamics with more rheologically realistic fluid.

Chapter 7: References

Adil, E., Bharucha, M.C., 2005 (4th edition). Management of gut dysmotility, Peripheral neuropathy. https://doi.org/10.1016/B978-0-7216-9491-7.50124-1

Aidun, C. K. , Clausen, J. R. 2010. Lattice -Boltzmann Method for Complex Flows. Annual Review of Fluid Mechanics, 42, 439-472. Available: 10.1146/annurev-fluid-121108-145519

Al-Shboul, O. A. 2013. The Importance of Interstitial Cells of Cajal in the Gastrointestinal Tract. Saudi Journal of Gastroenterology: Official Journal of the Saudi Gastroenterology Association, 19, 3-15. Available: 10.4103/1319-3767.105909

Alokaily S, Feigl K, Tanner F.2019. Characterization of peristaltic flow during the mixing process in a model human stomach. Phys. Fluids 31. https://doi.org/10.1063/1.5122665

Anandharamakrishnan, C. 2013. CFD Modelling of Biological Systems with Human Interface. In: SpringerBriefs in Food, H., and Nutrition (ed.) Computational Fluid Dynamics Applications in Food Processing. New York, NY: Springer.

Anvari, M., Myers, J., Malbert, C., Horowitz, M., Dent, J., Jamieson, G. 2000. Antral compensation after proximal gastric vagotomy. Journal of Gastrointestinal Surgery, 4, 526-530.

Aoki, S., Uesugi, K., Tatsuishi, K., Ozawa, H., Kayano, M. 1992. Evaluation of the correlation between in vivo and in vitro release of phenylpropanolamine HCl from controlled-release tablets. International journal of pharmaceutics, 85, 65-73.

Ashford, M. 2002. Gastrointestinal tract- physiology and drug absorption. In: Michael E. Aulton, K. M. G. T. (ed.) Aulton's Pharmaceutics: The Design and Manufacture of Medicines. Edinburg: Elsevier.

Azpiroz, F, Malagelada, J. 1984. Pressure activity patterns in the canine proximal stomach: response to distension. American Journal of Physiology-Gastrointestinal and Liver Physiology, 247, G265-G272.

Azpiroz, F, Malagelada, J. R. 1985. Physiological variations in canine gastric tone measured by an electronic barostat. American Journal of Physiology-Gastrointestinal and Liver Physiology, 248, G229-G237. Available: 10.1152/ajpgi.1985.248.2.G229

Azpiroz F, Malagelada J.R. 1987. Gastric Tone Measured by an Electronic Barostat in Health arid Postsurgical Gastroparesis. Gastroenterology.;92(4):934-43.

Bao, Y. B., Meskas, J. 2011. Lattice-Boltzmann Method for Fluid Simulations. Available:http://www.cims.nyu.edu/~billbao/report930.pdf.

Barnes HA, H. J., Walters K 1989. An introduction to rheology, Amsterdam, Elsevier.

Barrett, K. E., Boitano, S., Barman, S. M., Brooks, H. L. 2010. Ganong's review of medical physilogy, New York, McGraw-Hill.

Barton, J. H., Emanuel, E. J. 2005. The Patents-Based Pharmaceutical Development ProcessRationale, Problems, and Potential Reforms. JAMA, 294, 2075-2082. Available: 10.1001/jama.294.16.2075

Bateman, D. N., Whittingham, T. A. 1982. Measurement of gastric emptying by real-time ultrasound. Gut, 23, 524-527. Available: 10.1136/gut.23.6.524

Bauer, A. J., Publicover, N. G. , Sanders, K. M. 1985. Origin and spread of slow-waves in canine gastric antral circular muscle. American Journal of Physiology-Gastrointestinal and Liver Physiology, 249, G800-G806. Available: 10.1152/ajpgi.1985.249.6.G800

Bennett, M. V. L., Barrio, L. C., Bargiello, T. A., Spray, D. C., Hertzberg, E. , Sáez, J. C. 1991. Gap junctions: New tools, new answers, new questions. Neuron, 6, 305-320. Available: https://doi.org/10.1016/0896-6273(91)90241-Q

Berry, R., Miyagawa, T., Paskaranandavadivel, N., Du, P., Angeli, T. R., Trew, M. L., Windsor, J. A., Imai, Y., O'Grady, G., Cheng, L. K. 2016. Functional physiology of the human terminal antrum defined by high-resolution electrical mapping and computational Modelling. American Journal of Physiology-Gastrointestinal and Liver Physiology, 311, G895-G902. Available: 10.1152/ajpgi.00255.2016

Berthoud, H.R., Hennig, G., Campbell, M., Volaufova, J., Costa, M. 2002. Video-based spatio-temporal maps for analysis of gastric motility in vitro: effects of vagal stimulation in guinea-pigs. Neurogastroenterology , Motility, 14, 677-688. Available: 10.1046/j.1365-2982.2002.00369.x

Blair, P. J., Rhee, P.-L., Sanders, K. M., Ward, S. M. 2014. The Significance of Interstitial Cells in Neurogastroenterology. jnm, 20, 294-317. Available: 10.5056/jnm14060

Blanquet, S., Zeijdner, E., Beyssac, E., Meunier, J.-P., Denis, S., Havenaar, R. , Alric, M. 2004. A dynamic artificial gastrointestinal system for studying the behaviour of orally administered drug dosage forms under various physiological conditions. Pharmaceutical research, 21, 585-591.

Bohr, D. F. 1964. Electrolytes and smooth muscle contraction. Pharmacological reviews, 16, 85-111.

Bornstein, J. C., Costa, M. , Grider, J. R. 2004. Enteric motor and interneuronal circuits controlling motility. Neurogastroenterology, Motility, 16, 34-38. Available: 10.1111/j.1743-3150.2004.00472.x.

Boulby, P., Moore, R., Gowland, P., Spiller, R. C. 1999. Fat delays emptying but increases forward and backward antral flow as assessed by flow-sensitive magnetic resonance imaging. Neurogastroenterology and motility: the official journal of the European Gastrointestinal Motility Society, 11, 27-36. Available: 10.1046/j.1365-2982.1999.00133.x.

Bouzidi Mh, Firdaouss M, Lallemand P. Momentum transfer of a Boltzmann-lattice fluid with boundaries. Physics of fluids. 2001;13(11):3452-9.

Boyd, J., Buick, J., Cosgrove, J. A., Stansell, P. 2005. Application of the lattice-Boltzmann model to simulated stenosis growth in a two-dimensional carotid artery. Physics in Medicine and Biology, 50, 4783-4796. Available: 10.1088/0031-9155/50/20/003.

Brookes, S. J. H., Spencer, N. J., Costa, M. , Zagorodnyuk, V. P. 2013. Extrinsic primary afferent signalling in the gut. Nature Reviews Gastroenterology, Hepatology, 10, 286-296. Available: 10.1038/nrgastro.2013.29.

Brown, B. P., Schulze-Delrieu, K., Schrier, J. E. , Abu-Yousef, M. M. 1993. The configuration of the human gastroduodenal junction in the separate emptying of liquids and solids. Gastroenterology, 105, 433-440. Available: 10.5555/uri:pii:001650859390717Q.

Bueno, L., Fioramonti, J. , Ruckebusch, Y. 1975. Rate of flow of digesta and electrical activity of the small intestine in dogs and sheep. The Journal of Physiology, 249, 69-85. Available: 10.1113/jphysiol.1975.sp011003.

Burns, W. E. 2004. Jan Bondeson. The Two-Headed Boy and Other Medical Marvels. xxii + 295 pp., illus., figs., bibl. Ithaca, N.Y.: Cornell University Press, 2000. $29.95. Isis, 95, 121-121.

Camilleri, M., Malagelada, J. R., Brown, M. L., Becker, G. , Zinsmeister, A. R. 1985. Relation between antral motility and gastric emptying of solids and liquids in humans. American Journal of Physiology-Gastrointestinal and Liver Physiology, 249, G580-G585. Available: 10.1152/ajpgi.1985.249.5.G580.

Camilleri M, Brown ML, Malagelada J.R. 1986. Relationship between impaired gastric emptying and abnormal gastrointestinal motility. Gastroenterology. 91(1):94-9.

Camilleri M. 2006.Integrated upper gastrointestinal response to food intake. Gastroenterology. 2006.131(2):640-58.

Campbell, G. 1966. The inhibitory nerve fibres in the vagal supply to the guinea-pig stomach. The Journal of Physiology, 185, 600-612. Available: 10.1113/jphysiol.1966.sp008004.

Cannon, W. B. 1898. The movements of the stomach studied by means of the Roentgen rays. Am. J. Physiol, 1, 359-382.

Casteels, R., Kuriyama, H. 1966. Membrane potential and ion content in the smooth muscle of the guinea-pig's taenia coli at different external potassium concentrations. The Journal of Physiology, 184, doi: 10.1113/jphysiol.1966.sp007906.

Chen, J. Y., Chang, W. C. 1998. Modelling Differential Diffusion Effects in Turbulent Nonreacting/Reacting Jets with Stochastic Mixing Models. Combustion Science and Technology, 133, 343-375. Available: 10.1080/00102209808952039.

Chen, S., Doolen, G. D. 1998. Lattice-Boltzmann method for fluid flows. Annual Review of Fluid Mechanics, 30, 329-364. Available: 10.1146/annurev.fluid.30.1.329.

Cheng, L. K., Farrugia, G. 2013. New Advances in Gastrointestinal Motility Research. In: Cheng, K. L., Pullan, J. A. , Farrugia, G. (eds.) New Advances in Gastrointestinal Motility Research. Dordrecht: Springer Netherlands. Available: 10.1007/978-94-007-6561-0_1.

Cheng, L. K., Komuro, R., Austin, T. M., Buist, M. L., Pullan, A. J. 2007. Anatomically realistic multiscale models of normal and abnormal gastrointestinal electrical activity. World Journal of Gastroenterology, 13, 1378-1383.

Christensen, J., Glover, J. R., Macagno, E. O., Singerman, R. B. , Weisbrodt, N. W. 1971. Statistics of contractions at a point in the human duodenum. The American journal of physiology, 221, 1818-1823. Available: 10.1152/ajplegacy.1971.221.6.1818.

Code, C. H. 1968. Motor activity of the stomach. Handbook of Physiology ~ Alimentary Canal IV. Washington, DC: American Physiological Society.

Cooper, G. 2000. Actin, Myosin, and Cell Movement. In: 2 (ed.) The Cell: A Molecular Approach. Sunderland (MA): Sinauer Associates.

Corrias, A., Buist, M. L. 2007. A Quantitative Model of Gastric Smooth Muscle Cellular Activation. Annals of Biomedical Engineering, 35, 1595-1607. Available: 10.1007/s10439-007-9324-8.

Craig, R., Megerman, J. 1977. Assembly of smooth muscle myosin into side-polar filaments. The Journal of cell biology, 75, 990-996.

Cristensen,H., Gregersen, J. 2000. Gastro Intestinal Tone. Neurogastroenterol.Mot, 501-508.

Dabrowska, R., Hinkins, S., Walsh, M. P. , Hartshorne, D. J. 1982. The binding of smooth muscle myosin light chain kinase to actin. Biochemical and Biophysical Research Communications, 107, 1524-1531. Available: https://doi.org/10.1016/S0006-291X(82)80172-1.

Daniel, E. E., Wang, Y.-F. 1999. Gap junctions in intestinal smooth muscle and interstitial cells of Cajal. Microscopy Research and Technique, 47, 309-320. Available: 10.1002/(sici)1097-0029(19991201)47:5<309::Aid-jemt2>3.0.Co;2-k.

Daniel, B. I. 1992. Interstitial cells of Cajal: are they major players in control of gastrointestinal motility? Neurogastroenterology, Motility, 4, 1-24. Available: 10.1111/j.1365-2982.1992.tb00074.x.

Deloose, E., Janssen, P., Depoortere , Tack, J. 2012. The migrating motor complex: control mechanisms and its role in health and disease. Nat Rev Gastroenterol Hepatol., 271-285.

De Loubens C, Lentle RG, Hulls C, Janssen PWM, Love RJ, Chambers JP. 2014. Characterisation of mixing in the proximal duodenum of the rat during longitudinal contractions and comparison with a fluid mechanical model based on spatiotemporal motility data. PLoS ONE.9(4).

De Loubens. C, Lentle R.G, Love R.J, Hulls. C, Janssen P.W.M. 2013. Fluid mechanical consequences of pendular activity, segmentation and pyloric outflow in the proximal duodenum of the rat and the guinea pig. Journal of the Royal Society Interface. 10(83).

Dickens, E. J., Hirst, G. D. S. & Tomita, T. 1999. Identification of rhythmically active cells in guinea-pig stomach. Journal of Physiology-London, 514, 515-531. Available: DOI 10.1111/j.1469-7793.1999.515ae.x.

Dikeman, C. L., Fahey, G. C. 2006. Viscosity as Related to Dietary Fiber: A Review. Critical Reviews in Food Science and Nutrition, 46, 649-663. Available: 10.1080/10408390500511862.

Dikeman, C. L., Barry, K. A., Murphy, M. R., Fahey, G. C. 2007. Diet and measurement techniques affect small intestinal digesta viscosity among dogs. Nutrition Research, 27, 56-65. Available: https://doi.org/10.1016/j.nutres.2006.12.005.

Dikeman, C. L., Murphy, M. R., Fahey, G. C. 2006. Dietary fibers affect viscosity of solutions and simulated human gastric and small intestinal digesta. The Journal of nutrition, 136, 913-919.

Dikeman C. L, Fahey GC. Viscosity as Related to Dietary Fiber: A Review. 2006. Crit Rev Food Sci Nutr.;46(8):649-63.

Dikeman CL, Murphy MR, Fahey GC. Food intake and ingredient profile affect viscosity of ileal digesta of dogs. J Anim Physiol Anim Nutr. 2007;91(3-4):130-8.

Dillard, S., Krishnan, S., Udaykumar, H. S. 2007. Mechanics of flow and mixing at antroduodenal junction. World journal of gastroenterology, 13, 1365-1371. Available: 10.3748/wjg.v13.i9.1365.

Dooley, C. P., Reznick, J. B., Valenzuela, J. E. 1985. A continuous manometric study of the human pylorus. Gastroenterology, 89, 821-826. Available: https://doi.org/10.1016/0016-5085(85)90578-5.

Du, P., O'Grady, G., Gao, J., Sathar, S. , Cheng, L. K. 2013. Toward the virtual stomach: progress in multiscale Modelling of gastric electrophysiology and motility. WIREs Systems Biology and Medicine, 5, 481-493. Available: 10.1002/wsbm.1218.

Edwards D.A. 1961, Physiological concepts of the pylorus. Proc R Soc Med. Nov.54:930–933.

Edwards, F. R., Hirst, G. D. S. 2006. An electrical analysis of slow-wave propagation in the guinea-pig gastric antrum. The Journal of Physiology, 571, 179-189. Available: 10.1113/jphysiol.2005.100743.

Eslam Ezzatneshan 2019, Comparative study of the lattice Boltzmann collision models for simulation of incompressible fluid flows, Mathematics and Computers in Simulation, 156, 158-177.

Ehrlein, H., Schemann, M. 2005. Gastrointestinal motility. Technische Universität München: Munich.

Faas, H., Hebbard, G. S., Feinle, C., Kunz, P., Brasseur, J. G., Indireshkumar, K., Dent, J., Boesiger, P., Thumshirn, M., Fried, M. , Schwizer, W. 2001. Pressure-geometry relationship in the antroduodenal region in humans. American Journal of Physiology-Gastrointestinal and Liver Physiology, 281, G1214-G1220. Available: 10.1152/ajpgi.2001.281.5.G1214

Ferrua, M. J., Singh, R. P. 2010. Modelling the Fluid Dynamics in a Human Stomach to Gain Insight of Food Digestion. Journal of Food Science, 75, R151-R162. Available: 10.1111/j.1750-3841.2010.01748.x.

Ferrua, M. J., Kong, F., Singh, R. P. 2011. Computational Modelling of gastric digestion and the role of food material properties. Trends in Food Science, Technology, 22, 480-491. Available: https://doi.org/10.1016/j.tifs.2011.04.007.

Fischer, W., Pfitzer, G. 1989. Rapid myosin phosphorylation transients in phasic contractions in chicken gizzard smooth muscle. FEBS Letters, 258, 59-62. Available: 10.1016/0014-5793(89)81615-1.

Forte, J. G. 1996. Gastric Function. In: Greger, R., Windhorst, U. (eds.) Comprehensive Human Physiology: From Cellular Mechanisms to Integration. Berlin, Heidelberg: Springer Berlin Heidelberg. Available: 10.1007/978-3-642-60946-6_62.

Funakoshi, M. 2008. Chaotic mixing and mixing efficiency in a short time. Fluid Dyn Res, 40, 1–33.

Furness, J. B., Callaghan, B. P., Rivera, L. R., Cho, H.-J. 2014. The Enteric Nervous System and Gastrointestinal Innervation: Integrated Local and Central Control. In: Lyte, M. , Cryan, J. F. (eds.) Microbial Endocrinology: The Microbiota-Gut-Brain Axis in Health and Disease. New York, NY: Springer New York. Available: 10.1007/978-1-4939-0897-4_3.

Furness, J. B. 2006. The Enteric Nervous System, Massachusetts, Blackwell Publishing.

Furness, J. B. 2009. In: Squire, L. R. (ed.) Encyclopedia of Neuroscience. Oxford: Academic Press. Available: https://doi.org/10.1016/B978-008045046-9.01990-2.

Garrett, D. A., Failla, M. L., Sarama, R. J. 1999. Development of an in Vitro Digestion Method To Assess Carotenoid Bioavailability from Meals. Journal of Agricultural and Food Chemistry, 47, 4301-4309. Available: 10.1021/jf9903298.

Gerthoffer, W. T. 1991. Regulation of the contractile element of airway smooth muscle. American Journal of Physiology-Lung Cellular and Molecular Physiology, 261, L15-L28. Available: 10.1152/ajplung.1991.261.2.L15.

Gleysteen, J. J., Sarna, S. K. , Myrvik, A. L. 1988. Truncal vagotomy as a possible potentiator of gastric atony. The American Journal of Surgery, 155, 199-205. Available: https://doi.org/10.1016/S0002-9610(88)80693-7.

Goodarzi, M., Safaei, M., Karimipour, A., Hooman, K., Dahari, M., Kazi, S., Sadeghinezhad, E. Comparison of the finite volume and lattice -Boltzmann methods for solving natural convection heat transfer problems inside cavities and enclosures. Abstract and Applied Analysis, 2014. Hindawi Publishing Corporation.

Gregersen H. 2003.B Biomechanics of the gastrointestinal tract: new perspectives in motility research and diagnostics. New York: Springer Verlag.

Groedel, F. 1924. Die Roentgenuntersuchung des Magens Roentgendiagnostik in der Inneren Medizin. Munich: Lehmann Verlag. p. 502-5.

Groedel,F 1909. Atlas und Grundriss der Roentgendiagnostik in der Innere Medizin. Archives of The Roentgen Ray, 14, 228-229. Available: 10.1259/arr.1909.14.0103.

Gunawardene, A. R., Corfe, B. M., Staton, C. A. 2011. Classification and functions of enteroendocrine cells of the lower gastrointestinal tract. International Journal of Experimental Pathology, 92, 219-231. Available: 10.1111/j.1365-2613.2011.00767.x.

Guo, Z., Shu, C. 2013. Lattice -Boltzmann method and its applications in engineering, World Scientific.

Guo Z, Shi B, Wang N. 2000.Lattice BGK model for incompressible Navier–Stokes equation. Journal of Computational Physics. 165(1):288-306.

Guo Z. L, Zheng CG, Shi BC. 2002. Non-equilibrium extrapolation method for velocity and pressure boundary conditions in the lattice Boltzmann method. Chinese Physics.11(4):366-74.

Hanani, M., Farrugia, G., Komuro, T. 2005. Intercellular coupling of interstitial cells of Cajal in the digestive tract. In: Jeon, K. W. (ed.) International Review of Cytology - a Survey of Cell Biology, Vol. 242. San Diego: Elsevier Academic Press Inc.

Hansen, M. B. 2003. Neurohumoral Control of Gastrointestinal Motility. Physiol. Res., 1-52.

Hao, S., Wang, B., Wang, Y. 2015. Density-dependent gastro retentive microparticles motion in human gastric emptying studied using computer simulation. European Journal of Pharmaceutical Sciences, 70, 72-81.

Hardacre A. K, Lentle, R.G, Yap S.-Y, Monro JA. 2018. Predicting the viscosity of digesta from the physical characteristics of particle suspensions using existing rheological models. J R Soc Interface. 15(142):20180092.

Hardy, J., Pomeau, Y. , Pazzis, O. d. 1973. Time evolution of a two-dimensional model system. I. Invariant states and time correlation functions. Journal of Mathematical Physics, 14, 1746-1759. Available: 10.1063/1.1666248.

Harrison SM, Cleary PW, Sinnott MD. 2018. Investigating mixing and emptying for aqueous liquid content from the stomach using a coupled biomechanical-SPH model. Food Funct. 9(6):3202-19.

Hashitani, H., Garcia-Londoño, A. P., Hirst, G. D. S., Edwards, F. R. 2005. A typical slow-waves generated in gastric corpus provide dominant pacemaker activity in guinea pig stomach. The Journal of Physiology, 569, 459-465. Available: 10.1113/jphysiol.2005.097907.

Hasler, W. L. 2003. Physiology of gastric motility and gastric emptying. In: Yamada T, Alpers DH, K. N., Laine L, Owyang C, Powel DW (eds.) Textbook of Gastroenterology. Philadelphia: Lippincott, Williams, Wilkins.

Hausken, T., Li, X. N., Goldman, B., Leotta, D., Ødegaard, S. , Martin, R. W. 2001. Quantification of gastric emptying and duodenogastric reflux stroke volumes using three-dimensional guided digital colour Doppler imaging. European Journal of Ultrasound, 13, 205-213. Available: https://doi.org/10.1016/S0929-8266(01)00134-3.

Hausken, t., Mundt, m. , Samsom, m. 2002. Low antroduodenal pressure gradients are responsible for gastric emptying of a low-caloric liquid meal in humans. Neurogastroenterology, Motility, 14, 97-105. Available: 10.1046/j.1365-2982.2002.00307.x.

Hausken, T., Ødegaard, S., Matre, K. , Berstad, A. 1992. Antroduodenal motility and movements of luminal contents studied by duplex sonography. Gastroenterology, 102, 1583-1590. Available: https://doi.org/10.1016/0016-5085(92)91717-I.

Hellström, P. M., Grybäck, P., & Jacobsson, H. (2006). The physiology of gastric emptying. Best practice & research. Clinical anaesthesiology, 20(3), 397–407. https://doi.org/10.1016/j.bpa.2006.02.002.

Hirst, G. D. , Redwards, F. 2006. Electrical events underlying organized myogenic contractions of the guniea pig stomach. J. Physil, 659-665.

Hirst, G. D. S., Garcia-Londoño, A. P. , Edwards, F. R. 2006. Propagation of slow-waves in the guinea-pig gastric antrum. The Journal of physiology, 571, 165-177. Available: 10.1113/jphysiol.2005.100735.

Hoebler, C., Lecannu, G., Belleville, C., Devaux, M. F., Popineau, Y. , Barry, J. L. 2002. Development of an in vitro system simulating bucco-gastric digestion to assess the physical and chemical changes of food. Int J Food Sci Nutr, 53, 389-402. Available: 10.1080/0963748021000044732.

Holt, S., Cervantes, J., Wilkinson, A. A., Wallace, J. H. K. 1986. Measurement of gastric emptying rate in humans by real-time ultrasound. Gastroenterology, 90, 918-923. Available: https://doi.org/10.1016/0016-5085(86)90868-1.

Hooper, S. L., Hobbs, K. H., Thuma, J. B. 2008. Invertebrate muscles: Thin and thick filament structure; molecular basis of contraction and its regulation, catch and asynchronous muscle. Progress in Neurobiology, 86, 72-127. Available: https://doi.org/10.1016/j.pneurobio.2008.06.004

Horowitz, A., Menice, C. B., Laporte, R. , Morgan, K. G. 1996. Mechanisms of smooth muscle contraction. Physiological reviews, 76, 967-1003.

Houghton, L. A., Read, N. W., Heddle, R., Horowitz, M., Collins, P. J., Chatterton, B., Dent, J. 1988. Relationship of the motor activity of the antrum, pylorus, and duodenum to gastric emptying of a solid-liquid mixed meal. Gastroenterology, 94, 1285-1291. Available: 10.5555/uri:pii:0016508588906658.

Huizinga, J. D., Chen, J.-H. 2014. Interstitial cells of Cajal: update on basic and clinical science. Current gastroenterology reports, 16, 1-11.

Huizinga, J. D., Lammers, W. J. E. P. 2009. Gut peristalsis is governed by a multitude of cooperating mechanisms. Am J Physiol Gastrointest Liver Physiol, G1-8.

Huizinga, J. D. 2001. II. Gastric motility: lessons from mutant mice on slow-waves and innervation. American Journal of Physiology-Gastrointestinal and Liver Physiology, 281, G1129-G1134. Available: 10.1152/ajpgi.2001.281.5.G1129.

Hunt, J. N., Spurrell, W. R. 1951. The pattern of emptying of the human stomach. The Journal of Physiology, 113, 157-168. Available: 10.1113/jphysiol.1951.sp004562.

Hunt, J. N. 1949. The simultaneous estimation of the absorption of water and sulphaguanidine from the stomach of man. The Journal of physiology, 109, 134-141. Available: 10.1113/jphysiol.1949.sp004377.

Iglberger, K., Thürey, N., Rüde, U. 2008. Simulation of moving particles in 3D with the Lattice - Boltzmann method. Computers and Mathematics with Applications, 55, 1461-1468. Available: https://doi.org/10.1016/j.camwa.2007.08.022.

Imai, Y., Kobayashi, I., Ishida, S., Ishikawa, T., Buist, M., Yamaguchi, T. 2013. Antral recirculation in the stomach during gastric mixing. American Journal of Physiology - Gastrointestinal and Liver Physiology, 304, G536-G542. Available: 10.1152/ajpgi.00350.2012.

Indireshkumar, K., Brasseur, J. G., Faas, H., Hebbard, G. S., Kunz, P., Dent, J., Feinle, C., Li, M., Boesiger, P., Fried, M. 2000. Relative contributions of “pressure pump” and “peristaltic pump” to gastric emptying. American Journal of Physiology-Gastrointestinal and Liver Physiology, 278, G604-G616.

Indireshkumar K, Brasseur JG, Faas H, Hebbard GS, Kunz P, Dent J, *et al*. Relative contributions of ”pressure pump” and ”peristaltic pump” to gastric emptying. Am J Physiol. 2000;278(4):G604-16.

Ishida, S., Miyagawa, T., O'Grady, G., Cheng, L. K. , Imai, Y. 2019. Quantification of gastric emptying caused by impaired coordination of pyloric closure with antral contraction: a simulation study. Journal of The Royal Society Interface, 16, 20190266. Available: doi:10.1098/rsif.2019.0266.

Itoh T, Higuchi T, Gardner CR, Caldwell L. 1986. Effect of particle size and food on gastric residence time of non-disintegrating solids in beagle dogs. J Pharm Pharmacol.38(11):801-6.

James F, S. 1996. Rheological Methods In Food Process Engineering, freeman Press.

Janssen, Lentle, R. G. , M, P. W. 2011. The Physical process of Digestion, Newyork, Springer.

Katschinski, M., J Schirra, C. B., Langbein, S., Wank, U., D'amato, M. , Arnold, R. 1996. Intestinal phase of human antro-pyloro-duodenal motility: cholinergic and CCK-mediated regulation. European Journal of Clinical Investigation, 574-583.

Keet Jr, A. 1962. Diameter of the pyloric aperture in relation to the contraction of the canalis egestorius. Acta radiologica, 57, 31-44.

Keinke, O., Ehrlein, H.J. 1983. Effect of oleic acid on canine gastroduodenal motility, pyloric diameter and gastric emptying. Quarterly journal of experimental physiology, 68, 675-686. Available: 10.1113/expphysiol.1983.sp002757.

Kelly, K. A. 1980. Gastric emptying of liquids and solids: roles of proximal and distal stomach. American Journal of Physiology-Gastrointestinal and Liver Physiology, 239, G71-G76. Available: 10.1152/ajpgi.1980.239.2.G71.

Kelly, L. 2004. The digestive system. Essentials of Human Physiology for Pharmacy. CRC Press. Available: doi:10.1201/9780203495339.ch18.

Kimura, K., Ito, M., Amano, M., Chihara, K., Fukata, Y., Nakafuku, M., Yamamori, B., Feng, J., Nakano, T., Okawa, K., Iwamatsu, A., Kaibuchi, K. 1996. Regulation of Myosin Phosphatase by Rho and Rho-Associated Kinase (Rho-Kinase). Science, 273, 245-248. Available: 10.1126/science.273.5272.245.

King, P. M., Adam, R. D., Pryde, A., McDicken, W. N., Heading, R. C. 1984. Relationships of human antroduodenal motility and trans-pyloric fluid movement: non-invasive observations with real-time ultrasound. Gut, 25, 1384-1391. Available: 10.1136/gut.25.12.1384.

Kong, F., Singh, R. P. 2008. Disintegration of Solid Foods in Human Stomach. Journal of Food Science, 73, R67-R80. Available: 10.1111/j.1750-3841.2008.00766.x.

Kong, F., Singh, R. P. 2009. Digestion of Raw and Roasted Almonds in Simulated Gastric Environment. Food Biophysics, 4, 365-377. Available: 10.1007/s11483-009-9135-6.

Konturek, S. J., Thor, P. J., Bilski, J., Bielanski, W. , Laskiewicz, J. 1986. Relationships between duodenal motility and pancreatic secretion in fasted and fed dogs. American Journal of Physiology-Gastrointestinal and Liver Physiology, 250, G570-G574. Available: 10.1152/ajpgi.1986.250.5.G570.

Koppen, B. M. , Stanton, B. A. 2008. Berney, Levy Physiology, Philadelphia, Mosby Elsevier.

Kozu, H., Kobayashi, I., Nakajima, M., Uemura, K., Sato, S. , Ichikawa, S. 2010. Analysis of Flow Phenomena in Gastric Contents Induced by Human Gastric Peristalsis Using CFD. Food Biophysics, 5, 330-336. Available: 10.1007/s11483-010-9183-y.

Krans, J. L. 2010. The Sliding Filament Theory of Muscle Contraction. Nature Education, 3(9).

Krehbiel, C. R., Mathews, J. C. 2003. Absorption of Amino acids and Peptides. In D'Mello, J.P.F. Amino Acids in Animal Nutrition (2nd ed.). pp. 41–70. Amino Acids in Animal Nutrition, 41-70.

Krieger, I. M., Dougherty, T. J. 1959. A Mechanism for Non-Newtonian Flow in Suspensions of Rigid Spheres. Transactions of the Society of Rheology, 3, 137-152. Available: 10.1122/1.548848.

Kunz, P., Crelier, G. R., Schwizer, W., Borovicka, J., Kreiss, C., Fried, M. , Boesiger, P. 1998. Gastric emptying and motility: assessment with MR imaging--preliminary observations. Radiology, 207, 33-40. Available: 10.1148/radiology.207.1.9530296.

Kunz, P., Feinle, C., Schwizer, W., Fried, M. , Boesiger, P. 1999. Assessment of gastric motor function during the emptying of solid and liquid meals in humans by MRI. Journal of Magnetic Resonance Imaging, 9, 75-80. Available: 10.1002/(sici)1522-2586(199901)9:1<75::Aid-jmri10>3.0.Co;2-i.

Kwiatek, M. A., Menne, D., Steingoetter, A., Goetze, O., Forras-Kaufman, Z., Kaufman, E., Fruehauf, H., Boesiger, P., Fried, M. , Schwizer, W. 2009. Effect of meal volume and calorie load on postprandial gastric function and emptying: studies under physiological conditions by combined fiber-optic pressure measurement and MRI. American Journal of Physiology, 297, G894-901.

Kwiatek, M. A., Steingoetter, A., Pal, A., Menne, D., Brasseur, J. G., Hebbard, G. S., Boesiger, P., Thumshirn, M., Fried, M. , Schwizer, W. 2006. Quantification of distal antral contractile motility in healthy human stomach with magnetic resonance imaging. Journal of Magnetic Resonance Imaging, 24, 1101-1109. Available: 10.1002/jmri.20738.

Ladd, A. J. C., Verberg, R. 2001. Lattice -Boltzmann Simulations of Particle-Fluid Suspensions. Journal of Statistical Physics, 104, 1191-1251. Available: 10.1023/a:1010414013942.

Lammers, W. J. E. P., Donck, L. V., Stephen, B., Smets, D. , Schuurkes, J. A. J. 2009. Origin and propagation of the slow-wave in the canine stomach: the outlines of a gastric conduction system. American Journal of Physiology-Gastrointestinal and Liver Physiology, 296, G1200-G1210. Available: 10.1152/ajpgi.90581.2008.

Lee, K. Y., Kim, M. S., Chey, W. Y. 1980. Effects of a meal and gut hormones on plasma motilin and duodenal motility in dog. American Journal of Physiology-Gastrointestinal and Liver Physiology, 238, G280-G283. Available: 10.1152/ajpgi.1980.238.4.G280.

Lees-Green, R., Du, P., O'Grady, G., Beyder, A., Farrugia, G. , Pullan, A. 2011. Biophysically-based of the interstitial cells of Cajal: Current status and future perspectives. Frontiers in Physiology, 2. Available: 10.3389/fphys.2011.00029.

Lentle, R. G., de Loubens, C. 2015. A review of mixing and propulsion of chyme in the small intestine: fresh insights from new methods. Journal of Comparative Physiology B, 185, 369-387. Available: 10.1007/s00360-015-0889-5.

Lentle, R. G., Janssen, P. W. M. 2008. Physical characteristics of digesta and their influence on flow and mixing in the mammalian intestine: a review. Journal of Comparative Physiology B, 178, 673-690. Available: 10.1007/s00360-008-0264-x.

Lentle, R. G., Janssen, P. W. M. 2010. Manipulating Digestion with Foods Designed to Change the Physical Characteristics of Digesta. Critical Reviews in Food Science and Nutrition, 50, 130-145. Available: 10.1080/10408390802248726.

Lentle, R. G., Janssen, P. W. M. 2011. Local Motility, Flow and Mixing in Tubular Segments of the Gut. The Physical Processes of Digestion. New York, NY: Springer New York. Available: 10.1007/978-1-4419-9449-3_8.

Lentle, R. G., Hemar, Y., Hall, C. E. , Stafford, K. J. 2005. Periodic fluid extrusion and models of digesta mixing in the intestine of a herbivore, the common brushtail possum (Trichosurus

vulpecula). Journal of Comparative Physiology B, 175, 337-347. Available: 10.1007/s00360-005-0490-4.

Lentle, R. G., Janssen, P. W. M., Goh, K., Chambers, P. , Hulls, C. 2010. Quantification of the Effects of the Volume and Viscosity of Gastric Contents on Antral and Fundic Activity in the Rat Stomach Maintained Ex Vivo. Digestive Diseases and Sciences, 55, 3349-3360. Available: 10.1007/s10620-010-1164-y.

Lentle, R. G., Reynolds, G. W., Hulls, C. M., Chambers, J. 2016. Advanced spatiotemporal mapping methods give new insights into the coordination of contractile activity in the stomach of the rat. American Journal of Physiology-Gastrointestinal and Liver Physiology, ajpgi. 00308.2016.

Lentle R.G, Reynold, W. G., Janssen, P. W. M. 2013. Gastro intestinal Tone; its genisis and contribution to the physical process of digestion. Neurogastroenterol Motil., 931-942.

Lentle, R. G., Stafford, K. J., Hemar, Y., Aseruvujanon, P., Mellor, D. J., Moughan, P. J. 2008. Changes in the physical properties of stomach digesta during fasting in tammar wallabies (Macropus eugenii eugenii). Australian Journal of Zoology, 55, 383-389. Available: https://doi.org/10.1071/ZO07055.

Lentle, R. G, De Loubens. C, Hulls .C, Janssen PWM, Golding M.D, Chambers J. P. 2012.A comparison of the organization of longitudinal and circular contractions during pendular and segmental activity in the duodenum of the rat and guinea pig. Neurogastroenterol Mot. 24(7):686-e298.

Lentle R. G, Hemar Y, Hall C.E. 2006. Viscoelastic behaviour aids extrusion from and reabsorption of the liquid phase into the digesta plug: creep rheometry of hindgut digesta in the common brushtail possum Trichosurus vulpecula. J Comp Physiol.B176(5):469-75.

Lentle R.G, Stafford K.J, Kennedy M.S, Haslett S.J. 2002. Rheological properties of digesta suggest little radial or axial mixing in the forestomach of the tammar (Macropus eugenii) and the parma (Macropus parma) wallaby. Physiol Biochem Zool.;75(6):572-82.

Leopold, G. R. 1975. Gray Scale Ultrasonic Angiography of the Upper Abdomen. Radiology, 117, 665-671. Available: 10.1148/117.3.665.

Liao, D., Gregersen, H., Hausken, T., Gilja, O. H., Mundt, M. , Kassab, G. 2004. Analysis of surface geometry of the human stomach using real-time 3D ultrasonography in vivo. Neurogastroenterology , Motility, 16, 315-324. Available: 10.1111/j.1365-2982.2004.00522.x.

Lim YF, de Loubens C, Love RJ, Lentle RG, Janssen PWM. Flow and mixing by small intestine villi. Food, Function. 2015;6(6):1787-95.

Lind, J. F., Duthie, H. L., Schlegel, J. F., Code, C. F. 1961. Motility of the gastric fundus. American Journal of Physiology, 201, 197-202.

Loewenstein, W. R. 1981. Junctional intercellular communication: the cell-to-cell membrane channel. Physiol Rev, 61, 829-913. Available: 10.1152/physrev.1981.61.4.829.

Love, R. J., Lentle, R. G., Asvarujanon, P., Hemar, Y., Stafford, K. J. 2013. An Expanded Finite Element Model of the Intestinal Mixing of Digesta. Food Digestion, 4, 26-35. Available: 10.1007/s13228-012-0017-x.

Luff, S. E. 1996. Ultrastructure of sympathetic axons and their structural relationship with vascular smooth muscle. Anatomy and Embryology, 193, 515-531. Available: 10.1007/BF00187924.

Maeda, H., Yamagata, A., Nishikawa, S., Yoshinaga, K., Kobayashi, S., Nishi, K., Nishikawa, S. I. 1992. Requirement of c-kit for development of intestinal pacemaker system. Development, 116, 369-375.

Malbert, C. H., Serthelon, J. P., Dent, J. 1992. Changes in antroduodenal resistance induced by Cisapride in conscious dogs. American Journal of Physiology-Gastrointestinal and Liver Physiology, 263, G202-G208. Available: 10.1152/ajpgi.1992.263.2.G202.

Malbert CH, Mathis C. Antropyloric modulation of trans-pyloric flow of liquids in pigs. Gastroenterology. 1994;107(1):37-46.

Malbert CH, Ruckebusch Y. Relationships between pressure and flow across the gastroduodenal junction in dogs. Am J Physiol. 1991;260(4):G653-7.

Mansouri, M., Delenne, J. Y., El Youssoufi, M. S. , Seridi, A. 2009. A 3D DEM-LBM approach for the assessment of the quick condition for sands. Comptes Rendus Mécanique, 337, 675-681. Available: https://doi.org/10.1016/j.crme.2009.09.010.

Marciani, L., Gowland, P. A., Fillery-Travis, A., Manoj, P., Wright, J., Smith, A., Young, P., Moore, R., Spiller, R. C. 2001. Assessment of antral grinding of a model solid meal with echo-planar imaging. American Journal of Physiology-Gastrointestinal and Liver Physiology, 280, G844-G849. Available: 10.1152/ajpgi.2001.280.5.G844.

Marciani, L., Gowland, P. A., Spiller, R. C., Manoj, P., Moore, R. J., Young, P., Al-Sahab, S., Bush, D., Wright, J. , Fillery-Travis, A. J. 2000. Gastric Response to Increased Meal Viscosity Assessed by Echo-Planar Magnetic Resonance Imaging in Humans. The Journal of Nutrition, 130, 122-127. Available: 10.1093/jn/130.1.122.

Marciani L, Gowland PA, Spiller RC, Manoj P, Moore RJ, Young P, 2001. Effect of meal viscosity and nutrients on satiety, intragastric dilution, and emptying assessed by MRI. Am J Physiol.;280(6):G1227-33.

Marciani, L. 2011. Assessment of gastrointestinal motor functions by MRI: a comprehensive review. Neurogastroenterology & Motility, 23, 399-407. Available: DOI 10.1111/j.1365-2982.2011.01670.x.

Marciani L, Penny A. Gowland, Robin C. Spiller, Pretima Manoj, Rachel J. Moore, Paul Young, Shireen Al-Sahab, Debbie Bush, Jeff Wright, Annette J. Fillery-Travis, Gastric Response to Increased Meal Viscosity Assessed by Echo-Planar Magnetic Resonance Imaging in Humans, The Journal of Nutrition, Volume 130, Issue 1, January 2000, Pages 122–127, https://doi.org/10.1093/jn/130.1.122.

Marieb, E. N., Hoehn, K. 2013. Human anatomy, physiology, Boston, Pearson.

Martinez M.N, Amidon GL. 2002. A mechanistic approach to understanding the factors affecting drug absorption: a review of fundamentals. J Clin Pharmacol, 42(6), 620-43.

Marston, S. B. 1989. What is latch? New ideas about tonic contraction in smooth muscle. Journal of Muscle Research, Cell Motility, 10, 97-100. Available: 10.1007/bf01739965.

Mattila-Sandholm, T., Mättö, J., Saarela, M. 1999. Lactic acid bacteria with health claims—interactions and interference with gastrointestinal flora. International Dairy Journal, 9, 25-35. Available: https://doi.org/10.1016/S0958-6946(99)00041-2.

Matusovsky, O. S., Shelud'ko, N. S., Permyakova, T. V., Zukowska, M. , Sobieszek, A. 2010. Catch muscle of bivalve molluscs contains myosin- and twitchin-associated protein kinase phosphorylating myorod. Biochimica et Biophysica Acta (BBA) - Proteins and Proteomics, 1804, 884-890. Available: https://doi.org/10.1016/j.bbapap.2009.12.020.

Melville J, Macagno E, Christensen J. 1975. Longitudinal contractions in the duodenum: their fluid-mechanical function. Am J Physiol.;228(6):1887-92.

Meyer, J., Ohashi, H., Jehn, D., Thomson, J. 1981. Size of liver particles emptied from the human stomach. Gastroenterology, 80, 1489-1496.

Mills, Z. G., Mao, W., Alexeev, A. 2013. Mesoscale Modelling: solving complex flows in biology and biotechnology. Trends in Biotechnology, 31, 426-434. Available: https://doi.org/10.1016/j.tibtech.2013.05.001.

Minekus, M., Marteau, P, Havenaar, R & Huis in't Veld, JHH 1995. A multicompartimental dynamic computer-controlled model simulating the stomach and small intestine. Alternatives to laboratory animal, 23, 197-209.

Mitra, S. 2015. Anatomy: Part 1, Academy publishers.

Miyagawa, T., Imai, Y., Ishida, S., Ishikawa, T. 2016. Relationship between gastric motility and liquid mixing in the stomach. American Journal of Physiology - Gastrointestinal and Liver Physiology, 311, G1114-G1121. Available: 10.1152/ajpgi.00346.2016.

Mochiki, E., Kuwano, H., Nakabayashi, T., Garcia, M., Haga, N., Asao, T. 2001. Pyloric Relaxation Regulated Via Intramural Neural Pathway of the Antrum. Digestive Diseases and Sciences, 46, 2307-2313. Available: 10.1023/a:1012374408853.

Mohamad, A. A. 2011. Lattice -Boltzmann Method - Fundamentals and Engineering Applications with Computer Codes, springer.

Molly, K., Smet, I. D., Nollet, L., Woestyne, M. V. , Verstraete, W. 1996. Effect of Lactobacilli on the Ecology of the Gastro-intestinal Microbiota Cultured in the SHIME Reactor. Microbial Ecology in Health and Disease, 9, 79-89. Available: 10.3109/08910609609166446.

Molly, K., Woestyne, M. V., Smet, I. D. , Verstraete, W. 1994. Validation of the simulator of the human intestinal microbial ecosystem (SHIME) reactor using microorganism-associated activities. Microbial Ecology in Health and Disease, 7, 191-200.

Mostafa, R. M., Moustafa, Y. M. , Hamdy, H. 2010. Interstitial cells of Cajal, the Maestro in health and disease. World Journal of Gastroenterology, 16, 3239-3248.

Mösges, R., Büchner, B., Kleiner, M., Freitas, R., Hörschler, I. , Schröder, W. 2010. Computational fluid dynamics analysis of nasal flow. B-ENT, 6, 161-165.

Noah, T. K., Donahue, B., Shroyer, N. F. 2011. Intestinal development and differentiation. Experimental Cell Research, 317, 2702-2710. Available: http://dx.doi.org/10.1016/j.yexcr.2011.09.006.

O'Grady, G., Du, P., Cheng, L. K., Egbuji, J. U., Lammers, W. J. E. P., Windsor, J. A., Pullan, A. J. 2010. Origin and propagation of human gastric slow-wave activity defined by high-resolution mapping. American Journal of Physiology-Gastrointestinal and Liver Physiology, 299, G585-G592. Available: 10.1152/ajpgi.00125.2010.

Okike, N., Kelly, K. A. 1977. Vagotomy impairs pentagastrin-induced relaxation of canine gastric fundus. American Journal of Physiology-Endocrinology and Metabolism, 232, E504. Available: 10.1152/ajpendo.1977.232.5.E504.

Pal, A., Brasseur, J. G., Abrahamsson, B. 2007. A stomach road or "Magenstrasse" for gastric emptying. Journal of Biomechanics, 40, 1202-1210. Available: https://doi.org/10.1016/j.jbiomech.2006.06.006.

Pal, A., Indireshkumar, K., Schwizer, W., Abrahamsson, B., Fried, M. , Brasseur, J. G. 2004. Gastric flow and mixing studied using computer simulation. Proceedings of the Royal Society of London B: Biological Sciences, 271, 2587-2594.

Pallotta, N., Cicala, M., Frandina, C., Corazziari, E. 1998a. Antro-pyloric contractile patterns and trans-pyloric flow after meal ingestion in humans. The American Journal of Gastroenterology, 93, 2513-2522. Available: https://doi.org/10.1016/S0002-9270(98)00479-1.

Pappas, T., Debas, H., Chang, A. , Taylor, I. 1986. Peptide YY release by fatty acids is sufficient to inhibit gastric emptying in dogs. Gastroenterology, 91, 1386-1389.

Patarin, J., Blésès, D., Magnin, A., Guérin, S. , Malbert, C.-H. 2015. Rheological Characterization of Gastric Juices from Bread with Different Amylose/Amylopectin Ratios. Food Digestion: Research and Current Opinion, 6, 2-9. Available: 10.1007/s13228-014-0037-9.

Paterson, C. A., Anvari, M., Tougas, G. , Huizinga, J. D. 2000. Determinants of Occurrence and Volume of Trans-pyloric Flow During Gastric Emptying of Liquids in Dogs. Digestive Diseases and Sciences, 45, 1509-1516. Available: 10.1023/A:1005544423426.

Peng, Y., Shu, C., Chew, Y. T. 2004. A 3D incompressible thermal lattice -Boltzmann model and its application to simulate natural convection in a cubic cavity. Journal of Computational Physics, 193, 260-274. Available: https://doi.org/10.1016/j.jcp.2003.08.008.

Powley, T. L., Wang, X.-y., Fox, E. A., Phillips, R. J., Liu, L. W. C. , Huizinga, J. D. 2008. Ultrastructural evidence for communication between intramuscular vagal mechanoreceptors and interstitial cells of Cajal in the rat fundus. Neurogastroenterology , Motility, 20, 69-79. Available: 10.1111/j.1365-2982.2007.00990.x.

Raj, K., Goyal, M. D. , Ikuo Hirano, M. D. 1996. The enteric nervous system. The New England Journal of Medicine, 1106-1115.

Ramkumar, D., Schulze, K. S. 2005. The pylorus. Neurogastroenterology , Motility, 17, 22-30. Available: 10.1111/j.1365-2982.2005.00664.x.

Rao, S. S., Lu, C. , Schulze-Delrieu, K. 1996. Duodenum as a immediate brake to gastric outflow: A videofluoroscopic and manometric assessment. Gastroenterology, 110, 740-747. Available: https://doi.org/10.1053/gast.1996.v110.pm8608883.

Rein, M. J., Renouf, M., Cruz-Hernandez, C., Actis-Goretta, L., Thakkar, S. K., da Silva Pinto, M. 2013. Bioavailability of bioactive food compounds: a challenging journey to bioefficacy. British Journal of Clinical Pharmacology, 75, 588-602. Available: 10.1111/j.1365-2125.2012.04425.x.

Rhee, P.-L., Lee, J. Y., Son, H. J., Kim, J. J., Rhee, J. C., Kim, S., Koh, S. D., Hwang, S. J., Sanders, K. M. , Ward, S. M. 2011. Analysis of pacemaker activity in the human stomach. The Journal of Physiology, 589, 6105-6118. Available: 10.1113/jphysiol.2011.217497.

Rinaldi, P. R., Dari, E. A., Vénere, M. J., Clausse, A. 2012. A Lattice -Boltzmann solver for 3D fluid simulation on GPU. Simulation Practice and Theory, 25, 163-171. Available: https://doi.org/10.1016/j.simpat.2012.03.004.

Rovelstad, R. A. 1976. The incompetent pyloric sphincter. Digestive Diseases and Sciences, 21, 165-173.

Saladin, K. S. 2007. Anatomy Physiology-The unity of form and function, New York, McGraw Hill.

Sanders, K. M., Hwang, S. J. , Ward, S. M. 2010. Neuroeffector apparatus in gastrointestinal smooth muscle organs. The Journal of Physiology, 588, 4621-4639. Available: 10.1113/jphysiol.2010.196030.

Sanders, K. M., Ward, S. M. , Koh, S. D. 2014. Interstitial cells: regulators of smooth muscle function. Physiological reviews, 94, 859-907.

Sanders, K. M. 2008. Regulation of smooth muscle excitation and contraction. Neurogastroenterol Motil, 20 Suppl 1, 39-53. Available: 10.1111/j.1365-2982.2008.01108.x

Sanderss, K. M., Koh S D , M, W. S. 2006. Interstitial cells of Cajal as pacemakers in the gastrointestinal tract. Annu. Rev. Physiol, 307-343.

Sanger, G. J., Lee, K. 2008. Hormones of the gut-brain axis as targets for the treatment of upper gastrointestinal disorders. Nat Rev Drug Discov, 7, 241-254.

Sanger, Paul, L., Andrews, J, G. 2002. Abdominal Vagal afferent neurons: an important target for the treatment of gastro intestinal dysfunction. Current opinion in Pharmacology, 650-656.

Sayegh, A. I., Reeve, J. R., Jr., Lampley, S. T., Hart, B., Gulley, S., Esdaile, A. R., Sharma, S. K., Webb, T., Williams, C. S., Pruitt, F. 2005. Role for the enteric nervous system in the regulation of satiety via cholecystokinin-8. J Am Vet Med Assoc, 226, 1809-16. Available: 10.2460/javma.2005.226.1809.

Schemann, M. 2005. Control of Gastrointestinal Motility by the “Gut Brain” - The Enteric Nervous System. Journal of Pediatric Gastroenterology and Nutrition, 41, S4-S6. Available: 10.1097/01.scs.0000180285.51365.55.

Schulze, K. 2006. Imaging and of digestion in the stomach and the duodenum. Neurogastroenterology , Motility, 18, 172-183. Available: 10.1111/j.1365-2982.2006.00759.x.

Schulze-Delrieu, K. , Shirazi, S. S. 1983. Neuromuscular differentiation of the human pylorus. Gastroenterology, 84, 287-292.

Schulze-Delrieu, K., Wall, J. P. 1983. Determinants of flow across isolated gastroduodenal junctions of cats and rabbits. American Journal of Physiology - Gastrointestinal and Liver Physiology, 245, G257-G264.

Schulze-Delrieu, K., Herman, R. J., Shirazi, S. S. , Brown, B. P. 1998. Contractions move contents by changing the configuration of the isolated cat stomach. American Journal of Physiology-Gastrointestinal and Liver Physiology, 274, G359-G369. Available: 10.1152/ajpgi.1998.274.2.G359.

Schulze-Delrieu, K. 1992. Clearance patterns of the isolated guinea pig duodenum. Gastroenterology, 102, 849-856.

Sembulingam, K. 2012. Essentials of Medical Physiology, New Delhi, Jaypee Brothers Medical Publishers (P) Ltd.

Shahidullah, M., Kennedy, T., Parks, T. 1975. The vagus, the duodenal brake, and gastric emptying. Gut, 16, 331-33.

Shi, X., Lim, S. P. 2007. A LBM–DLM/FD method for 3D fluid–structure interactions. Journal of Computational Physics, 226, 2028-2043. Available: https://doi.org/10.1016/j.jcp.2007.06.031.

Siegel JA, Urbain JL, Adler LP, Charkes ND, Maurer AH, Krevsky B, *et al*. Biphasic nature of gastric emptying. Br Med J. 1988;29(1):85-9.

Singh, S., Singh, R. P. 2010. Gastric digestion of foods: Mathematical Modelling of flow field in a human stomach. Food engineering interfaces. Springer.

Sobieszek, A. 2016. Helical model of smooth muscle myosin filament and the ribbons made of caldesmon: history revisited. European Biophysics Journal, 1-7. Available: 10.1007/s00249-016-1175-5.

Song, Z. M., Brookes, S. J. H., Costa, M. 1996. Projections of specific morphological types of neurons within the myenteric plexus of the small intestine of the guinea-pig. Cell and Tissue Research, 285, 149-156. Available: 10.1007/s004410050630.

Spiller RC, Trotman IF, Higgins BE, Ghatei MA, Grimble GK, Lee YC, *et al*. The ileal brake-inhibition of jejunal motility after ileal fat perfusion in man. Br Med J. 1984;25(4):365-74.

Stanghellini V, Ghidini C, Maccarini MR, Paparo G, Corinaldesi R, Barbara L. Fasting and postprandial gastrointestinal motility in ulcer and non-ulcer dyspepsia. Gut. 1992;33(2):184-90.

Succi, S. 2001. The Lattice -Boltzmann Equation for Fluid Dynamics and Beyond, Clarendon Press.

Sukop, M. C. 2006. Lattice -Boltzmann Modelling: An Introduction for Geoscientists and Engineers, Springer.

Sukop MC, Thorne DTJ. 2007. Lattice Boltzmann Modelling: An Introduction for Geoscientists and Engineers. New York: Springer.

Szurszewski, J. H. 1997. The enigmatic electrical slow-wave : A mirror on 100 years of research in gut motility. Gastroenterology, 113, 1785-1787. Available: 10.1053/gast.1997.v113.agast971131785.

Takahashi, Toku. 2012. Mechanism of Interdigestive Migrating Motor Complex. J Neurogastroenterol Motil., 18, 246-257.

Takahashi, T., Sakata, T. 2002. Large Particles Increase Viscosity and Yield Stress of Pig Cecal Contents without Changing Basic Viscoelastic Properties. The Journal of Nutrition, 132, 1026-1030. Available: 10.1093/jn/132.5.1026.

Takahashi, T., Sakata, T. 2004. Viscous properties of pig cecal contents and the contribution of solid particles to viscosity. Nutrition, 20, 377-382. Available: https://doi.org/10.1016/j.nut.2003.12.011.

Takahashi, T. 2011. Flow Behaviour of Digesta and the Absorption of Nutrients in the Gastrointestine. Journal of Nutritional Science and Vitaminology, 57, 265-273. Available: 10.3177/jnsv.57.265.

Takaki, M. 2003. Gut Pacemaker Cells: the Interstitial Cells of Cajal (ICC). Journal of Smooth Muscle Research, 39, 137-161. Available: 10.1540/jsmr.39.137.

Takayama, I., Horiguchi, K., Daigo, Y., Mine, T., Fujino, M. A. , Ohno, S. 2002. The Interstitial Cells of Cajal and a Gastroenteric Pacemaker System. Archives of Histology and Cytology, 65, 1-26. Available: 10.1679/aohc.65.1.

Terragni, R., Vignoli, M., Rossi, F., Laganga, P., Leone, V. F., Graham, J. P., Russo, M. , Saunders, J. H. 2012. Stomach wall evaluation using helical hydro-computed tomography. Veterinary Radiology, Ultrasound, 53, 402-405. Available: 10.1111/j.1740-8261.2012.01928.x.

Thomas, A. 2006. Gut motility, sphincters and reflex control. Anaesthesia, Intensive Care Medicine, 7, 57-58. Available: https://doi.org/10.1383/anes.2006.7.2.57.

Troncon, L. E., Bennett, R. J., Ahluwalia, N. K., Thompson, D. G. 1994. Abnormal intragastric distribution of food during gastric emptying in functional dyspepsia patients. Gut, 35, 327-332. Available: 10.1136/gut.35.3.327.

Van Citters, G. W., Lin, H. C. 1999. The ileal brake: A fifteen-year progress report. Current Gastroenterology Reports, 1, 404-409. Available: 10.1007/s11894-999-0022-6.

Van Helden, D. F., Laver, D. R., Holdsworth, J., Imtiaz, M. S. 2010. Generation and propagation of gastric slow-waves. Clinical and Experimental Pharmacology and Physiology, 37, 516-524. Available: 10.1111/j.1440-1681.2009.05331.x.

Ward, S. M., Sanders, K. M., Hirst, G. D. S. 2004. Role of interstitial cells of Cajal in neural control of gastrointestinal smooth muscles. Neurogastroenterology, Motility, 16, 112-117. Available: 10.1111/j.1743-3150.2004.00485.x.

Webb, R. C. 2003. Smooth Muscle Contraction And Relaxation. Advances in Physiology Education, 27, 201-206.

Weitschies, W., Blume, H., Mönnikes, H. 2010. Magnetic Marker Monitoring: High resolution real-time tracking of oral solid dosage forms in the gastrointestinal tract. European Journal of Pharmaceutics and Biopharmaceutics, 74, 93-101. Available: https://doi.org/10.1016/j.ejpb.2009.07.007.

Weitschies W, Blume H, Mönnikes H. 2010. Magnetic marker monitoring: high resolution real-time tracking of oral solid dosage forms in the gastrointestinal tract. Eur J Pharm Biopharm. 74(1):93-101.

Westfall, W. D. 2006. Goodman and Gilman's The Pharmacological Basis of Therapeutics New York: McGraw-Hill.

Wheelon H, T. J. 1921. Rhythmicity of the pyloric sphincter. Am J Physiol, 54, 460–473.

Weitschies W, Blume H, Mönnikes H. 2010 .Magnetic Marker Monitoring: High resolution real-time tracking of oral solid dosage forms in the gastrointestinal tract. European Journal of Pharmaceutics and Biopharmaceutics;74(1):93-101.

Wilbur, B. G., Kelly, K. A. 1973. Effect of proximal gastric, complete gastric, and truncal vagotomy on canine gastric electric activity, motility, and emptying. Annals of surgery, 178, 295-303. Available: 10.1097/00000658-197309000-00009.

Word, R. A., Tang, D. C., Kamm, K. E. 1994. Activation properties of myosin light chain kinase during contraction/relaxation cycles of tonic and phasic smooth muscles. Journal of Biological Chemistry, 269, 21596-21602.

Worlicek, H., Dunz, D., Engelhard, K. 1989. Ultrasonic examination of the wall of the fluid-filled stomach. Journal of Clinical Ultrasound, 17, 5-14. Available: 10.1002/jcu.1870170103.

Xu, J.-Q., Harder, B. A., Uman, P., Craig, R. 1996. Myosin filament structure in vertebrate smooth muscle. The Journal of cell biology, 134, 53-66.

Xue, Z., Ferrua, M. J. , Singh, P. 2012. Computational fluid dynamics Modelling of granular flow in human stomach. Alimentos hoy, 21, 3-14.

Yoo, J., Chen, X. 2006. GIT physicochemical Modelling-a critical review. International Journal of Food Engineering, 2, 1-10.

Zhang, J. 2011. Lattice -Boltzmann method for microfluidics: models and applications. Microfluidics and Nanofluidics, 10, 1-28. Available: 10.1007/s10404-010-0624-1.

Zou, Q., He, X. 1997. On pressure and velocity boundary conditions for the lattice -Boltzmann BGK model. Physics of Fluids, 9, 1591-1598. Available: 10.1063/1.869307.

Zu, W.-H., Zhang, J.-H., Chen, D.-D., Xu, Y.-Q., Wei, Q. , Tian, F.-B. Immersed Boundary-Lattice -Boltzmann Method for Biological and Biomedical Flows. 2014a Berlin, Heidelberg. Springer Berlin Heidelberg, 383-392.

Ördög, T., Ward, S. M. , Sanders, K. M. 1999. Interstitial cells of Cajal generate electrical slow-waves in the murine stomach. The Journal of Physiology, 518, 257-269. Available: 10.1111.

Appendix 1: Background information on the human stomach

Morphology and Glandular Histology of gastric wall

Like the other parts of the GI tract, the stomach wall constitute of different types of tissues (Figure A1)(Forte, 1996, Koppen *et al*., 2008, Mitra, 2015), namely

- Epithelial mucosa
- Sub-mucosa
- Muscularis propria (muscular layer)
- Serosa (fibrous layer)

Epithelial mucosa

The gastric mucosa lines the cavity of the GI tract. It has folded (rugae) structure when the stomach is empty. The rugae stretch out when the food reaches the stomach to accommodate more food. The gastric mucosa consists of three layers, namely: the columnar epithelial lining, the lamina propria and the muscularis mucosa.

The epithelial layer is a single layer of columnar epithelial cells. There are a number of different types of cells present in this layer. Lamina Propria is a loose connective tissue layer immediately below the epithelium (Koppen *et al*., 2008). This layer contains collagen and elastin fibrils. This layer is rich in capillaries and nerve fibres. The muscularis mucosa is the innermost layer of mucosa, and the functions of this layer are uncertain (Forte, 1996).

The gastric mucosa contains deep narrow depressions called gastric pits, into which the gastric glands are opening. The main glandular epithelial cells in the gastric pits are:

- Chief cells
- Parietal cells

- Mucus secreting cells
- Neuroendocrine cells

The chief cells also referred to as peptic cells or zymogenic cells, are found at the base of the gastric glands, which secretes pepsinogen (PG-l) and gastric lipase (Forte, 1996, Barrett *et al.*, 2010). The hydrochloric acid below pH 5 (Mitra, 2015) transforms inactive pepsinogen into active pepsin. Pepsin is an endopeptidase, which breaks long-chain protein molecules into peptides (short chains of amino acids). Gastric lipase catalyses the hydrolysis of triacylglycerols (fats) into fatty acids and glycerols (Youssef Gargouri, 1988). The production of enzymes from the chief cells is regulated by gastrin.

The parietal cells or the oxyntic cells present throughout the length of the glands are hydrochloric acids and intrinsic factor producing cells (Mitra, 2015, Sembulingam, 2012, Sjaastad *et al.*, 2010, Saladin, 2007). The hydrochloric acid reduces the gastric pH to 2 (Mitra, 2015). The hydrochloric acid partially hydrolysis the proteins and prevent bacterial colonization (Mitra, 2015).

Hydrochloric acid is produced by the action of carbonic anhydrase, which forms carbonic acid (H2CO3) from CO2. Subsequent dissociation of carbonic acid generates H^+ ions and the bicarbonate ion ($HCO3^-$). $HCO3^-$ is exchanged for chloride ion (Cl^-) and enters into the bloodstream. The Cl^- and H^+ ions are excreted to the lumen by interchanging a potassium ion. When parietal cells are stimulated by gastrin, the concentrations of H^+ ions rise significantly in the lumen, cause the lumen pH to fall (Sjaastad *et al.*, 2010).

The intrinsic factor secreted by partial cells is essential for vitamin B12 absorption (Sjaastad, 2010, Bruce M. Koppen, 2008, Saladin, 2007). The absence of intrinsic factor leads to anaemia, as vitamin B12 is essential for red blood cell maturation (Forte, 1996). According to Koppen (2008), secretion of intrinsic factor is the only gastric function essential for human life.

The mucus-secreting cells are exocrine cells that secrets a polymer matrix present in the mucus called the mucin (Verdugo, 1990, Specian and Oliver, 1991). The slippery, viscous and gel-like mucus coats the stomach wall to protects the gastric mucosa from acid, alcohol, pepsin and other luminal agents (Forte 1996). These cells also secrete sodium bicarbonate ($NaHCO_3$) rich fluid other than mucin. The production of sodium bicarbonate is influenced by the low mucosal pH (Forte 1996), which is helpful to neutralize the highly acidic environment of the stomach. The secretion

of mucin is merocrine, yet the apocrine method of secretion is also observed under stress (Specian and Oliver, 1991). According to Sjaastaad (2010), these cells are stem cells of new epithelial cells, but Forte (1996) specifies that they act as a stem cell only for chief cells.

Neuroendocrine cells are alternatively called enteroendocrine cells (Gunawardene *et al.,* 2011) are located around the base of the gland and secrete different types of hormones and paracrine messengers to regulate digestion (Marieb and Hoehn, 2013, Saladin, 2007). The G cells, D cells, enterochromaffin-like cells (ECL) and enterochromaffin (EC) cells are the enteroendocrine cells present in the stomach(Sembulingam, 2012, Mitra, 2015).

EC cell secretes serotonin (Sembulingam, 2012), an enteric neurotransmitter that affects neural modulation of gut smooth muscle function(Ormsbee and Fondacaro, 1985). Enterochromoffin-like (ECL) cells synthesise and secrete histamine, which is a physiological stimulant of gastric acid production (Håkanson and Sundler, 1991). ECL cells are stimulated by gastrin.

The G cells secrete gastrin that activates the hydrochloric acid production by stimulating the parietal cells and chief cells. Gastrin influence the release of histamine that in turn stimulates parietal cells to release HCl (Kelly, 2004). Gastrin gastric contractile activity but relaxes the pyloric sphincter (Sembulingam, 2012, Kelly, 2004).

The D cells secrete somatostatin, which inhibits the HCl secretion. Here gastric acid secretion is regulated by the interplay of gastrin and somatostatin. The somatostatin prevents the release of gastrin, secretin and histamine. The somatostatin release is activated by the low pH of the chyme in the antrum.

The collection of different epithelial cells which opens to a gastric pit is called gastric glands. According to the topographic area, the types of epithelial cell and population present in gastric gland changes (Schubert and Peura, 2008).

Gastric glands

There are three types of gastric glands, distinguishable from one another by location and type of glandular cells present, namely cardiac glands, fundic glands and pyloric glands (Barrett *et al.,* 2010, Sjaastad *et al.,* 2010, Sembulingam, 2012, Saladin, 2007, Forte, 1996). In contrast, Schubert *et al*. (2008) explain that cardiac glands are formed due to abnormal gastric refluxes. They

conclude as the autopsy and endoscopic studies prove that cardiac mucosa is absent in over 50% of the population. So, according to them, only two glandular regions exists in the stomach.

A gastric gland is located at the base of an apical pit called the gastric pit, and the progenitor cells are located at the isthmus (Schubert and Peura, 2008, Sjaastad *et al.,* 2010, Saladin, 2007). The mucous producing cells migrate upward, and acid-secreting cells move toward the base of the gland from the progenitor cell zone. The parietal cells become inactive as it moves deeper and the turn over a period of the parietal cells is around 54 days (Schubert and Peura, 2008).

The cardiac glands

The glands that are situated in the cardiac region of the stomach are short and mucus-secreting. The mucus-secreting surface mucous cells are abundant in these glands, but a few parietal and chief cells are also present (Forte, 1996).

Fundic glands

The glands present in the fundus and corpus of the stomach is called fundic or oxyntic, or parietal glands. Major cell types of the fundic gland are the parietal cells, chief cells, mucus-secreting cells and the enterochromaffin-like cells (ECL).

Pyloric glands

The glands located in the distal stomach, near the antrum and pyloric region are called pyloric glands. Gastric pits in this region are very deep and reach halfway down to the muscularis mucosa. The mucus-secreting glands are abundant in these glands; in addition to that, G cells, D cells, and EC cell types are also present.

Some secretory cells which are normally seen in the intestinal wall are found in the stomach in special circumstances. The tuft cell is found in the hyperplastic human, that capable of detecting and transmitting the environmental signals to the brain (Saqui-Salces *et al.*, 2011). A condition known as intestinal metaplasia mutates the gastric glands, and they start to act like an intestinal gland (Inada *et al.,* 2001).

Sub-mucous layer

The sub-mucous layer contains the nerve trunks, blood vessels and lymph vessels along with the submucosal plexus (Meissner's plexus) of the ENS (Koppen *et al*., 2008).

Muscularis propria (the muscular layer)

The muscularis propria is a three-layered muscle tissue made of smooth muscles. Refer to chapter 2 of this thesis for details

Regulation of gastric secretions

The gastric secretion is under neural and hormonal control with three different phases: the cephalic phase, gastric phase, and the intestinal phase.

The cephalic phase

The cephalic phase occurs before food is ingested, whereupon the sight, smell, taste, or even the thought of food (Sjaastad *et al*. 2010) activates vagal efferent fibres that stimulate the gastric secretion.

The gastric phase

Consumed food and semi-digested protein activate gastric secretion (Sjaastad *et al*., 2010). This phase accounts for two-thirds of the gastric enzyme secretions that occur in the body in response to a meal.

Although food stimulates gastric juice secretion in this phase, the buffering effect of the food decreases the acidity of the stomach. A study using pH electrodes at various locations of the stomach had shown that pH profile increases in postprandial state at proximal and distal stomach (Fletcher *et al*., 2001). The intra-gastric pH in healthy subjects during fasting is in the range of 1.3 - 2.5, and intake of a meal increase pH to 4.5 to 5.8, but the pH again drops to 3 within 1 hour after eating (Kong and Singh, 2008).

Role of Ghrelin in the gastric phase

Recent studies suggest that ghrelin, a 28-amino acid peptide has a major role in increasing food intake and body weight gain (Date *et al*., 2002, Zheng *et al*., 2009). Ghrelin is produced in a distinct type of endocrine cell in the stomach, and ghrelin induces feeding by direct stimulation of gastric

vagal afferents. It is observed that both central and peripheral administration of ghrelin stimulates food intake in humans and rodents (Zheng *et al*., 2009).

The studies suggest (Date *et al*., 2002; Toshinai *et al*., 2001) that starvation and insulin-induced hypoglycemia can up-regulate the ghrelin production, but feeding, hyperglycemia and obesity down-regulate it (Date *et al.,* 2002, Toshinai *et al.,* 2001). However, injection of ghrelin to completely vagotomised mice, did not stimulate food intake; this is contradicting the early hypothesis that ghrelin can cross the blood-brain barrier (Date *et al.*, 2002).

The intestinal phase of gastric secretion

The intestinal phase begins when the chyme reaches the duodenum (Saladin 2007), and this initially enhances the gastric secretion but inhibits it soon after (Saladin 2007). Stretching the duodenum and the presence of peptides and amino acids in the chyme stimulates the secretion via vagovagal reflexes and gastrin produced by G cells. However, the presence of acid and semi-digested fats in the duodenum triggers the entero-gastric reflex that sends inhibitory signals to the stomach via ENS (Saladin 2007). Enteroendocrine cells in the duodenum secrete secretin, cholecystokinin (CCK), and gastric inhibitory peptide (GIP). All these three hormones annihilate gastric secretion and motility (Saladin 2007).

Secretin, a hormone produced by the duodenum, is a polypeptide made of 27 amino acids. This is essential for water homeostasis. When the chyme is very acidic, secretin is secreted into the bloodstream, and this stimulates the acinar cells of the pancreas to secrete water and bicarbonate that drain into the duodenum. This will dilute the acidity of the chyme and thereby protect the intestinal lining from damage.

The presence of hydrochloric acid, amino acid, or fatty acid in the duodenum stimulates enteroendocrine cells to secrete CCK. CCK stimulates the gallbladder to release stored bile into the intestine that provides satiety. A gastric inhibitory polypeptide is secreted by the intestinal mucosa. GIP blocks the HCl secretion but stimulates the insulin secretion from islets of Langerhans. Debas *et al*. conducted a study to decide the physiological role of cholecystokinin (CCK) in the inhibition of gastric emptying (Pappas *et al.,* 1986). Four dogs were administrated CCK intravenously to simulate the physiological condition. By monitoring the gastric emptying

of the volume, they proved that CCK is a potent inhibitor of gastric emptying. They noticed that both Penta gastrin and heptadeca peptide gastrin also inhibits gastric emptying, but the dosage required is much higher.

Stomach wall motor activity during inter meal interval: The migrating motor complex

The aborally propagating contraction waves (APCs) in the stomach that occurs between the meal is called the migrating motor complex (MMCs) (Takahashi and Toku, 2012, Deloose *et al.*, 2012) and is controlled by the intrinsic nervous system (Brierley *et al.*, 2001). The empty stomach stays quiescent for 1-2 hrs, and then a series of peristaltic contractions begin. During inter meal interval, the pyloric sphincter is relaxed so that the antral contractions cause large undigested particles to be flushed out of the stomach. Four phases of MMCs are identified in human and dogs (Takahashi *et al*., 2012).

MMC Phase-I is identified as a smooth muscle quiescent period that lasts for 45 to 60 minutes during the post prandial period in which no action potentials or contractions are observed.

MMC Phase-II is a 30minute long intermittent irregular APCs where the frequency of contraction increases progressively (Takahashi *et al*., 2012).

Phase-III sometimes called the gastric Phase-III, is the most active phase of MMC, where regular bursts of APCs originates across the stomach (Deloose *et al*. 2012). Phase-III lasts for 90-120 minutes in humans and dogs (Takahashi and Toku, 2012). The MMC Phase-III APCs can be induced in humans by intravenous administration of motilin (Tack *et al.*, 2016), erythromycin or ghrelin (Miyano *et al.*, 2013) and serotonin or somatostatin (Deloose *et al.*, 2012).

MMC ***Phase-IV*** is a short period of transition between the barrage of contractions in phase 3 and the inactivity of phase-I.

Role of Motilin in regulating MMC

Relation of Motilin (a 22-amino acid polypeptide hormone, released into the general circulation by endocrine M cells) with MMC phase-III in human and dog is well established (Itoh, 1997, Zheng *et al.*, 2009, Takahashi and Toku, 2012), but not observed in pig (Romanski and W, 2009).

Romanski (2009) observed that Phase-III of MMC was evoked by motilin in the gastroduodenal region of sheep and dog. The study conducted by Takahashi *et al*. (2012) supporting that observation by identifying no Phase-III MMC in dogs after duodectomy. Romanski (2009) suggested that motilin induces MMC Phase-III directly through motilin receptors present in the smooth muscles. According to Takahashi *et al*. (2012), duodenum stores motilin, and duodectomy causes motilin deprivation. They augmented the point by inducing MMC Phase-III in duodenectomized dogs by administrating exogenous motilin.

A study (Luiking *et al.,* 2003) conducted in humans suggested that motilin induces Phase-III only in the antrum region. They believe that the cooperation of ENS with motilin induces the MMC phase-III in the gastro-duodenal region. It is supported by the fact that the motilin receptors in the antrum are localized principally in

the enteric nerve plexus (Luiking *et al.,* 2003). However, according to Takahashi (Takahashi and Toku 2012), "it has not been well established whether motilin acts through intrinsic neurons, extrinsic neurons or smooth muscles."

Role of ghrelin in regulating MMC

Ghrelin, a peptide hormone known as the hunger hormone, is secreted by the ghrelinergic cells in the GI tract. A recent study suggests that ghrelin, which is from the same peptide family as motilin, is also involved in the regulation of the MMC (Miyano *et al.,* 2013). But this is contradicting the observations of (Takahashi and Toku, 2012), where the administration of ghrelin in dogs did not induce Phase-III. So according to them, motilin regulates gastric phase III contractions in dogs and humans, while ghrelin regulates gastric phase III-like contractions in rats and mice.

Miyano *et al*. (2013) noticed that ghrelin did not enhance phase II contractions in vagotomised suncus. This observation strongly suggests that the ghrelin directly acts on the vagal afferent pathways and induces gastric phase II contractions through the vagus nerve.